学 位 論 文

Development of Remote Inflammation through Interneuron Network in the Spinal Cord

(脊髄の介在ニューロンネットワークを介した遠隔炎症の発症)

2022 年3 月

北 海 道 大 学

ナダ　ナスロ　アアブヅルモネイモ　サイェド

アヘメド　ハラカ

Nada Nasr AbdelMoneim Sayed Ahmed Halaka

学 位 論 文

Development of Remote Inflammation through Interneuron Network in the Spinal Cord

(脊髄の介在ニューロンネットワークを介した遠隔炎症の発症)

202２ 年3 月

北 海 道 大 学

ナダ　ナスロ　アアブヅルモネイモ　サイェド

アヘメド　ハラカ

Nada Nasr AbdelMoneim Sayed Ahmed Halaka

TABLE OF CONTENTS Page#

List of Publications and Presentations

List of Publications:

1. Rie Hasebe#, Kaoru Murakami#, Masaya Harada#, **Nada Halaka**#, Hiroshi Nakagawa, Fuminori Kawano, Yoshinobu Ohira, Tadafumi Kawamoto, Fiona E. Yull, Timothy S. Blackwell, Junko Nio-Kobayashi, Toshihiko Iwanaga, Masahiko Watanabe, Nobuhiro Watanabe, Harumi Hotta, Toshihide Yamashita, Daisuke Kamimura, Yuki Tanaka#, and Masaaki Murakami; ATP spreads inflammation to other limbs through crosstalk between sensory neurons and interneurons. *J. Exp. Med.*, Under revision
2. Omran M.H., Aly M.K., **Nasr N**., Massoud A.A., Youssef S.S., Bader El Din N.G., Dawood R.M., Atef K, Moustafa R.I., Nabil W., Tabll A.A., El Awady M.K.. A; Study of CC-Chemokine Receptor 5 (CCR5) Polymorphism on the Outcome of HCV Therapy in Egyptian Patients. *Hepat Mon*. 13(12): e13721

List of Presentations:

A- Poster presentations:

1. **Nada Halaka**, Daisuke Kamimura, Munezumi Fujita, Masaaki Murakami. Further Understanding to the role of NEED4 gene, and number of other genes in the development of keloid Scar , and hypertrophic scar as a model for inflammatory Diseases. 5th Hokkaido university interdepartmental symposium. 2019 November 6th Graduate school of Medicine , Hokkaido university, Japan.
2. **Nada Halaka**, Munezumi Fujita, Daisuke Kamimura, Naoki Murao, Yuhei Yamamoto, Masaaki Murakami. NEDD4 SP3-mediated activation of the inflammation amplifier is related to chronic inflammation of keloid. 4th Hokkaido university Cross symposium. 2019 January 25th . Graduate school of Medicine, Hokkaido university, Japan.
3. **Nada Halaka**, Daisuke Kamimura, Munezumi Fujita, Masaaki Murakami. Genetic differential study for the Hypertrophic scars (HTS) and Keloid disease (KD)
   The 9th IGM Exchange Meeting, 2018 December 17, Graduate School of Medicine, Hokkaido University.

B- Oral presentations:

1. Moataza H. Omran, **Nada Halaka**, Mahmoud Khamis, Mohamed A. EL Ghor, Mostafa K. El Awady Studying of Interleukin-10 Gene Polymorphism and Its Association as a

Predictive Marker in HCV Infection .. The 4 th International Conference of the Arab Society for Medical Research13 – 16 th September 2014,El Ain el Sokhna , Egypt.

Summary

Background and purpose:

Rheumatoid arthritis (RA) is a chronic inflammatory disease accompanied by joint inflammation, synovial hypertrophy, and progressive destruction of cartilage and bone, and affects 1% of the adult population worldwide. One criterion of the diagnosis and a fundamental characteristic of RA is remote inflammation, which results in widespread and severe malformation and immobility on both sides of joint. Although several studies have suggested that a neural mechanism is involved in the spreading inflammation of RA, the molecular links of inflammatory and neural pathways have not been uncovered.

We previously found an amplification mechanism of inflammatory response, so called "IL-6 amplifier", in which a simultaneous activation of IL-6-STAT3 and other cytokines (e.g. IL-17, TNF-α, and growth factors)-NF-κB pathways, induces an excessive activation of NF-κB in tissue-specific non-immune cells, resulting in chronic inflammation through a local recruitment of immune cells and robust production of inflammatory cytokines such as IL-6 *per se* and chemokines. Accordingly, we have defined inflammation as an IL-6-mediated accumulation of immune cells and/or proliferation of immune cells and regional non-immune cells, followed by the dysregulation of local homeostasis including the dysfunction of tissues and/or organs. Furthermore, we also discovered “gateway reflex” as the regulatory mechanism of IL-6 amplifier by activation of specific neural circuit. Environmental factors such as gravity, weak electricity, pain, stress, and light stimulate specific neural circuits to produce neurotransmitter locally, and induce or inhibit (only by light stimulation) IL-6 amplifier that subsequently creates a specific gateway for immune cells at blood barrier, and then promote or suppress (only by light stimulation) an onset of chronic inflammatory diseases.

Based on our original discoveries regarding IL-6 amplifier and gateway reflex, we hypothesized that a local neural regulation for bilateral inflammation may trigger initial inflammation and promotes the subsequent recruitment of immune cells by releasing attracting factors such as chemokines via the IL-6 amplifier.

In my doctoral research, I aimed to clarify the underlying molecular mechanism of how specific neural circuit interconnects with bilateral inflammation for spreading pathology.

Materials and methods:

To explore the molecular basis via neural pathways for spreading inflammation, F759 mice in which IL-6-mediated STAT3 activation is enhanced due to an amino acid substitution, Y759F in gp130 (IL-6 signal transducer in the IL-6R complex) at the binding site of SOCS3 for the negative regulation of IL-6 signaling, and spontaneous development of an RA-like disease in both sides of the ankle joints at around one year of age occur, were used as a representative cytokine-induced arthritis model as well as in a collagen-induced arthritis model (CIA) throughout my study.

Since we hypothesized that spreading inflammation in RA might depend on neural pathways distributed on both sides, F759 mice were injected with IL-6 plus IL-17A, saline, or a neurotransmitter ATP, with or without anti-IL-6R, anti-IL-17A, control IgG, A438079 (ATP receptor P2X7 antagonist) at unilateral or bilateral ankle joints. For some experiments, F759 mice induced arthritis by cytokine injections undergo deafferention for the sensory neurons at one side of the dorsal root ganglions (DRGs) beside the fifth lumbar cord (L5) or spinal cord cut. These mice were then assessed for the disease severity based on two bilaterally parameters: (1) swelling of the ankle and (2) restricted mobility of the ankle joints. The severity of each parameter was graded on a scale of 0–3, where 0 indicates no change; 1, mild change; 2, medium change; and 3, severe change. Averages for a single point in one leg ankle joint from each mouse were used. Ipsilateral and/or contralateral ankle joints, DRG at third to sixth lumbar cords (L3-L6) and nineth to thirteenth thoracic cords (T9-13), were used for examining recruitment of immune cells and neural activation status, and identification of specific sensory neuron and interneuron by immunohistochemistry (IHC), for quantifying c-fos (neural activation status), cytokine, and chemokine expression levels by real-time PCR, and for measuring cytokine and neurotransmitter levels by ELISA. For assessing NF-κB activity, ankle joints from NF-κB-reporter Tg/F759 mice induced arthritis by IL-6 plus IL-17A injections were collected and synovial tissues were homogenized in passive lysis buffer. After centrifugation, the supernatants were collected and analyzed for luciferase activities using Luciferase reporter assay system. To investigate the neural networks in spinal cord that connect sensory pathways between the ankle joints, herpes simplex virus 2 (HSV2) was employed to trace neural connections regardless of the presence of synapses. The presence of HSV2 was detected by IHC and quantified by real-time PCR.

Results:

We found that surgical ablation or pharmacological inhibition of neural pathway at one side of ankle prevented inflammation development on the other side. Mechanistic analysis showed that ATP induced by activation of the IL-6 amplifier in collagen type1+ non-immune cells in one side of the ankle joint activates Nav1.8+ TRPV1+/- sensory neurons, which further stimulate the regional sensory neural pathway involving the lower thoracic spinal cord that contains proenkephalin+ interneurons. On the contralateral side, the response of sensory neurons in L4-L6 DRGs releases ATP, which induces inflammatory mediators, including cytokines and chemokines, by activating the IL-6 amplifier in collagen type1+ non-immune cells, including fibroblasts and endothelial cells, through a ATP receptor, P2RX7.

Discussion:

It is known that spreading inflammation is common in RA. The present study clarifies the molecular link for spreading inflammation between bilateral ankle joints in cytokine-induced and CIA models. Cytokine injections into one ankle joint of F759 mice induce ATP release from non-immune cells and subsequently activate afferent sensory pathways with c-fos induction on both sides of L5 DRG toward the contralateral ankle joint through a proenkephalin+ interneuron network in the thoracic cords, suggesting that the inflammation signal from one side activates sensory neurons in both the ipsilateral and contralateral sides. A previous report showed that RA synovial fibroblasts (RASFs) are able to migrate and contribute to the spread of the disease between bilateral synovial tissues in SCID mice. Although the authors identified RASFs as one key factor for spreading inflammation from a single joint to multiple ones, how RASFs reach the other joints remains to be elucidated. The present study suggests that the local neural regulation for bilateral inflammation may trigger the initial inflammation and promotes the subsequent recruitment of RASFs by releasing chemokines via IL-6 amplifier. Thus, a regional sensory neuron-interneuron connection between the ankle joints through the thoracic spinal cord is critical for spreading inflammation via the bilateral expression of ATP, which activates a neural pathway and enhances the IL-6 amplifier.

Conclusion:

My doctoral study suggests that blockade of the sensory neuron-interneuron axis may be a therapeutic target for various inflammatory diseases including RA, in which inflammation spreads to remote positions.

Keywords

- Spreading inflammation
- IL-6 amplifier
- sensory neuron-interneuron interaction
- ATP

List of Abbreviation

Ach	Acetyl choline
ATP	Adenosine tri-phosphate
BBB	Blood brain barrier
bDMARD	biological disease modifying anti-Rheumatoid drugs
CCL20	C-C Motif Chemokine ligand 20
CD4	Cluster of Differentiation 4
CD8	Cluster of Differentiation 8
CGRPα	Calcitonin gene related peptide alpha
CIA	Collagen induced arthritis
CLCF1	cardiotrophin-like cytokine factor 1
CNS	Central Nervous System
CNTF	Ciliary Neurotrophic Factor
CT-1	cardiotrophin-1
DRG	Dorsal root ganglia
EAE	Experimental autoimmune encephalomyelitis
ERK	Extracellular-signal-regulated kinase
Gab	GRB associated binding protein
GP130	Glycoprotein 130
GWAS	Genome wide association study
HSV2	Herpes simplex virus 2
HTLV-1	Human T-cell leukemia virus
IFN-α	Interferon-alpha
IL-6	Interleukin-6
IL-11	Interleukin-11
IL-17A	Interleukin-17A
IL-27	Interleukin-27
IL-31	Interleukin-31
JAK	Janus Kinase signal transducer
LIF	Leukemia inhibitory factor
L5	Fifth lumbar cord
MAPK	Mitogen-activated protein kinases
MHC	Major Histocompatibility complex

MOG	Myelin oligodendrocyte glycoprotein
MS	Multiple Sclerosis
NA	Noradrenaline
NANC	non-noradrenergic, non-cholinergic transmitter
NF-κB	Nuclear Factor kappa-light-chain-enhancer of activated B cells
NO	Nitric oxide
OSM	Oncostatin M
PD1	Programmed cell death-1
RA	Rheumatoid arthritis
SNP	Single nucleotide polymorphism
Socs3	Suppressor Of Cytokine Signaling 3
STAT3	Signal Transducer and Activator of transcription 3
TCR	T cell receptor
TGF-β	Transforming Growth factor beta
Th1	T- helper 1
Th2	T-helper 2
Th17	T helper 17 cell
TNF-α	Tumor necrosis factor alpha
TRPV1	Transient Receptor Potential Cation Channel Subfamily V Member 1
TNFis	Tumor Necrosis Factor Inhibitors

1. Introduction

1-1. Rheumatoid arthritis (RA)

RA is chronic inflammatory disease **(Lefèvre et al., 2009)**, and affects 1% of the adult population worldwide. RA symptoms include chronic joint inflammation, synovial hypertrophy, and progressive destruction of cartilage and bone that lead to weakening of the joints, pain, and severe disability. The clinical symptoms, such as pain, difficulty to move, inflammation in the joints, negatively affect the patients' well-being and ability to work, and induce psychological stress **(Mausset-Bonnefont et al., 2019)**. One criterion for the diagnosis and a fundamental characteristic of RA is remote inflammation, which results in widespread and severe malformation and immobility on both sides of the joints **(Arnett et al., 1988; Clarke et al., 1994)**. Similar symptoms are also observed in other inflammatory diseases including psoriasis, pulmonary fibrosis, glomerulonephritis, and sympathetic ophthalmitis. Several studies have suggested that a neural mechanism is involved in these symptoms **(Kelly et al., 2007; Kidd et al., 1989; Shenker et al., 2003)**; however, the detailed molecular mechanism that links inflammatory and neural pathways has not been demonstrated. To this aim, animal models of RA are essential.

The collagen-induced arthritis (CIA) mouse model has been extensively studied, since it shares several pathological and immunological features with the human pathology, and allows testing innovative treatments in preclinical studies. In the CIA model, arthritis development and severity are assessed using a clinical scoring system based on peripheral joint swelling and redness **(Mausset-Bonnefont et al., 2019)**. However, it is still unknown how RA spread over different joints.

1-2. Interleukin-6 (IL-6)

IL-6, which was discovered in 1986, is a pleiotropic cytokine involved not only in immune responses but also in inflammation, hematopoiesis, bone metabolism, embryonic development, and other fundamental processes **(Hirano, 1998; Ishihara and Hirano, 2002)**.

IL-6 is a prototypical member of the IL-6 family of cytokines, which is composed of 10 members including IL-6, IL-11, IL-27, oncostatin M (OSM), leukemia inhibitory factor (LIF), ciliary neurotrophic factor (CNTF), cardiotrophin 1 (CT-1), cardiotrophin-like cytokine factor1

(CLCF1), IL-35 and IL-39 **(Murakami et al., 2019)**. Studies in the 1980s showed that IL-6 is produced by cardiac myxoma cells **(Hirano et al., 1987)** and Castleman's germinal center cells **(Yoshizaki et al., 1989**), and is present at high amounts in the synovial fluid of RA patient **(Hirano et al., 1988; Houssiau et al., 1988)**, suggesting its pathogenic role in autoimmune diseases and chronic inflammatory diseases **(Hirano, 1992; 1998)**.

IL-6 is a multifunctional cytokine with biological activities that include regulation of immune response, inflammation, and hematopoiesis. IL-6 also possesses several proinflammatory properties, such as stimulating the production of chemokines and adhesion molecules in lymphocytes, inducing acute-phase proteins in liver cells and increasing neutrophil counts in the blood **(Hashizume and Mihara, 2011)**.

1-3. Pathogenicity of IL-6 in RA development

IL-6 has been demonstrated as a pivotal cytokine in RA pathogenesis by contributing to perturbation of both innate and adaptive immune system **(Raimondo et al., 2017)**. Increased level of IL-6 is detected in the sera and synovial fluid of RA patients, which appears to be responsible for disease severity and progression **(Ogata et al., 2019)**. In concert with other pro-inflammatory mediators, IL-6 consequently promotes differentiation of B cells and T cells to antibody-secreting cells and IL-17-secreting T helper 17 (Th17) cells, respectively. IL-6 also stimulates endothelial cells to produce chemokines, which lead to recruitment of other immune cells at the site of inflammation **(Ogura et al., 2008)**. Moreover, IL-6 induces secretion of acute-phase proteins, such as C-reactive protein (CRP) in hepatocytes, activates fibroblast-like synoviocytes to produce IL-6 in the joint synovia, and induces autoantibody production from B-cells **(Biggioggero et al., 2019; Ogata et al., 2019; Raimondo et al., 2017)**. Synovial fibroblastic cells produce large amounts of IL-6, when stimulated by inflammatory cytokines such as IL-1, TNFα, and IL-17, and that IL-6 augments the proliferation of synovial fibroblastic cells in the presence of soluble IL-6R **(Hashizume and Mihara, 2011)**. As a pathogenic mechanism of bone destruction in RA, osteoclasts activated by inflammatory cytokines are responsible for focal bone erosion. Osteoclasts are often seen in the synovium at sites of cartilage destruction in RA patients. The receptor activator of NF- κB (RANK) and its ligand (RANKL) are essential factors for osteoclastogenesis. IL-6 and soluble IL-6R, induce RANKL expression in RA fibroblast-like synoviocytes (RAFLS). **(Hashizume and Mihara, 2011)**.

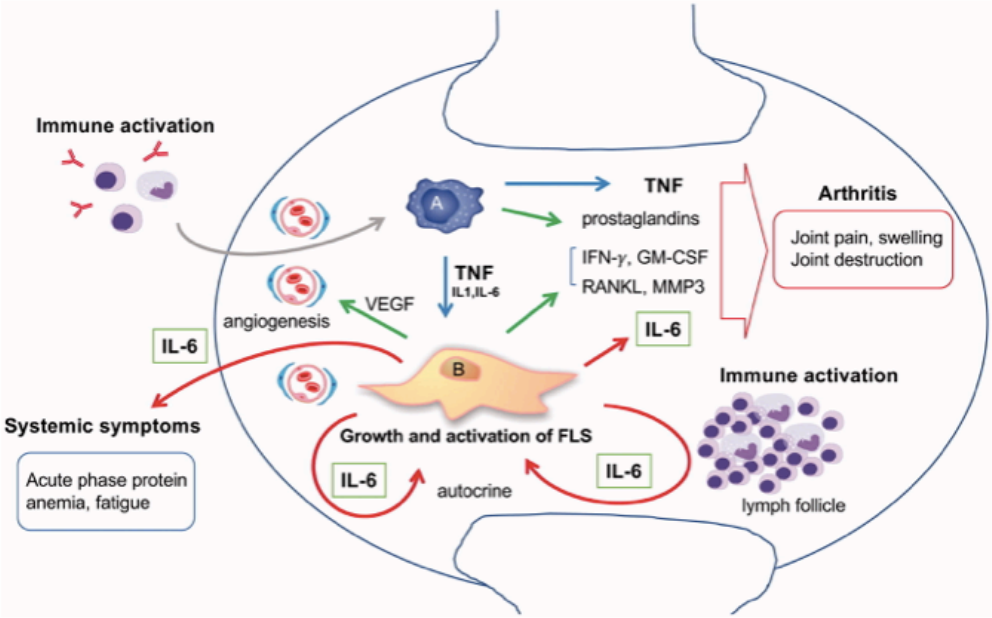

Fig. 1 Summary of pathogenic role of IL-6 in RA (Raimondo et al., 2017)

1-4. Anti-IL-6 receptor therapy in RA

IL-6 action is the result of interaction with IL-6 receptor (IL-6R), composed of a non-signaling-receptor subunit IL-6Rα existing as both soluble and membrane-bound (present only on T cells, hepatocytes, activated B cells, neutrophils, and macrophages); and two signal-transducing gp130 subunits, which transduce signal through Janus kinase (JAK)-signal transducer and the activator of the transcription (JAK-STAT) pathway. IL-6 may interact with membrane-bound subunit in a classical (*cis*-) signaling pathway, which activates acute-phase response, and is involved in metabolic effects, infection defense, and tissue regeneration. On the other hand, an interaction between complex IL-6/soluble IL-6R and gp130 subunits activates *trans*-signaling pathway in different cell types such as endothelial, smooth muscle, and neural cells, resulting in IL-6-mediated proinflammatory effects. Furthermore, the central role of IL-6 in a number of RA extra-articular manifestations and comorbidities has been definitely demonstrated. As an example, IL-6 interferes with several nervous functions, such as neuronal development and survival, synaptic plasticity, and central pain sensitization via stimulation of DRG in neuronal cells, which express gp130 subunits enabling IL-6 *trans*-signaling. Moreover, IL-6 can influence on hypothalamic-pituitary-adrenal axis, resulting in hypersecretion of adrenocorticotropic hormone without a reciprocal increase of cortisol. Those described effects on central nervous and endocrine systems suggest a direct role of IL-6 in generating/amplifying mood disorders and RA systemic symptoms such as pain and fatigue **(Raimondo *et al.*, 2017)**. As a result blocking the IL-6

activity through deteriorating the IL-6 pathway became the target for the new generation of RA drugs by creating IL-6R antagonists **(Raimondo *et al.*, 2017)**. The first IL-6R blocker to be introduced to the markets was tocilizumab, a humanized anti-IL-6R monoclonal antibody. The successful use of tocilizumab in RA has encouraged the development of other biological agents specifically targeting the IL-6 pathway, through attacking IL-6R as another IL-6R blocker,as sarilumab. Upon IL-6 stimulation, gp130 transduces two major signaling pathways: the JAK–STAT3 pathway, which is mediated by the YxxQ motif of gp130, and the SHP2–Gab-Ras-Erk–MAPK pathway, which is regulated by Y759, a cytoplasmic SOCS3 binding residue in gp130**(Fukada et al., 1996; Kamimura et al., 2003; Ohtani et al., 2000)**. Both tocilizumab and sarilumab are monoclonal antibodies that bind to both soluble and membrane-bound IL-6R, preventing the interaction of IL-6 with both the IL-6R and the signal transducer gp130 complex. The result is the inhibition of both the *cis*- and *trans*-signaling cascades involving the JAK-STAT pathway **(Narváez et al., 2021)**. However anti-IL-6R therapy cannot be used for all RA patients **(Nakagawa et al., 2010)**, and in about 30% of those patients as a result of serious adverse events, a decision of ceasing treatment has to be taken **(June and Olsen, 2016)**. This increases the need to further and deep understanding of the molecular and neuronal pathways that control the RA disease progression.

1-5. F759 knock-in mouse line

F759 knock-in mouse line (F759) that expresses a mutant variant of gp130, where tyrosine at 759^{th} position is substituted by phenyl alanine (F), those mice shows enhanced IL-6-mediated STAT3 activation due to a lack of SOCS3-mediated negative feedback of IL-6 signaling **(Ohtani *et al.*, 2000)**. As age increases, F759 mice spontaneously develop a RA-like disease in both sides of the ankle joints at around one year of age. Mechanistic analyses clarified that an enhanced IL-6 signal in type 1 collagen+ (Col1α)+ non-immune cells, but not in immune cells, is responsible for the development of F759 arthritis. Importantly, F759 arthritis was developed even in RAG-deficient F759 mice (**Sawa et al., 2006**), indicating that constitutive activation of IL-6 signaling in non-immune cells is involved in the development of autoimmune diseases **(Atsumi et al., 2002)**. F759 arthritis is also dependent on Th17 cells expressing IL-17A and IL-6 in a non-RAG-deficient background and the subsequent activation of the IL-6 amplifier in the affected joints by cytokines from activated CD4+ T cells **(Murakami et al., 2011; Ogura *et al.*, 2008)** Interestingly, ankle-joint injections of IL-17A and IL-6 in young F759 mice also caused an arthritic disease within two weeks, significantly facilitating

mechanistic analyses of the joint inflammation in vivo with a minimal effect by immune cells **(Atsumi et al., 2017; Harada et al., 2015; Meng et al., 2016; Murakami et al., 2013; Murakami *et al.*, 2011; Okuyama et al., 2018a; Ota et al., 2020; Tanaka et al., 2018)**. Thus, F759 mice are useful murine model for RA.

1-6. IL-6 amplifier

By using F759 mice, we discovered the IL-6 amplifier, which is a fundamental molecular mechanism of tissue-specific inflammation and enhances the activation of NF-κB in non-immune cells including synovial fibroblasts, endothelial cells, and chondrocytes, followed by regionally expressing excessive chemokines, cytokines, and growth factors in animal models and patients of RA and osteoarthritis (**Fig. 2) (Harada *et al.*, 2015; Murakami *et al.*, 2013; Murakami *et al.*, 2011; Ogura *et al.*, 2008; Okuyama et al., 2018b; Tanaka et al., 2017)** In this system, hyper-activation of the NF-κB signal is induced by the simultaneous stimulation of NF-κB and STAT3, followed by the local induction of inflammation **(Atsumi et al., 2014; Harada *et al.*, 2015; Lee et al., 2013; Murakami *et al.*, 2013; Murakami *et al.*, 2011; Ogura *et al.*, 2008)**Because one NF-κB target, IL-6, stimulates STAT3 during inflammation, its autocrine and/or paracrine action helps maintain STAT3 activation to express inflammatory mediators via the IL-6 amplifier in various inflammatory diseases **(Hirano and Murakami, 2020; Murakami *et al.*, 2019).** We further showed that the IL-6 amplifier plays a role in other tissue-specific inflammatory diseases in many organs including the skin, kidney, central nervous system (CNS), and lungs **(Arima et al., 2012; Arima et al., 2015b; Arima et al., 2017b; Fujita et al., 2019; Higuchi et al., 2020; Lee *et al.*, 2013; Murakami *et al.*, 2019; Stofkova et al., 2019)** Accordingly, we have defined inflammation as an IL-6-mediated accumulation of immune cells and/or proliferation of immune cells and regional non-immune cells, followed by the dysregulation of local homeostasis including the dysfunction of tissues and/or organs. It has been proposed that autoimmune diseases are caused by a break-down of self-tolerance due to multiple genetic and/or environmental factors, suggesting that the dysregulation of immune responses is fundamental for autoimmune diseases. This agrees with the theory that certain autoimmune diseases like RA, develop in specific tissues as a result of cognate antigen-recognition by CD4+ T cells, particularly, when these diseases are associated with class II major histocompatibility complex (MHC) alleles. Consistent with this, joint-specific antigen specific peptides such as derivatives of aggrecan, fibrillin, and collagen have been identified in humans **(Murakami and Hirano, 2011)**.

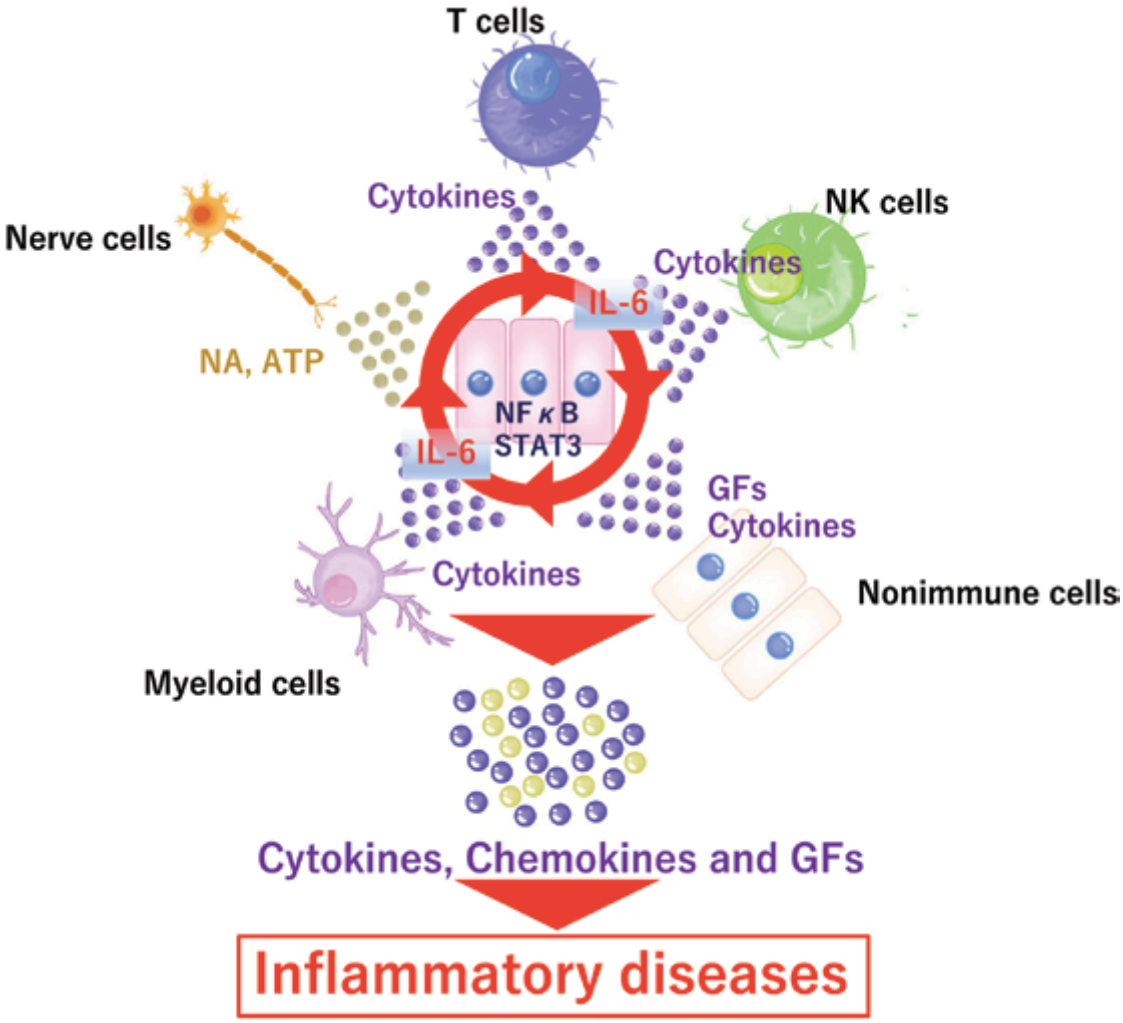

Fig. 2 The IL-6 amplifier. In non-immune cells, such as fibroblasts and endothelial cells, the simultaneous activation of NF-κB and STAT3 induces excessive NF-κB activation. Then, excess chemokines, growth factors (GFs) and IL-6 are locally produced. Eventually, local homeostasis is disturbed by the accumulation of immune cells as well as the growth of local non-immune cells, leading to inflammatory pathologies. IL-6 is one of only a few STAT3 stimulators in many inflammatory diseases **(Murakami et al., 2021)**.

1-7 Gateway reflex

We have reported five gateway reflexes, which are triggered by gravity, pain, stress, light, and artificial electric stimulation, respectively **(Fig. 3)**. Each gateway reflex regulates gateway in different sites of the CNS and retina during the development of tissue-specific inflammation. We identified several neural circuits that include ganglions, nuclei and different neurons and neurotransmitters. All gateways are established by the secretion of noradrenaline (NA) from the sympathetic pathway to activate the IL-6 amplifier at specific vessels.

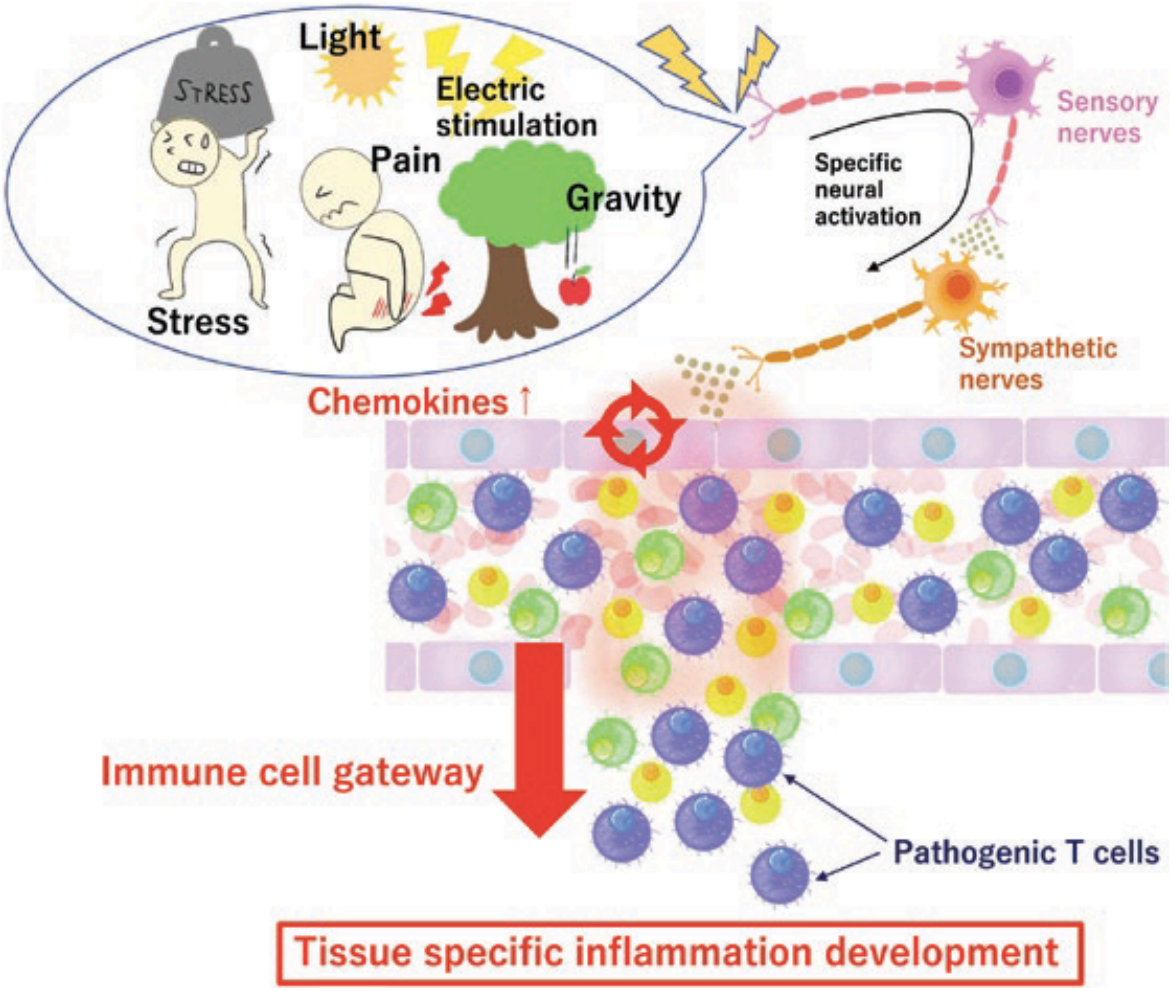

Fig. 3 The gateway reflexes. The activation of specific neural circuits by environmental stimuli as well as artificial electric stimulations on muscles results in the production of local neurotransmitters, such as NA, and increases chemokine expression at specific blood vessels via IL-6 amplifier activation. When CNS-specific or retina-specific autoreactive CD4+ T cells are present in the blood, they accumulate at gates in the CNS or retina, respectively, to disrupt the blood barriers and induce inflammatory diseases. Five types of gateway reflexes triggered by gravity, pain, stress, light or electric stimulation have been reported **(Uchida et al., 2021)**.

In 2017, we discovered the 2nd generation of the gateway reflex, named stress gateway reflex. Regarding the stress gateway reflex, gateway-mediated micro-inflammation in the brain activated a new neural pathway via ATP to dysregulate distant organs. It is well known that stress is involved in many diseases. We have identified a stress-related nerve circuit that causes gastrointestinal failure and sudden death in the presence of autoreactive T cells that migrate to the CNS from the blood **(Fig. 4; Arima et al., 2017)**. We employed transfer experimental autoimmune encephalomyelitis (EAE) mice under two stress conditions that have no obvious negative effect on the body: light sleep and wet bed environments. Severe gastrointestinal inflammation and heart failure were observed in mice with either stress in the presence of myelin-specific autoreactive T cells.

Mechanistically, the stress stimulation activated some noradrenergic neurons in the PVN, which projects to two specific blood vessels surrounded by the third ventricle, dentate gyrus and thalamus, establishing gateways for the autoreactive T cells (**Arima et al., 2017**). Considering that the dentate gyrus and PVN are stress-related brain regions **(Yun et al., 2018), (Moretto et al., 2017)**, it is reasonable that these blood vessels play a role in stress responses. We hypothesized that increased permeability in the absence of autoreactive T cells might suppress stress responses by activating neurons at the vessels to activate neurons in the dorsomedial hypothalamic nucleus (DMH)/anterior hypothalamic part (AHP). Consistently, some neurons in the DMH reduce the activation of PVN neurons to reduce the stress responses **(Stotz-Potter et al., 1996; Vetrugno et al., 1993)**

In the stress gateway reflex **(Fig. 4)**, PVN-derived noradrenergic neurons upregulate chemokine expression including CCL5 at the blood vessels in a manner dependent on nor-adrenaline mediated IL-6 amplifier activation at the vessels, thus recruiting autoreactive T cells and MHC class II+ monocytes from the blood, followed by the activation of autoreactive T cells via antigen presentation. Cytokines expressed by the autoreactive T cells accelerated the IL-6 amplifier in endothelial cells and triggered microinflammation at the blood vessels **(Arima et al., 2017)**.

ATP is a neurotransmitter and is expressed in several cells after cytokine stimulation **(Burnstock, 2006)**. ATP produced by the microinflammation locally functioned as a neurotransmitter. ATP directly activated neurons in the DMH/AHP followed by activating

neurons in the dorsal motor nucleus of vagal nerve (DMX) **(Arima et al., 2017**). The activation of the efferent vagus nerve projected from the DMX yielded severe gastrointestinal inflammation via massive ACh secretion, followed by hyperkalemia with sudden death **(Uchida *et al.*, 2021)**.

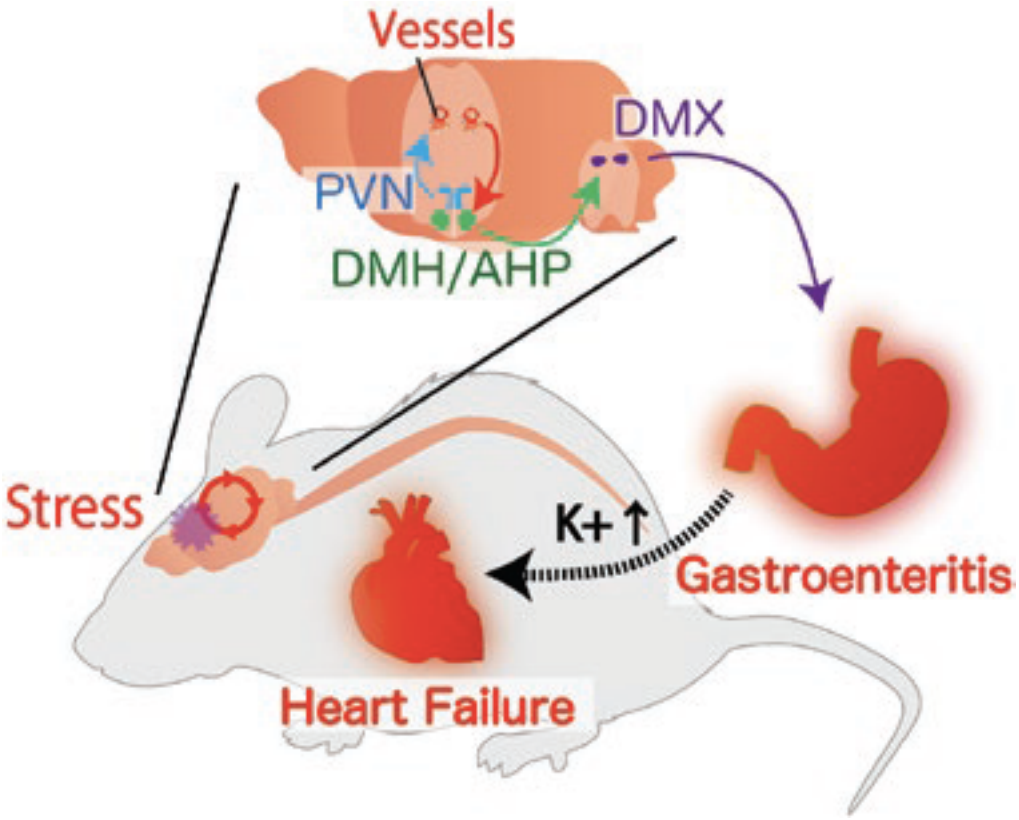

Fig. 4 The stress gateway reflex. Chronic stresses including light sleep induce the activation of noradrenergic neurons in the PVN followed by the establishment of gateways for immune cells at specific blood vessels in the brain, particularly in the presence of myelin specific CD4+ T cells in the blood. Myelin-specific CD4+ T cells accumulate at the specific vessels together with MHC class II+ monocytes to develop micro-inflammation there. ATP produced by the microinflammation functions as a neurotransmitter to directly activate neurons in the DMH/AHP, followed by the hyper-activation of neurons of the DMX, especially projecting to the stomach and the upper level of the intestine. The resulting activated efferent vagus nerve causes gastrointestinal inflammation in a manner dependent on ACh followed by hyperkalemia with heart failure and sudden death. (**Uchida et al., 2021**)

Therefore, we assume that gateways can be artificially controlled to open and close at specific vessel sites. Thus, the concept of the gateway reflex might resemble neuromodulation medicine,

which treats diseases by artificially controlling neural circuits. For this purpose, it is critical to identify neural circuits of the whole body and clarify nerve–vessel relationships. Elucidating these relationships may lead to novel therapeutic strategies for inflammatory diseases mediated by NF- κB targets including IL-6 and chemokines in response. During the gateway reflexes, the IL-6 amplifier at the specific vessels is activated by noradrenaline produced by specific sympathetic activation via some environmental or artificial stimuli. Autoreactive T cells at the gateway produce other cytokines such as IL-17 and TNF-α, which along with IL-6 stimulate NF- κB and STAT3 in regional non-immune cells, resulting in more chemokine and IL-6 production to breach the blood barriers. Thus, gateway reflexes are associated with the local neural regulation of autoimmune responses.

1-8 Hypothesis and Objectives

One criterion for the diagnosis and a fundamental characteristic of RA is remote inflammation, which results in widespread and severe malformation and immobility at both sides of the joints **(Arnett et al., 1988; Clarke et al., 1994)**. Similar symptoms are also observed in other inflammatory diseases including psoriasis, pulmonary fibrosis, glomerulonephritis, and sympathetic ophthalmitis. Although several studies suggest that a neural pathway may be involved in these symptoms **(Kelly et al., 2007; Kidd et al., 1989; Shenker et al., 2003)**, the detailed mechanism has not been demonstrated. In my doctoral research, I aimed to clarify the underlying molecular mechanism that links inflammatory and neural pathways for spreading inflammation.

2. Materials and Methods

2-1. Mouse strains

C57BL/6 mice were purchased from Japan SLC (Shizuoka, Japan). F759 mice were backcrossed with C57BL/6 mice for more than 10 generations. Adult (8–10 weeks of age) male mice were used in all experiments. Type I collagen-Cre mice were provided by Dr. G. Karsenty (Baylor College of Medicine, Houston, TX) and were crossed with $STAT3^{flox/flox}$ mice (provided by Dr. S. Akira, Osaka University, Japan) **(Takeda et al., 1998)** and $IKK\gamma^{flox/flox}$ mice **(Schmidt-Supprian et al., 2000)**. NFκB-reporter transgenic mice in a C57BL/6 background were also backcrossed with F759 mice and used **(Sadikot and Blackwell, 2008)**. All mice were maintained under specific pathogen-free conditions according to the protocols of Osaka University Medical School. All animal experiments were performed following the guidelines of the Institutional Animal Care and Use Committees of the Graduate School of Frontier Biosciences and Graduate School of Medicine, Osaka University, and the Institute for Genetic Medicine, Hokkaido University. The protocols for animal experiments were approved by the Institutional Animal Care and Use Committees of the Graduate School of Frontier Biosciences and Graduate School of Medicine, Osaka University, and Hokkaido University.
We used Sham operated mice as a control mice in all experiments.

2-2. Antibodies and Reagents

The following antibodies were used for staining: anti-c-Fos rabbit polyclonal antibodies (Abcam, product no. ab190289), anti-Nav1.8 rabbit polyclonal antibodies (a gift from Dr. Watanabe), anti-phosphorylated-c-fos (Ser32) rabbit monoclonal antibody (D82C12) (Cell Signaling Technologies, no. 5368S), anti-HSV2 rabbit whole antisera (Novus Biologicals, no. NB120-9534), anti-pro-enkephalin guinea pig polyclonal antibodies (a gift from Dr. M. Watanabe), anti-TRPV1 guinea pig polyclonal antibodies (a gift from Dr. M. Watanabe), anti-calretinin chicken polyclonal antibodies (Encor Biotechnology, no. CPCA-Calret),anti-phosphorylated STAT3 (Tyr705) Rabbit monoclonal antibody (D3A7) (Cell Signaling Technologies, no. 9145), anti-vimentin (Abcam, no. ab92547), anti-phosphorylated NF-κB p65 ($pSer^{276}$) rabbit polyclonal antibodies (Sigma-Aldrich, no. SAB4504488), anti-P2RX7 goat polyclonal antibodies (Abcam, no. ab93354), anti-mouse CD31 rat monoclonal antibody (BD Pharmingen, no. 550274), Alexa Fluor 647 labeled anti-phosphorylated CREB (Ser133) rabbit monoclonal antibody (clone 87G3, Cell Signaling Technologies, no. 14001S), Alexa Fluor 546

donkey anti-rabbit IgG (H+L)(Thermo Fisher Scientific, no. A10040), Alexa Fluor 488 donkey anti-rabbit IgG (H+L)(Thermo Fisher Scientific, no. A21206), Alexa Fluor 555 donkey anti-rabbit IgG (H+L) (Thermo Fisher Scientific, no. A31572), Alexa Fluor 488 donkey anti-goat IgG (H+L)(Thermo Fisher Scientific, no. A11055), Alexa Fluor 647 goat anti-chicken IgG (H+L) (Thermo Fisher Scientific, no. A21449), Alexa Fluor 488 donkey anti-guinea pig IgG (H+L) (Jackson ImmunoResearch, no. 756-545-148), and Alexa Fluor 555 donkey anti-rat IgG (H+L) (Abcam, no. ab150154). VECTASTAIN Elite ABC Kit Peroxidase (Rabbit IgG) and ImmPACT DAB Substrate Kit Peroxidase were purchased from Vector Laboratories. The following antibodies were used for in vivo neutralization: anti-mouse IL-17 Ab (R &D Systems, no. MAB421) and anti-IL-6R Ab (Chugai Pharmaceutical Co.). Mouse IL-17A was purchased from Peprotech. Human soluble IL-6Rα was purchased from R&D systems. Human IL-6 was obtained from Toray Industries. A438079 hydrochloride (no. 2972), A803467 (no. 2976), and IKK 16 (no. 2539) were purchased from Tocris Bioscience. Fluoro Gold (FG) was purchased from Fluorochrome (no. 52-9400), and ATP from Sigma-Aldrich (no. A6559). ATP Measuring Reagent Kit was purchased from TOYO Ink (no. LL100-1), Bradykinin EIA Kit (Human, Rat, Mouse) (no. EK-009-01) and CGRP EIA Kit (Rat, Mouse)(no. EK-015-09) from Phoenix Pharmaceuticals, Human IL-6 ELISA Set (no. 555220) from BD Biosciences, IL-17 mouse ELISA (no. BMS6001) from Thermo Fisher Scientific, LEGEND MAX Human IL-6 ELISA Kit (no. 430507) from BioLegend, Luciferase reporter assay system (no. E1500) from Promega, and Norepinephrine EIA Kit (no. VA-10-0200) from LDN. Alexa Fluor-488- (no. C22841) and Alexa Fluor-555- (no. C22843) conjugated Cholera Toxin B subunit, and Zenon Rabbit IgG Labeling Kit, Alexa Fluor 488 (no. Z25302) and Alexa fluor 555 (no. Z25305) were purchased from Thermo Fisher Scientific.

2-3. Joint injections

IL-6, IL-17A, ATP, A803467, A438079, FG, HSV2 (ATCC), Alexa Fluor labeled CTB, anti-mouse IL-17 antibody, and anti-IL-6R antibody were injected into the ankle and knee joints of mice after washing extensively with saline and then injected into the joints of mice.

2-4. Clinical assessment of cytokine-induced arthritis

F759 mice injected with IL-6 and IL-17A were assessed for signs of arthritis as described previously (Atsumi *et al.*, 2017; Harada *et al.*, 2015; Meng *et al.*, 2016; Murakami *et al.*, 2013; Murakami *et al.*, 2011). Briefly, the severity of the arthritis was based on two bilaterally assessed parameters: (1) swelling of the ankle and (2) restricted mobility of the ankle joints.

The severity of each parameter was graded on a scale of 0–3, where 0 indicates no change; 1, mild change; 2, medium change; and 3, severe change. Averages for a single point in one leg ankle joint from each mouse were used.

2-5. Deafferentation

Deafferentation was conducted as described previously (**Kawano et al., 2007**). Briefly, a skin incision was made along the vertebra between the thoracic-to-sacral level, the left dorsal root of the spinal cord at the L4-5 segmental levels or L4-6 segment levels was exposed, and the afferent fibers between the spinal cord and DRGs at L5 or L4-L6 were transected. Mice in the sham-operated control group had their left DRGs and roots exposed, but the nerve supply was kept intact. The contralateral side was kept intact for all mice. Fourteen days of ambulation were allowed after the surgery.

2-6. Partial sciatic nerve ligation

Partial sciatic nerve ligation (Seltzer model) was performed as described previously **(Malmberg and Basbaum, 1998; Seltzer et al., 1990)**. Briefly, a skin incision was made on the hip, and the sciatic nerve was exposed and ligated with 6-0 PGA suture (Akiyama, Tokyo) around approximately 1/3 to 1/2 the diameter of the nerve. In sham-operated mice, the nerve was exposed but not ligated.

2-7. Real-time PCR

Total RNA was prepared from L5 DRG using sepasol-RNA I (Nacalai Tesque), chloroform (Sigma-Aldrich), and isopropanol (Sigma-Aldrich) or prepared from ankle joint tissue using a GenElute Mammalian Total RNA Kit (Sigma-Aldrich). The RNA was then treated with DNase I (Sigma-Aldrich) and used for reverse transcription with M-MLV reverse transcriptase (Promega) using an Oligo(dT)18 primer. The cDNA product was used in each real-time PCR reaction. Genomic DNA was prepared from L5 DRG and mouse ankle joints injected with HSV2 using the alcohol precipitation carrier Ethachinmate (Nippon Gene) and isopropanol.
A 7300 Fast Real-Time PCR system and PROBE qPCR Master Mix (KAPA Biosystems) were used to quantify the levels of c-fos and HPRT mRNA and HSV2 DNA. The TaqMan PCR primer pairs were as follows:

Table 1. Primers and probes

Gene	Sequence	
Mouse *Hprt*	Forward	5'- AGCCCCAAAATGGTTAAGGTTG -3'
(TAMURA)	Reverse	5'- CAAGGGCATATCCAACAACAAAC -3'
	Probe	5'- GATCCAACAAAGTCTGGCCTGTATCCAACAC -3'
Mouse *fos*	Forward	5'- CCTTCTCCAGCATGGGCTC -3'
(TAMURA)	Reverse	5'- CGTGGGGATAAAGTTGGCACTA -3'
	Probe	5'- GTGTCAACACAGGACTTTTGCGCAGAT -3'
HSV2	Forward	5'- CGCATCAAGACCACCTCCTC -3'
(TAMURA)	Reverse	5'- GCTCGCACCACGCGA -3'
	Probe	5'- GCGGCGATGCGCCCCAG -3'

The conditions for TaqMan real-time PCR were 40 cycles at 95 °C for 3 s followed by 40 cycles at 60 °C for 30 s. The relative mRNA expression levels were normalized to the levels of HPRT mRNA. The relative HSV2 DNA replication levels were normalized to the levels of genomic DNA quantity.

A 7300 Fast Real-Time PCR system (Applied Biosystems) and SYBR green qPCR Master Mix (KAPA Biosystems) were used to quantify the levels of IL-6, CCL2, CCL3, CCL21, CXCL2, and HPRT mRNA.

The PCR primer pairs were as follows:

Table 2. Primers and probes

Gene	Sequence	
Mouse *Hprt*	Forward	5'- GATTAGCGATGATGAACCAGGTT -3'
	Reverse	5'- CCTCCCATCTCCTTCATGACA -3'
Mouse *Il6*	Forward	5'- GAGGATACCACTCCCAACAGACC -3'
	Reverse	5'- AAGTGCATCATCGTTGTTCATACA -3'
Mouse *Ccl2*	Forward	5'- CCGGCTGGAGCATCCACGTGT -3'
	Reverse	5'- TGGGGTCAGCACAGACCTCTCTCT -3'

Mouse *Ccl21*	Forward	5'- GGGTCAGGACTGC TGCCTTA -3'
	Reverse	5'- CGGGATGGGACAGCCTAAA -3'
Mouse *Cxcl2*	Forward	5'- CGCTGTCAATGCCTGAAGAC -3’
	Reverse	5'- ACACTCAAGCTCTGGATGTTCTTG -3’

The conditions for real-time PCR were 40 cycles at 94 °C for 15 s followed by 40 cycles at 60 °C for 60 s.

The relative mRNA expression levels were normalized to the levels of HPRT mRNA.

2-8. Frozen and Paraffin Embedded Section Preparations and Immunohistochemistry

Spines and ankle joints were harvested, and spinal cord segments were separated. Individual spinal cord segments and ankle joints were embedded in a SCEM compound (SECTION-LAB, Hiroshima). The cut surface was covered with adhesive film (Cryofilm type IIIC (16UF), SECTION-LAB), and frozen sections (10 to 20 μm) were prepared with a cryostat (CM3050S) or a macrotome (CM3600XP, Leica Microsystems, Germany) according to a method described previously (Kawamoto and Kawamoto, 2014). For paraffin embedded sections, ankle joints were harvested, fixed with 10% phosphate buffered formalin, and embedded in paraffin. The resulting sections were stained with the antibodies described above and counterstained with Hoechst 33342 (Invitrogen, Tokyo), followed by analysis with a BZ-9000 microscope (KEYENCE, Osaka) or LSM980 (Carl Zeiss, Germany).

2-9. Quantification of immunostaining

The phosphorylated c-fos+ areas were measured using Image J (Wayne Rasband, NIH). Colocalization was measured using the Coloc module of Imaris software (Bitplane).

2-10. Spinal cord cut

A skin incision was made along the vertebra at the thoracic level, and muscle on the spine was removed. The spinal cord was exposed and cut lengthwise at the T9-13 levels. Mice in the sham-operated control group had the muscle on the spine removed, but the spinal cord was kept intact.

2-11. Luciferase reporter Assay

Ankle joints from NF-κB-reporter Tg/F759 mice were collected, and synovial tissues were homogenized in passive lysis buffer (Promega, Tokyo). After centrifugation, the supernatants

were collected, and the total protein amount was adjusted using the Bradford assay. The luciferase activities of tissue lysates were measured using the Luciferase reporter assay system (Promega, Tokyo).

2-12. ATP assay

Ankle joints from individual mice were collected and soaked in 10 mL of distilled water containing 10 mM HEPES-NaOH and 250 mM sucrose for 30 min. After 10 min of 3000 rpm centrifugation at 4°C, the supernatants were collected. The levels of ATP were determined with a luciferin-luciferase assay using an ATP Measuring Reagent Kit (TOYO Ink, Tokyo) according to the manufacturer's instructions, except that the homogenization step was omitted.

2-13. ELISA

IL-6 levels in the cell culture supernatant and mouse sera were determined using ELISA kits (BD Biosciences, Tokyo). The levels of norepinephrine, CGRP, bradykinin, and substance P in mouse ankle joints were determined using ELISA kits (LDN, Nordhorn, Germany; Phoenix Pharmaceuticals, Burlingame, CA; or R&D systems, Tokyo). The level of neuropeptide Y in the mouse ankle joint was determined using ELISA kits (EMD Millipore Corporation, U.S.A.). Human IL-6 and mouse IL-17 levels in the sera were determined using ELISA kits (Biolegend and eBioscience, respectively).

2-14. Cells and stimulation conditions

The type 1 collagen+ endothelial BC1 cell line (**Murakami *et al.*, 2013**) was obtained from Dr. M. Miyasaka (Osaka University). W26 synovial fibroblasts were prepared as described previously (**Igarashi et al., 2010**). For stimulation, the cells were plated in 96-well plates (1×10^4 cells/well) and stimulated with human IL-6 (50 ng/mL; Toray Industries) plus human soluble IL-6Rα (50 ng/mL; R&D Systems), mouse IL-17A (50 ng/mL; R&D Systems), and/or ATP (100 μM; Sigma-Aldrich) for 24 h. The cell culture supernatant was collected for ELISA, and cell growth was assessed by the MTT assay (see below).

2-15. MTT assay

Cell growth was determined with thiazolyl blue tetrazolium bromide according to the manufacturer's instructions (Sigma-Aldrich, Tokyo)

2-16. Collagen-induced arthritis

CIA was induced in C57BL/6 mice essentially as previously described **(Kitabayashi et al., 2010; Sasai et al., 1999)**. Mice were injected intradermally in their backs with 200 μg of chicken type II collagen (Sigma-Aldrich) plus 250 μg of Mycobacterium bovis Bacillus Calmette-Guerin cell wall skeleton (BCG-CWS) emulsified in CFA. Three weeks after the initial injection, a booster injection containing 200 μg of chicken type II collagen plus 250 μg of BCG-CWS emulsified in CFA was given intradermally in the base of the tail. Clinical arthritis activity was evaluated every 2 or 3 days after the second immunization for 21 days. Arthritis severity in the metacarpophalangeal, metatarsophalangeal, and ankle joints was scored using the following scale: 0 = no arthritis, 1 = small degree of arthritis, 2 = mild swelling, 3 = moderate swelling, and 4 = severe swelling. The arthritic score was the sum of the scores from the involved joints in the hind limb.

2-17. Brain microinjection

The head of an anesthetized mouse was fixed in a stereotaxic device. The fur above the skull was shaved, the skin was cleaned with 70% ethanol, and a small incision was made. A 30-gauge needle was slowly lowered toward the ACC (AP 0.7 mm; ML 0.3 mm; VD 1.75 mm), and MK801 was injected as described previously (3 μg/μL delivered as 0.5 μL over 90 s) (Arima et al., 2015a; Kim et al., 2011).

2-18. Statistical analysis

The Student’s t-test (two-tailed) or Welch’s t-test was used for the statistical analyses of differences between two groups. Dunnett's test was used for multiple comparisons. The Wilcoxon rank-sum test was used for the statistical analyses of the clinical scores of the arthritis models. Statistical analysis was performed assuming a normal distribution. P values less than 0.05 are considered statistically significant.

3. Results

3-1. Sensory neurons are critical for spreading inflammation between joints

We previously established cytokine-induced and nonimmune cell-triggered arthritis in F759 mice by ankle-joint injections of IL-17A and IL-6 **(Atsumi *et al.*, 2017; Harada *et al.*, 2015; Meng *et al.*, 2016; Murakami *et al.*, 2013; Murakami *et al.*, 2011; Okuyama *et al.*, 2018a; Ota *et al.*, 2020; Tanaka *et al.*, 2018)**. Histological analysis showed that the synovial cavity is narrowed by hypertrophic synovial fibroblasts and that immune cells accumulate in the cytokine-injected ankle joint (Murakami et al., 2011) **(Fig. 5)**.

One advantage of this model is that inflammation can be induced both uni- and bilaterally, which enables us to investigate spreading inflammation from one ankle joint to the other and its molecular mechanism. Inflammation in each joint can be similarly induced even when cytokines are injected in either the left or right ankle joint (data not shown). Because we hypothesized that spreading inflammation might depend on neural pathways distributed on both sides, we performed deafferentation of the sensory neurons at one side of the dorsal root ganglions (DRGs) beside the fifth lumbar cord (L5) to investigate whether the sensory pathway is involved in the development of the arthritis in both ankle joints. We then injected IL-17A and IL-6 into both ankle joints of F759 mice. The deafferentation of sensory neurons at one side of the L5 DRG reduced the development of arthritis in both ankles **(Fig. 6, A and B)**. We then investigated whether inflammation on one side triggers the development of inflammation on the other side. We injected cytokines or saline into the left ankle and investigated the regional cell status in the right ankle joint. We found that CD11b+MHC class II+ cells were increased, while T cells were not present 10 days after the cytokine injection **(Fig. 7)**, suggesting that resident myeloid cells were activated. To investigate cytokine-induced arthritis development in the contralateral joint, we injected cytokines or saline into the left ankle and a small concentration of cytokines into the right ankle in both groups. The clinical scores of the right ankle joint were significantly enhanced by the IL-17A and IL-6 injections in the left ankle joint **(Fig. 8)**. These results suggested that neural pathways, most likely sensory pathways between the ankle joints, are involved in the development of the bilateral joint inflammation of the cytokine-induced arthritis.

We next examined neural activation after inducing inflammation in one ankle joint. Injections of IL-17A and IL-6 induced the expression of c-fos, which is an indicator of neural activation, in ipsilateral L5 DRG, but not ipsilateral L3, L4 or L6 DRG **(Fig. 9)**. On the other hand, c-fos expression was broadly induced in contralateral L4-L6 DRGs, but not L3 DRG **(Fig. 10)**, suggesting that the neural activation induced in the ankle joint transduced through ipsilateral L5 DRG and contralateral L4-L6 DRGs. The direct neural connection between the ankle joint and DRG was confirmed by detecting a retrograde neural tracer, Fluoro-Gold (FG), which was injected into the right ankle joint. We found that 90.9% of FG+ cells were neurons positive for Nav1.8 but negative for TRPV1. Nav1.8 and TRPV1 double positive cells were 9.1% of FG+ cells in the L5 DRG **(Fig. 11)**. Consistent with these results, activated c-fos+ sensory neurons were Nav1.8+TRPV1- or Nav1.8+TRPV1+ in the contralateral L5 DRG after cytokine injection **(Fig. 12, A and B)**. These results suggest that ankle joint inflammation on one side induced Nav1.8+TRPV1- sensory activation in the ipsilateral L5 DRG, and the neural signal subsequently traveled to Nav1.8+TRPV1+/- sensory neurons on the contralateral side to L4-L6 DRGs. Thus, we demonstrated that a sensory neural pathway is involved in bilateral ankle joint inflammation.

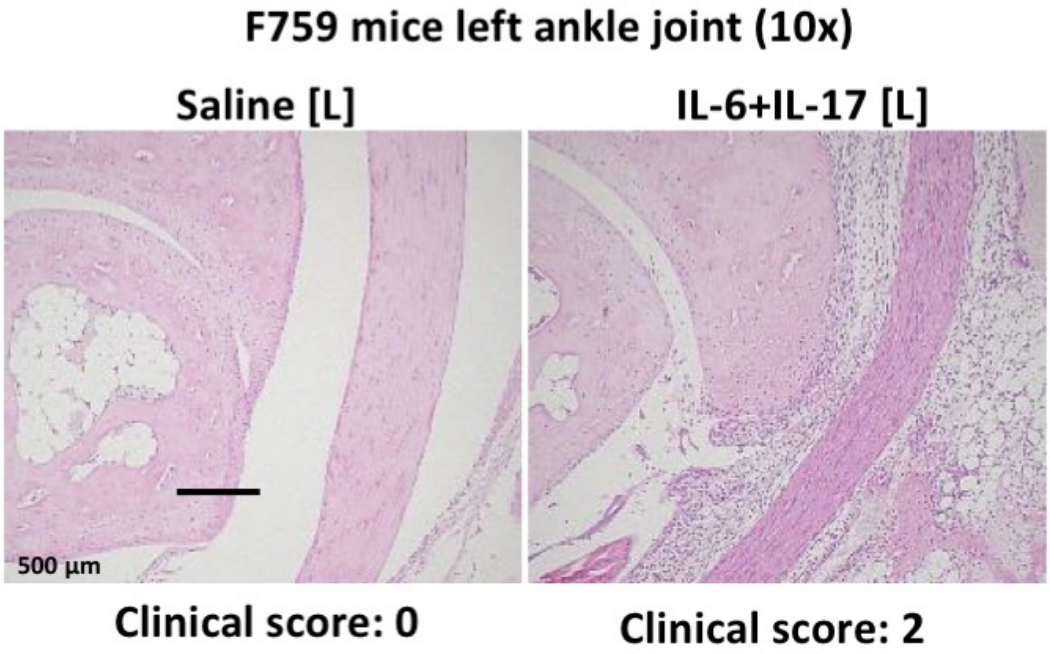

Fig. 5 Histological analysis of the left ankle joint of F759 mice on day 7 with saline or cytokine injections (IL-17A and IL-6 (0.1 µg each)) on days 0, 1, and 2. Experiments were performed at least three times independently; representative data are shown.

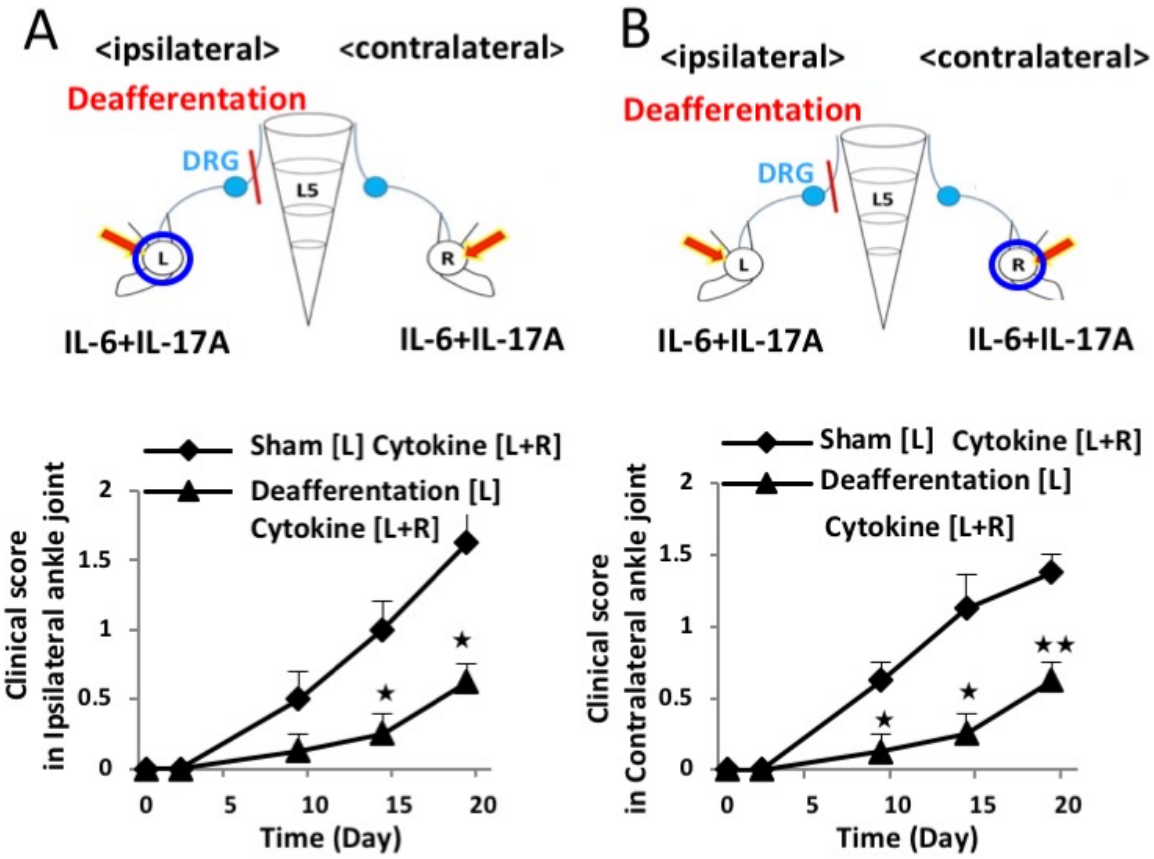

Fig. 6 Clinical arthritis scores of the left (A) and right (B) ankles of F759 mice deafferented or sham-operated at L5 DRG of the left side. IL-17A and IL-6 (0.1 μg each) were injected into both ankles on days 0, 1, and 2 (n = 4 per group). Mean scores ± SEM are shown. *P* values were calculated using Student's t-tests (★, $P < 0.05$; ★★, $P < 0.01$). Diagrams depicted illustrate the experimental settings. L, left ankle; L5, fifth lumbar vertebral level; DRG, dorsal root ganglion; R, right ankle. Arrows indicate cytokine or saline injection, and blue circles indicate the ankle joint assessed for arthritis.

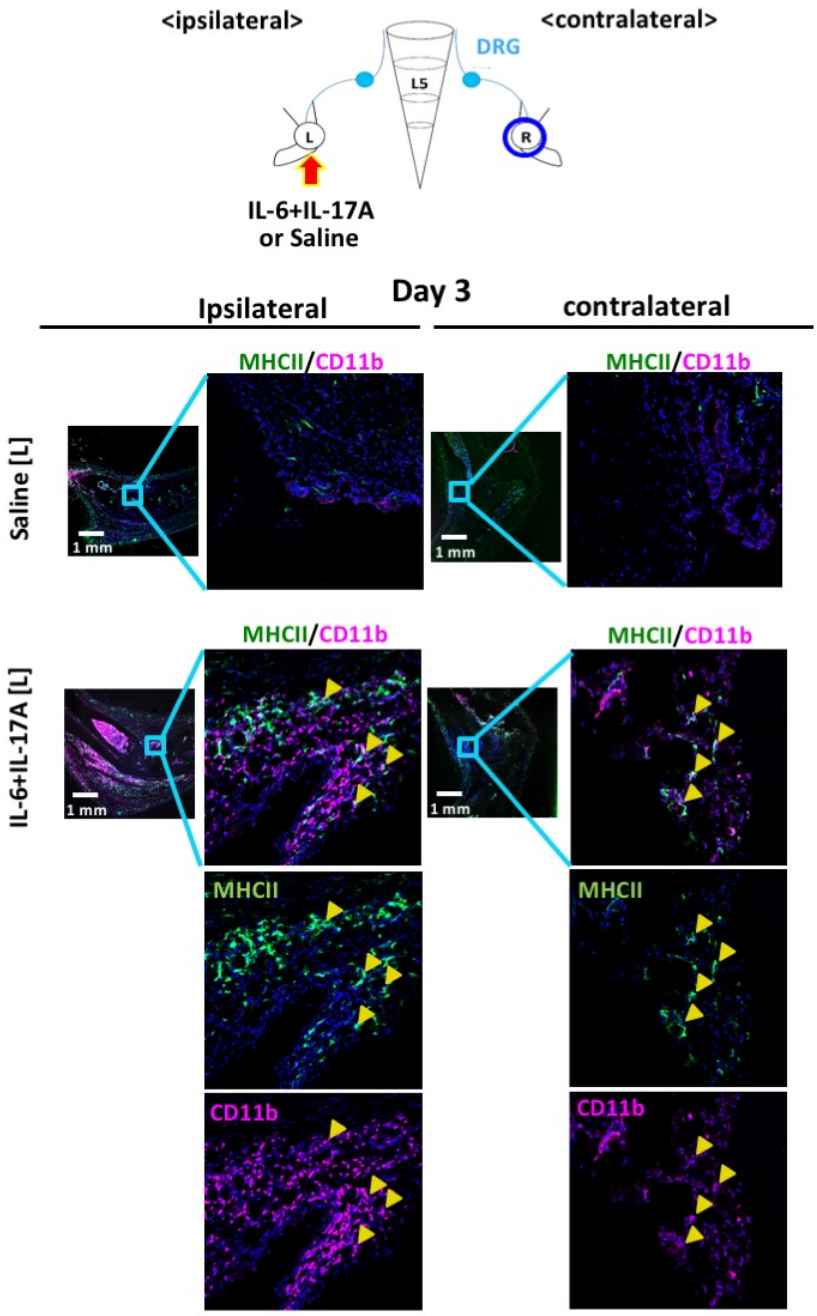

Fig. 7 CD11b+MHCII+ cells in the ankle joints of F759 mice on day 3 after IL-17A and IL-6 or saline injections. IL-17A and IL-6 or saline (1 μg each) were injected in the left ankle joint on day 0, 1, and 2 (n=2 per group). Green, MHC II. Magenta, CD11b. Blue, nuclei. Bar, 50 μm. Arrow heads show CD11b+MHCII+ cells Diagram depicted illustrates the experimental setting. L, left ankle; L5, fifth lumbar vertebral level; DRG, dorsal root ganglion; R, right ankle. Arrow indicates cytokine or saline injection, and blue circle indicates the ankle joint assessed.

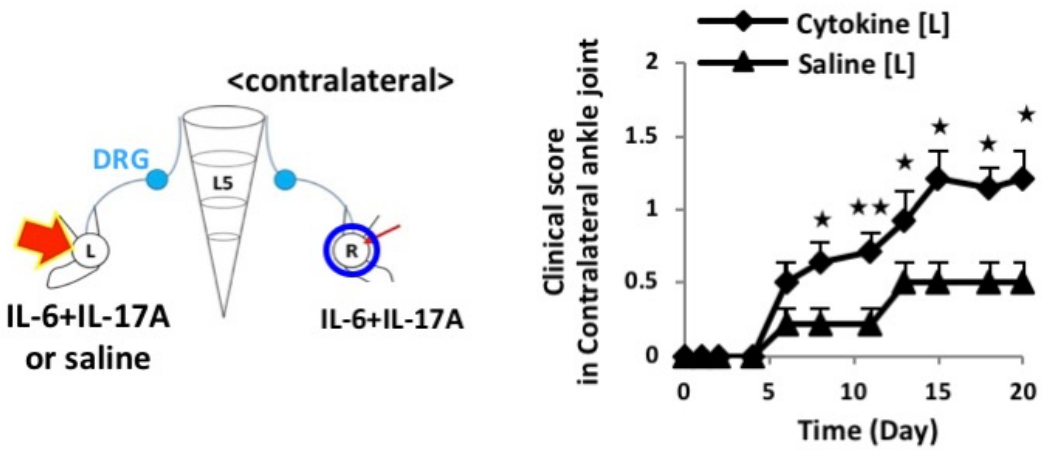

Fig. 8 Clinical arthritis scores of the right ankle joint of F759 mice after IL-17A and IL-6 injections at a low dose (0.01 μg each) in the right ankle joint and high dose (1 μg each) or saline injection in the left ankle joint on days 0, 1, and 2 (n = 14 per group). Mean scores ± SEM are shown. *P* values were calculated using the Wilcoxon rank-sum test (★, $P < 0.05$). Diagram depicted to the left of the graphs illustrates the experimental setting. L, left ankle; L5, fifth lumbar vertebral level; DRG, dorsal root ganglion; R, right ankle. Arrow indicates cytokine or saline injection, and blue circle indicates the ankle joint assessed for arthritis

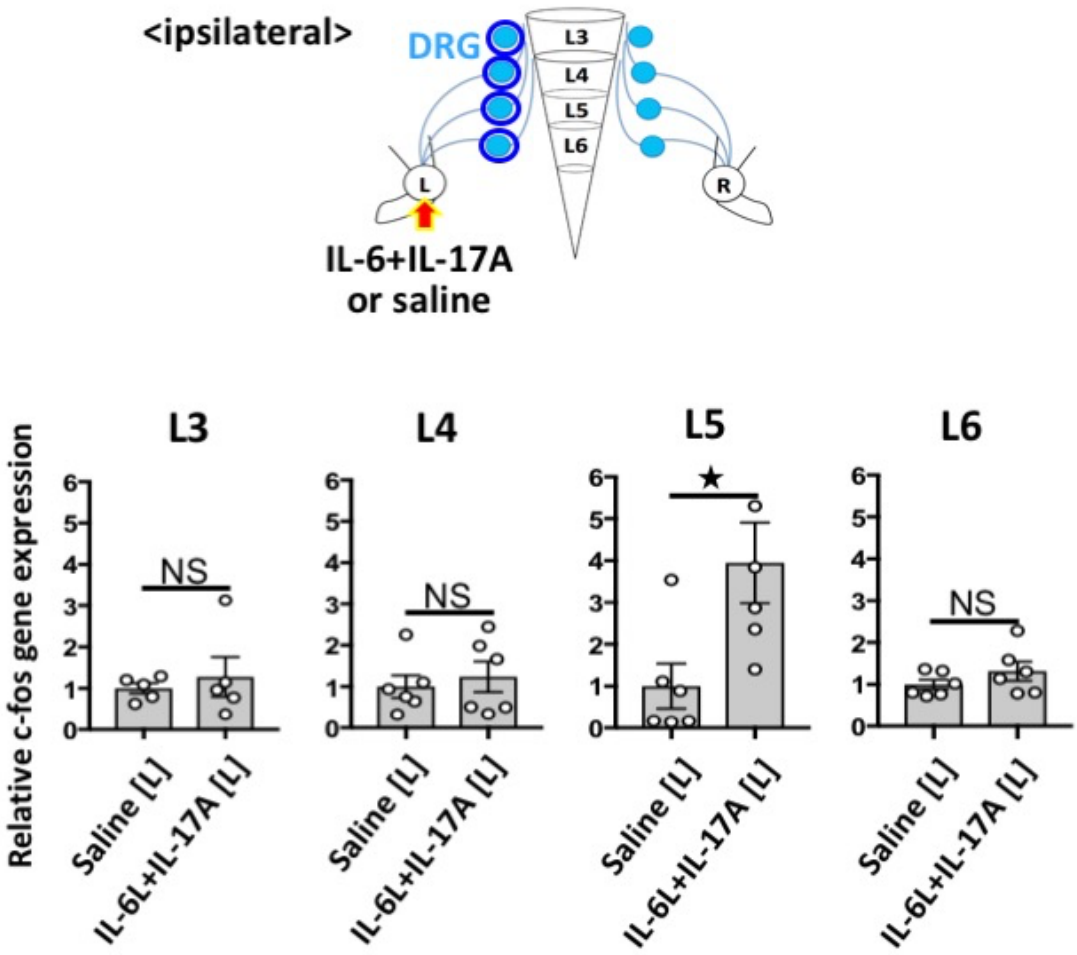

Fig. 9 IL-17A and IL-6 (1 μg each) or saline were injected into the left ankle joint on days 0, 1, and 2. c-fos expression in ipsilateral L3, L4, L5, and L6 DRGs on day 3 using real-time PCR (n = 5-6 per group). Mean scores ± SEM are shown. *P* values were calculated using Student's t-tests (★, $P < 0.05$; NS, not significant). Diagram depicted above illustrates the experimental setting. L, left ankle; L3-6, third to fifth lumbar vertebral levels; DRG, dorsal root ganglion; R, right ankle. Arrow indicates cytokine or saline injection, and blue circles indicate the DRG examined.

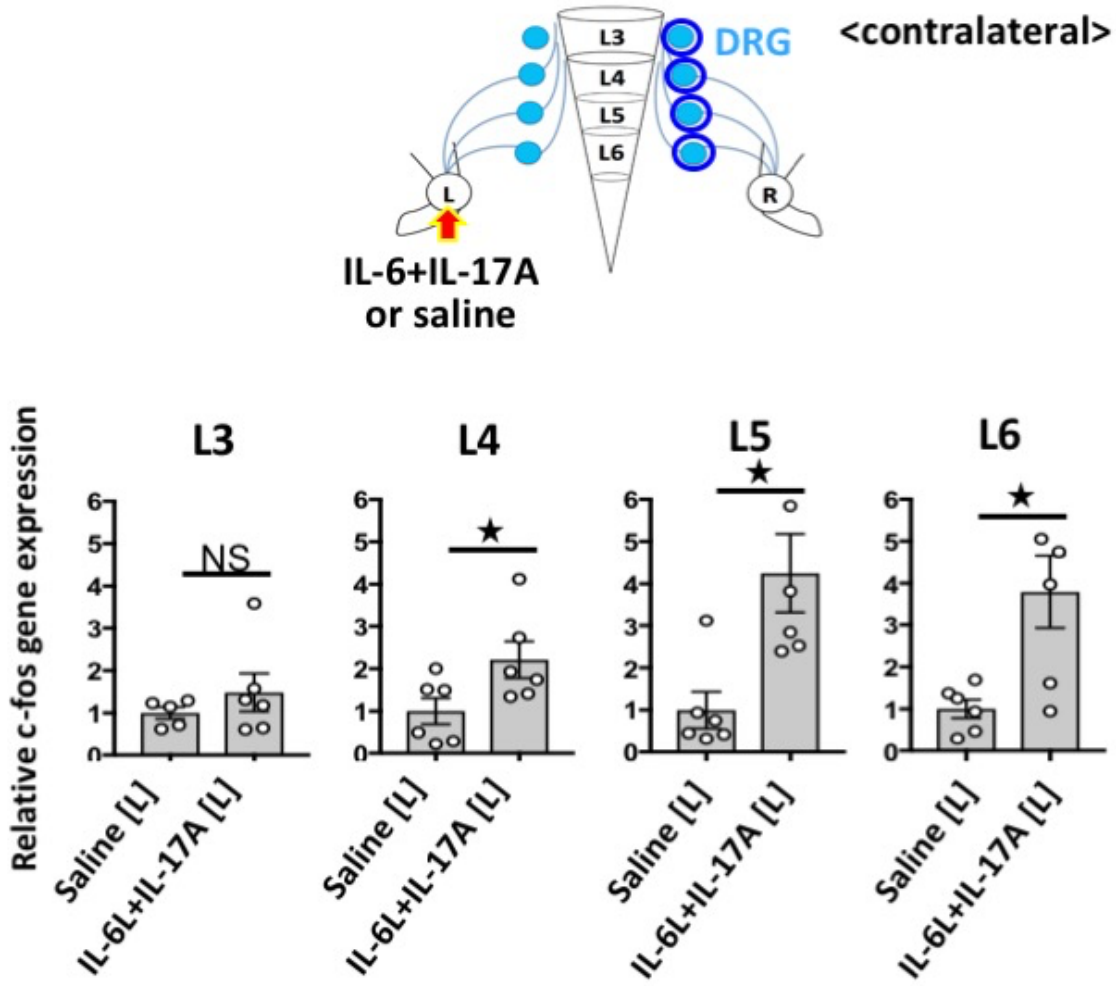

Fig. 10 IL-17A and IL-6 (1 μg each) or saline were injected into the left ankle joint on days 0, 1, and 2. c-fos expression in contralateral L3, L4, L5, and L6 DRGs on day 3 using real-time PCR (n = 5-6 per group). Mean scores ± SEM are shown. *P* values were calculated using Student's t-tests (★, $P < 0.05$; NS, not significant). Diagram depicted above illustrates the experimental setting. L, left ankle; L3-6, third to fifth lumbar vertebral levels; DRG, dorsal root ganglion; R, right ankle. Arrow indicates cytokine or saline injection, and blue circles indicate the DRG examined.

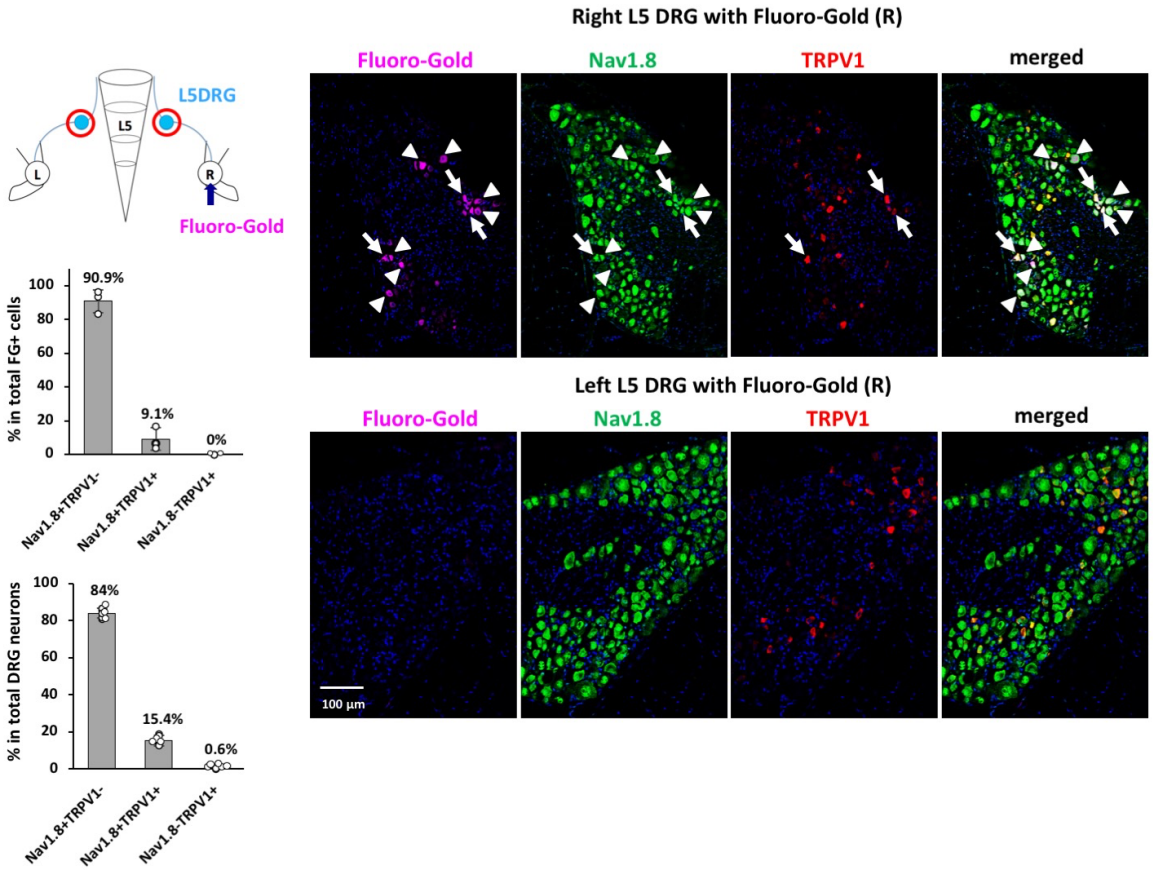

Fig. 11 Fluoro-Gold was injected into the right ankle joint of F759 mice, followed by the detection of Fluoro-Gold and staining of Nav1.8 and TRPV1 in the ipsilateral (right, R) and contralateral (left, L) L5 DRG on day 7. The number of FG+ cells, Nav1.8+TRPV1-, Nav1.8+TRPV1+, and Nav1.8-TRPV1+ cells was counted (n = 3 for the upper graph, n=6 for the lower graph). The upper graph shows the percentage of FG+ cells in the total number of Nav1.8+TRPV1-, Nav1.8+TRPV1+, and Nav1.8-TRPV1+ cells. The lower graph shows the percentage of Nav1.8+TRPV1-, Nav1.8+TRPV1+, and Nav1.8-TRPV1+ cells in the total number of DRG neurons. Data represent the mean ± SD. Magenta, Fluoro-Gold. Green, Nav1.8. Red, TRPV1. Blue, Nuclei. Bar, 100 µm. Diagram illustrates the experimental setting. L, left ankle; L5, fifth lumbar vertebral level; DRG, dorsal root ganglion; R, right ankle. Arrow indicates Fluoro-Gold injection, and the red circles indicate the L5 DRGs examined.

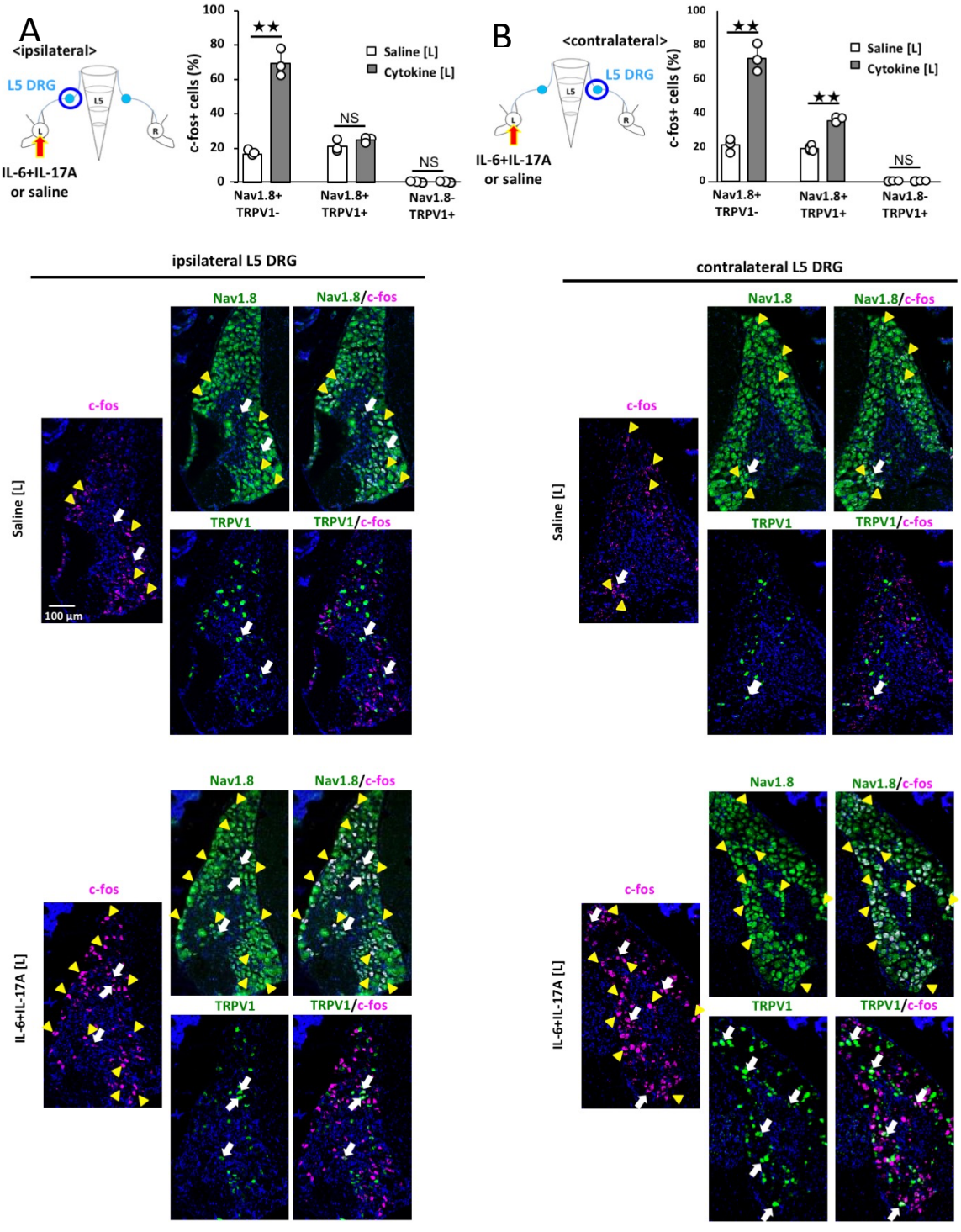

Fig. 12 IL-17A and IL-6 (1 μg each) or saline were injected into the left ankle joint on days 0, 1, and 2, followed by staining of c-fos, Nav1.8, and TRPV1 in the ipsilateral (A) or contralateral (B) L5 DRG on day 3. (Bottom) Magenta, c-fos. Green, Nav1.8 or TRPV1. Blue, nuclei.

Yellow arrowheads show c-fos+Nav1.8+TRPV1- neurons. White arrows show c-fos+Nav1.8+TRPV1+ neurons. The number of c-fos+, Nav1.8+TRPV1-. Nav1.8+TRPV1+, and Nav1.8-TRPV1+ was counted (n = 3 per group). Bar graphs shows the percentage of c-fos+ cells in the total number of Nav1.8+TRPV1-, Nav1.8+TRPV1+, and Nav1.8-TRPV1+ neurons, respectively. Bar, 100 μm. Mean scores ± SEM are shown. *P* values were calculated using Student's t-tests (★★, $P < 0.01$; NS, not significant).

3-2. Proenkephalin+ interneurons in the spinal cord connect to sensory neurons between the joints, forming a critical network for the spreading inflammation

To investigate the neural networks in spinal cord that connect sensory pathways between the ankle joints, we employed herpes simplex virus 2 (HSV2) to trace neural connections regardless of the presence of synapses(**Norgren and Lehman, 1998; Turner and Jenkins, 1997**). We injected HSV2 into one side of the ankle joint. HSV2 was present in the injected side of L5 DRG on day 4 **(Fig. 13A)** reached the dorsal horn of L5 on day 5 **(Fig. 13B)**, and was detected on the same side of the thoracic cords (T13) by day 7 **(Fig. 13C)**. It was then detected on the contralateral right side of T10-T13 by day 10 **(Fig. 13D)** and in the contralateral DRGs (L4-6) on day 14 after virus injection ((**Fig. 13E)** and data not shown). These HSV2 tracing experiments were confirmed by quantitative PCR **(Fig. 14)**. Thus, we confirmed a neural connection between bilateral ankle joints, at least through the left and right DRGs and lower thoracic cords. Because HSV2 was present on both sides of the thoracic cords at T10-T13, we examined the presence of interneurons connected to sensory pathways between the ankle joints through the DRGs. We performed a lengthwise spinal cord cut in the lower level of the thoracic cords (T9-13) and rested the mice 14 days for recovery from the surgical operation, followed by the induction of inflammation in one ankle joint. The injections of IL-17A and IL-6 induced the expression of c-fos in contralateral L5 DRG in sham-operated mice, but negligible changes in c-fos expression in contralateral L5 DRG were observed in mice that underwent a lengthwise spinal cord cut **(Fig. 15)**, suggesting the importance of T9-13 interneurons for spreading inflammation between joints.

We then investigated activated neurons in the spinal cord after cytokine injection in one side of the ankle joints. Phosphorylated-c-fos+ activated neurons were present mainly in the injected side of the L5 dorsal horn 15 min after the cytokine injection, and the activated neurons increased in both sides at 30 min **(Fig. 16)**. Some neurons around the central canal of the L5 cord were also activated 15 to 30 min after the cytokine injection (**Fig. 16A)**. Interestingly, we found activated neurons mainly on the injected side of the T13 dorsal horn but not in T11-T12, L1-L4, or L6 15 min and 30 min after the cytokine injection (**Fig. 16B** and data not shown). Additionally, neurons around the central canal of the T10 cord were activated 30 min after the cytokine injection (**Fig. 16C)**. These results suggested that the neural pathway related to spreading inflammation is a sensory neuron-interneuron connection between the ankle joints.

To investigate markers of the interneurons involved in spreading inflammation, we employed antibodies against several interneuron markers including proenkephalin and calretinin [35]. We found that most activated c-fos+ neurons in L5 and T13 expressed proenkephalin but not calretinin 15 min after cytokine injection in the ipsilateral ankle joint **(Fig. 17, A and B)**. These results suggest that proenkephalin+ interneurons in the spinal cord connect to sensory neurons between the joints, forming a critical network for the spreading inflammation.

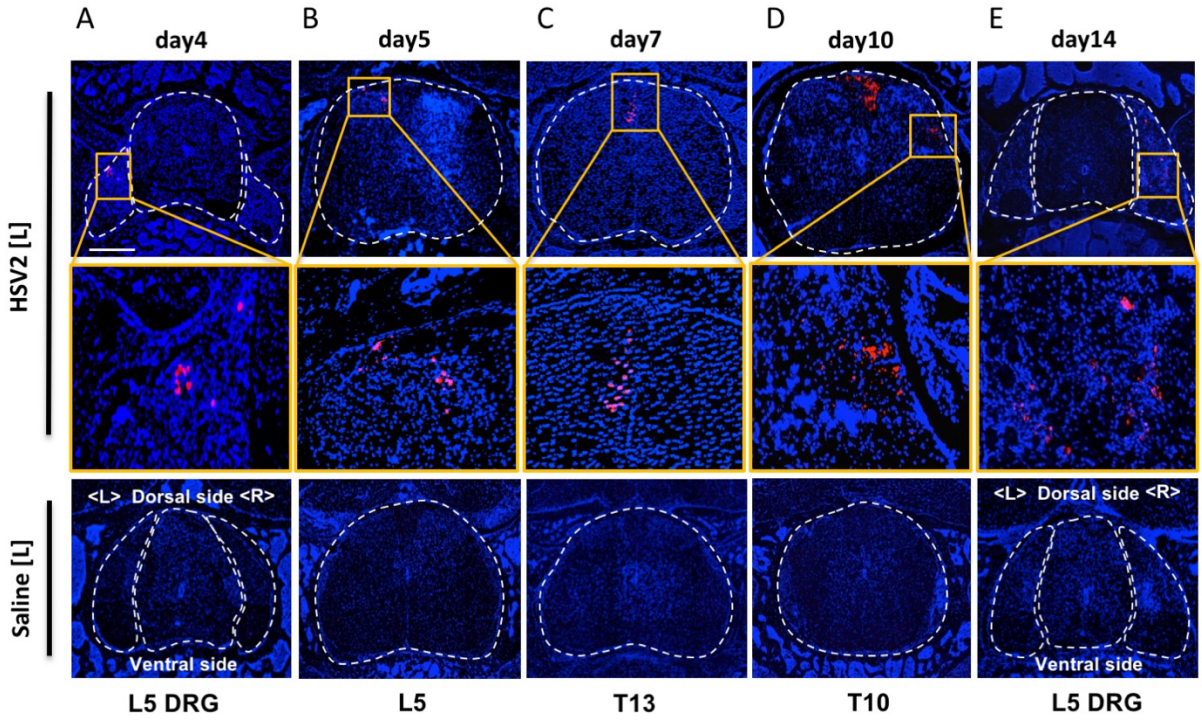

Fig. 13 (A-E) HSV2 (4.5×10^5 pfu) or saline was injected into the left ankle joint of F759 mice, followed by the staining of HSV2 in the spinal cord and DRG at L5 on day 4 (A), L5 on day 5 (B), T13 on day 7 (C), T10 on day 10 (D), and L5 DRG on day 14 (E). Nuclear staining by Hoechst 33342 is shown in blue. Broken lines outline the spinal cord and DRG. Magnified images in the orange boxes are shown in the middle row. Sections from control F759 mice given saline injection are shown in the bottom. Experiments were performed at least three times independently; representative data are shown.

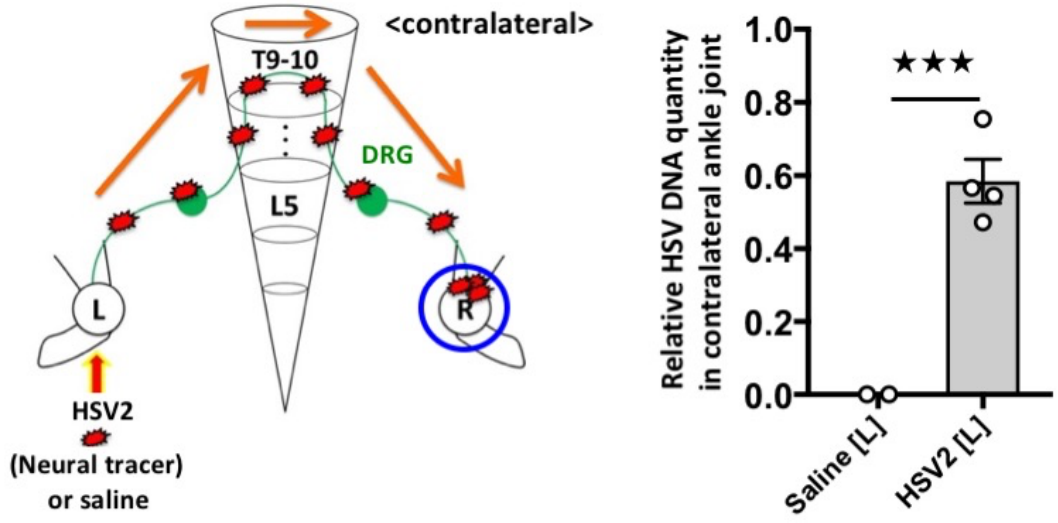

Fig. 14 HSV2 (4.5×10^5 pfu) or saline was injected into the left ankle joints of F759 mice on day 0, followed by the detection of HSV2 DNA in the contralateral (right) ankle joint on day 20 by real-time PCR (n = 2-4 per group). Mean scores ± SEM are shown. *P* values were calculated using Student's t-tests (★★★, $P < 0.001$). Diagram illustrates the experimental setting. L, left ankle; L5, fifth lumbar vertebral level; T9-T13, ninth to thirteenth thoracic cord; DRG, dorsal root ganglion; R, right ankle. Arrow indicates HSV2 injection. Blue circle indicate the ankle examined.

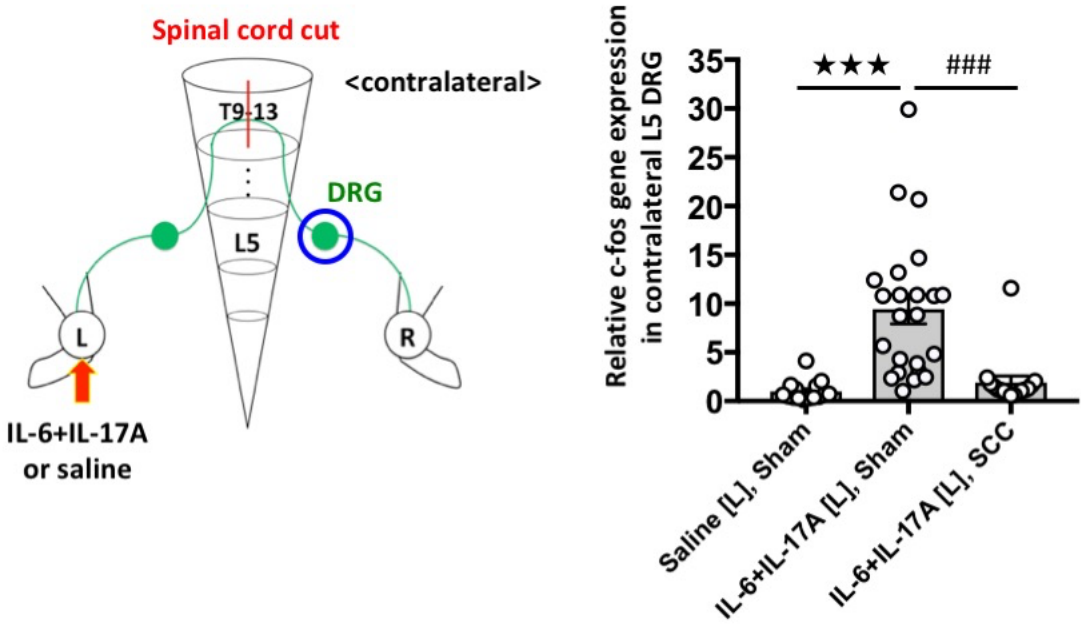

Fig. 15 c-fos expression of the right L5 DRG in F759 mice who underwent a spinal cord cut (SCC, T9-T13) or sham operation. IL-17A and IL-6 (1 μg each) or saline were injected into the left ankle on days 0, 1, and 2, and c-fos expression was examined by real-time PCR on day 3 (n = 15-23 per group). Mean scores ± SEM are shown. *P* values were calculated using Dunnett's test (★★★ and ###, $P < 0.001$). Diagram illustrates the experimental setting. L, left ankle; L5, fifth lumbar vertebral level; T9-T13, ninth to thirteenth thoracic cord; DRG, dorsal root ganglion; R, right ankle. Arrow indicates cytokine or saline injection. Blue circle indicates the DRG examined.

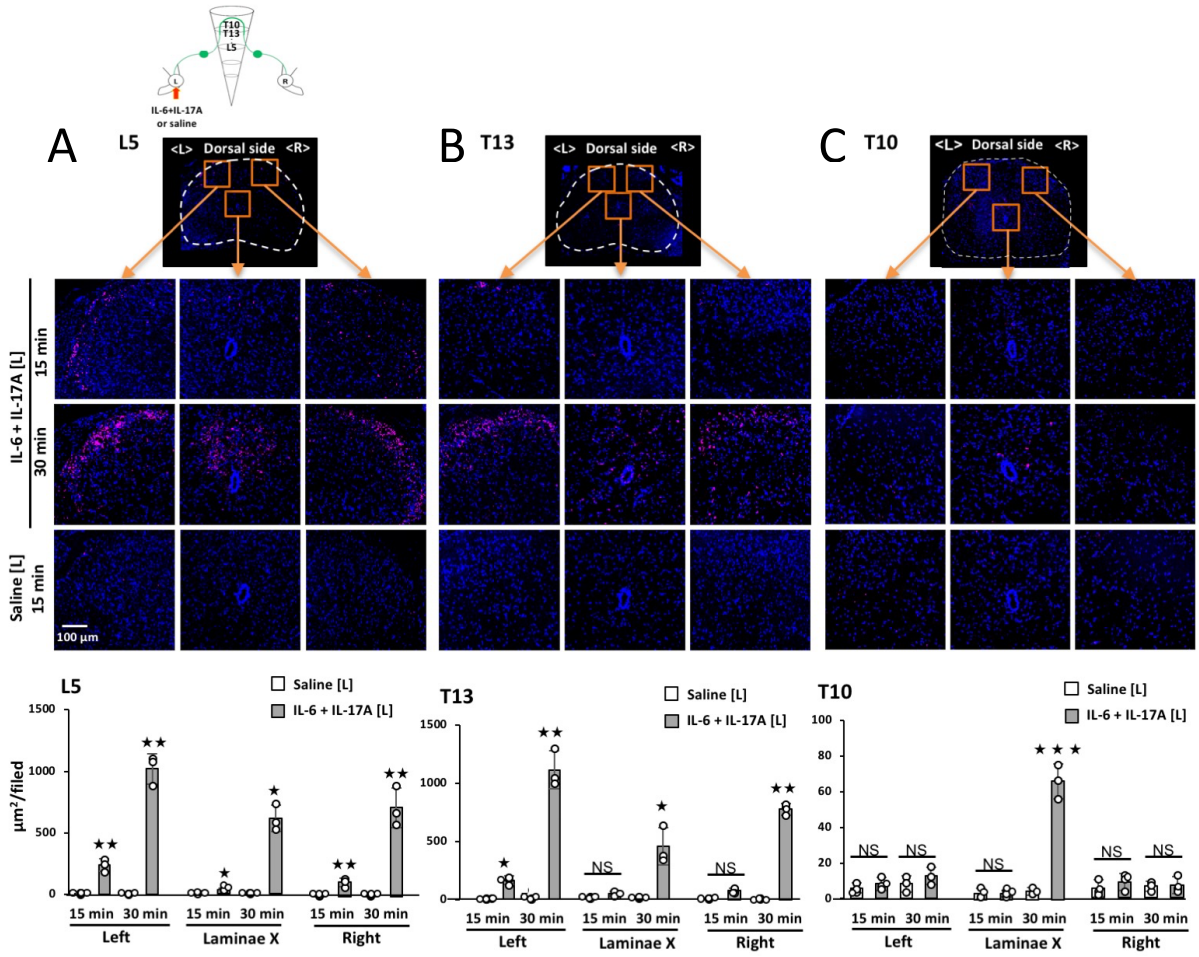

Fig. 16 IL-17A and IL-6 (1 μg each) or saline were injected into the left ankle joint of F759 mice on day 0, followed by the analysis of phosphorylated c-fos expression in (A) the L5 spinal cord, (B) T13 spinal cord, and T10 spinal cord 15 min or 30 min after the last injection. Magenta, phosphorylated-c-fos, Blue, nuclei. Bars, 100 μm. Phosphorylated c-fos positive areas per field (225,625 μm^2) were quantified (n=3 per group). Experiments were performed three times independently; representative data are shown. Mean scores ± SEM are shown. *P* values were calculated using Student's t-test (A, B) or Welch's t-test (C) (★ $P < 0.05$; ★★ $P < 0.01$; ★★★ $P < 0.001$; NS, not significant). Diagram illustrates the experimental setting. L, left ankle; L5, fifth lumbar spinal cord; T13, thirteenth thoracic spinal cord; T10, tenth thoracic spinal cord; DRG, dorsal root ganglion; R, right ankle. Arrow indicates cytokine or saline injection.

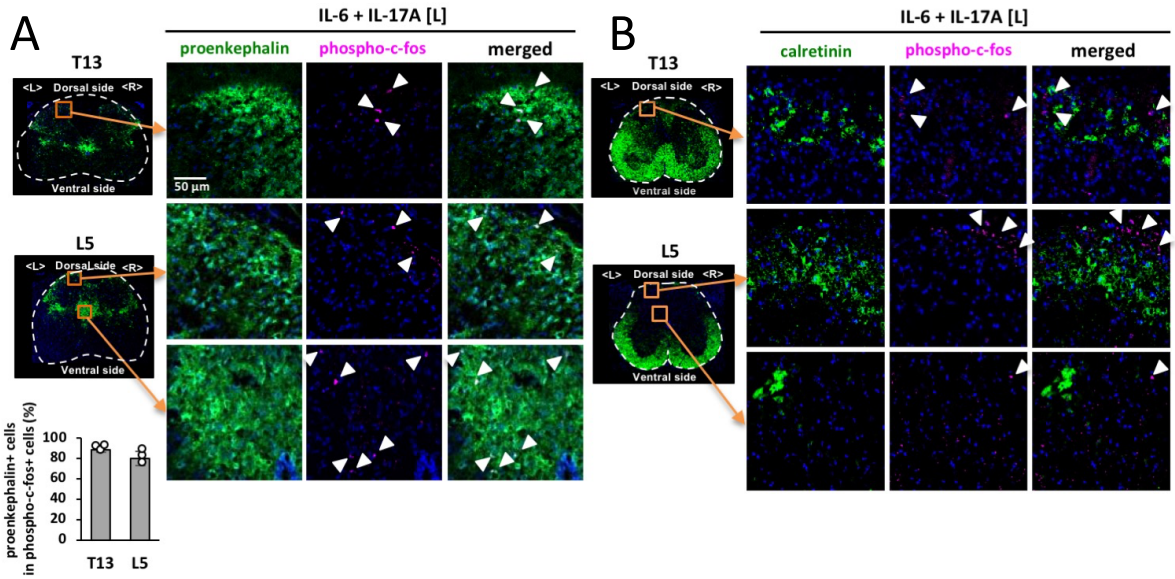

Fig. 17 IL-17A and IL-6 (1 μg each) or saline were injected into the left ankle joint of F759 mice on day 0, followed by the analysis of phosphorylated c-fos and (A) proenkephalin or (B) calretinin expression in the L5 and T13 spinal cord 15 min after the last injection. Green, proenkephalin (A) or calretinin (B). Magenta, phosphorylated c-fos. Blue, nuclei. Bar, 50 μm. Arrowheads show phosphorylated c-fos signals. Experiments were performed three times independently; representative data are shown.

3-3. Ipsilateral ankle joint inflammation increased ATP in the contralateral ankle joint to trigger remote inflammation development

We then investigated neurotransmitter levels in the contralateral ankle joint. Many neurotransmitters are believed to be related to arthritis pathogenesis. For example, extracellular ATP is increased in the synovial fluid of RA patients **(Peirs et al., 2015)**, and norepinephrine (NE) production from synovial TH+ cells has been correlated with the severity of inflammation in RA patients (**Miller et al., 2002)**. Substance P, CGRP, and bradykinin play a role in the development of arthritis models. Additionally, neuropeptide Y is reported to increase in synovial fluid from the joints of RA patients **(Grassel, 2014; Larsson et al., 1991; O'Connor et al., 2004; Xie et al., 2014)**. Among these neurotransmitters, only ATP was increased in the contralateral ankle joint after inflammation induction in the ipsilateral joint **(Fig. 18)**. Consistently, ATP synthase expression was increased in Nav1.8+ neurons in the contralateral ankle joint by IL-17A and IL-6 stimulation **(Fig. 19)**. Additionally, NF-κB activation and IL-6 and CCL2 expressions in the contralateral ankle joint were suppressed by the injection of A438079 in the same joint **(Fig. 20)** (**Donnelly-Roberts et al., 2009; McGaraughty et al., 2007**). Finally, the injection of A438079 into the contralateral ankle joint suppressed arthritis development **(Fig. 21)**. These results strongly suggest inflammation in the ipsilateral ankle joint increases ATP to induce arthritis in the contralateral ankle joint.

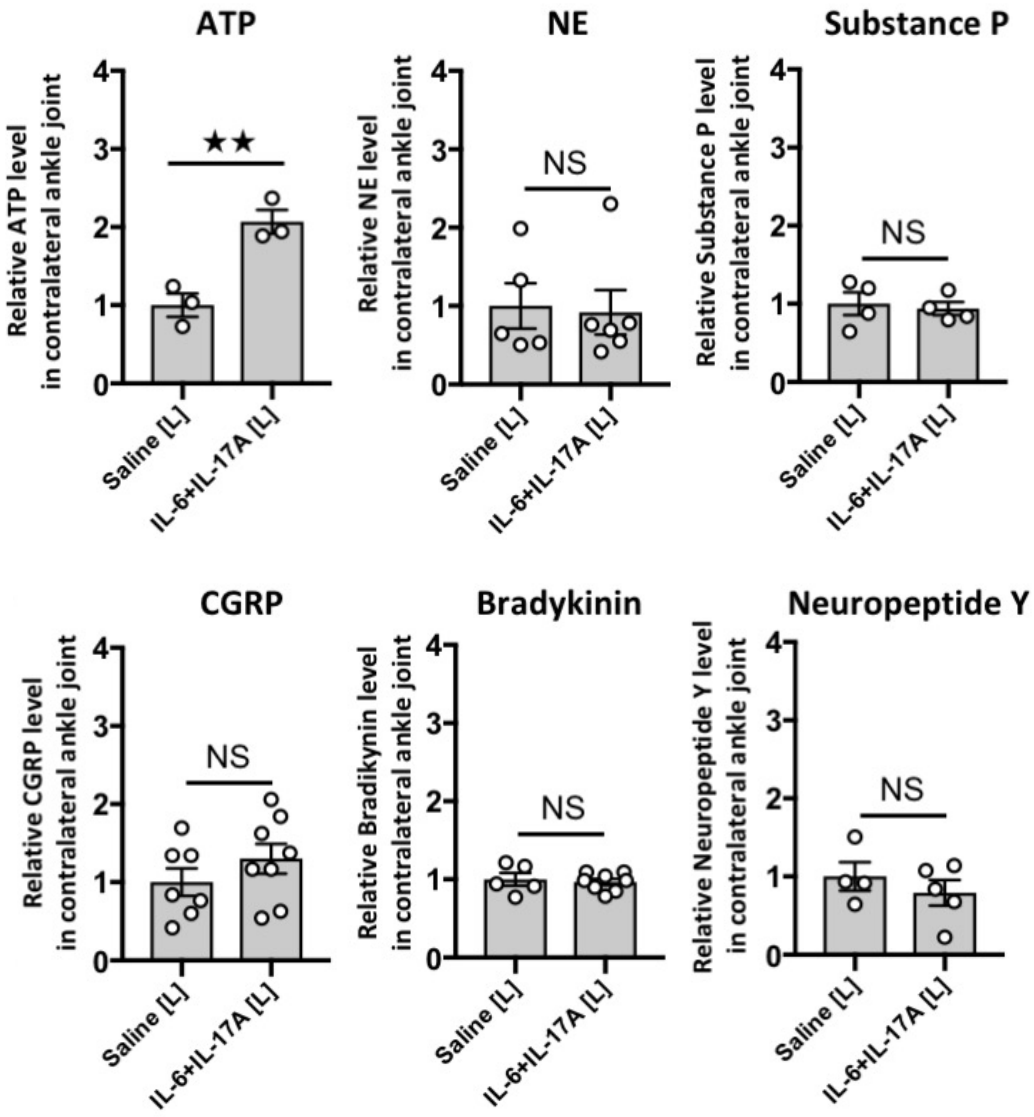

Fig. 18 IL-17A and IL-6 (1 μg each) or saline were injected into the left ankle joints of F759 mice on days 0, 1, and 2, followed by the analysis of ATP (n = 3 per group), norepinephrine (NE) (n = 5-6 per group), substance P (n = 4 per group), CGRP (n = 7-8 per group), bradykinin (n = 5-8 per group), and neuropeptide Y (n = 4-5 per group) levels in the contralateral (right) ankle joint on day 3. Mean scores ± SEM are shown. *P* values were calculated using Student's t-tests (★★ $P < 0.01$; NS, not significant).

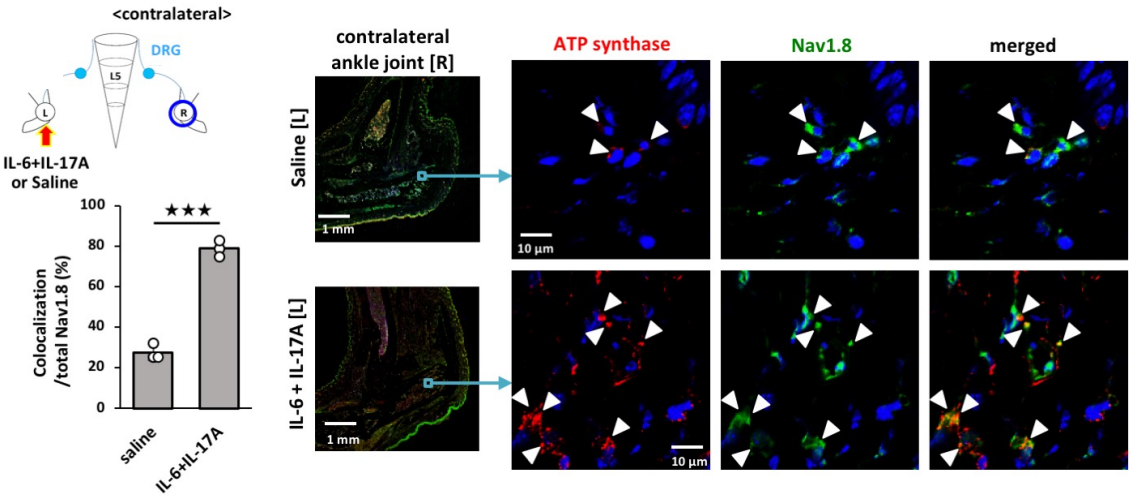

Fig. 19 IL-17A and IL-6 (1 μg each) or saline were injected into the left ankle joints of F759 mice on days 0, 1, and 2, followed by immunostaining for ATP synthase and Nav1.8 in the contralateral (right) ankle joint on day 3. The colocalization of ATP synthase and Nav1.8 was quantified using Z-stack images (n=3 per group). The bar graph shows the percentage of the colocalized signal volume in the total signal volume of Nav1.8. Red, ATP synthase. Green, Nav1.8. Blue, nuclei. Arrowheads show merged signals. Bar, 1 mm or 10 μm. Mean scores ± SD are shown. *P* values were calculated using Student's t-tests (★★★ $P < 0.001$). Diagram illustrates the experimental setting. L, left ankle; L5, fifth lumbar vertebral level; DRG, dorsal root ganglion; R, right ankle. Arrow indicates cytokine or saline injection. Blue circle indicates the ankle joint examined.

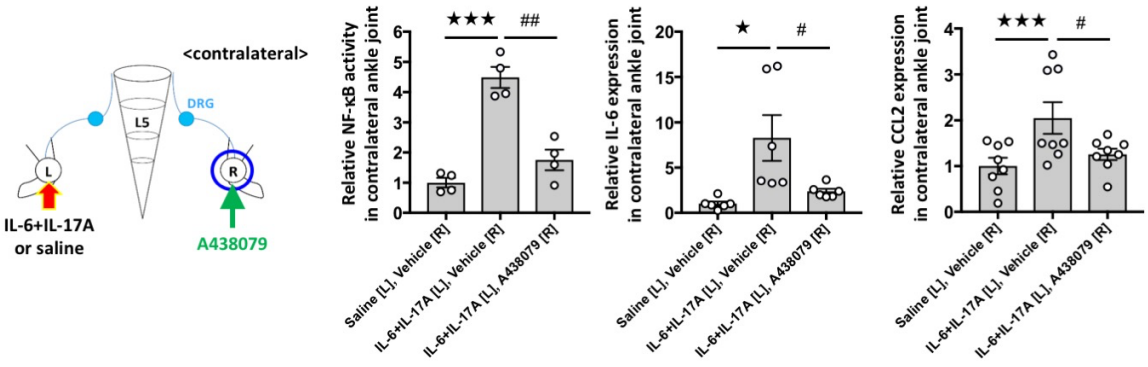

Fig. 20 IL-17A and IL-6 (1 μg each) or saline were injected into the left ankle joint of F759 mice on days 0, 1, and 2 in the presence or absence of A438079 in the contralateral (right) ankle joint, followed by the analysis of NF-κB activation and IL-6 and CCL2 levels in the contralateral ankle joint on day 3 (n = 4-6 per group). Mean scores ± SEM are shown. *P* values were calculated using Student's t-tests (★ and # $P < 0.05$; ## $P < 0.01$; ★★★ $P < 0.001$). Diagram illustrates the experimental setting. L, left ankle; L5, fifth lumbar vertebral level; DRG, dorsal root ganglion; R, right ankle. Arrow indicates cytokine, saline or A438079 injection. Blue circle indicates the ankle joint examined.

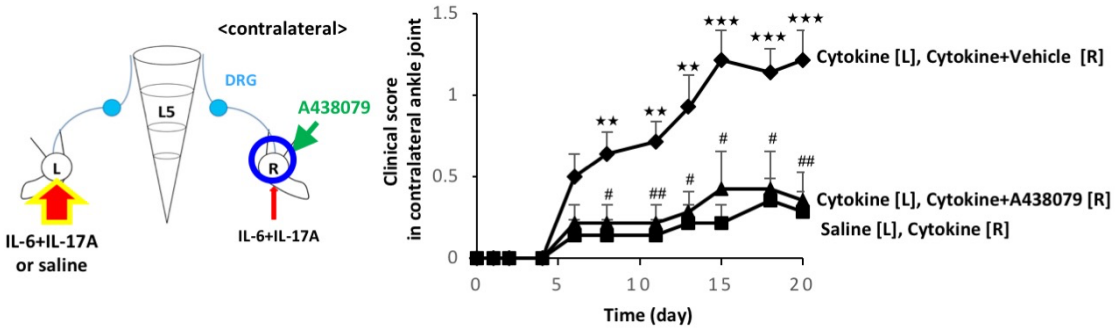

Fig. 21 IL-17A and IL-6 (1 μg each) or saline were injected into the left ankle joint, and a low dose of IL-17A and IL-6 (0.01 μg each) with A438079 (10 μg) was injected into the right ankle joint of F759 mice on days 0, 1 and 2. Clinical arthritis scores of the right ankle joint were evaluated (n = 4-5 per group). Mean scores ± SEM are shown. *P* values were calculated using Wilcoxon rank-sum test (# $P < 0.05$; ★★ and ## $P < 0.01$; ★★★ $P < 0.001$). Diagram illustrates the experimental setting. L, left ankle; L5, fifth lumbar vertebral level; DRG, dorsal root ganglion; R, right ankle. Arrow indicates cytokine, saline or A438079 injection. Blue circle indicates the ankle joint examined.

3-4. Sensory neuron-interneuron interactions between joints are critical for ATP induction in the contralateral joint

We next investigated functional neural connections between the ankle joints. All of the following events suppressed ATP induction in the contralateral ankle joint after cytokine injections into the other joint: the deafferentation of sensory neurons at L5 DRG on the cytokine-injected side **(Fig. 22A)**; a lengthwise T9-13 spinal cord cut, which induced the ablation of interneurons between bilateral ankle joints in the lower thoracic cords **(Fig. 22B)**; and the deafferentation of contralateral L4-L6 DRG sensory nerves **(Fig. 22C)**. These results strongly suggest that functional sensory neuron-interneuron connections exist between the ankle joints and are sufficient for ATP induction in the contralateral ankle joint.

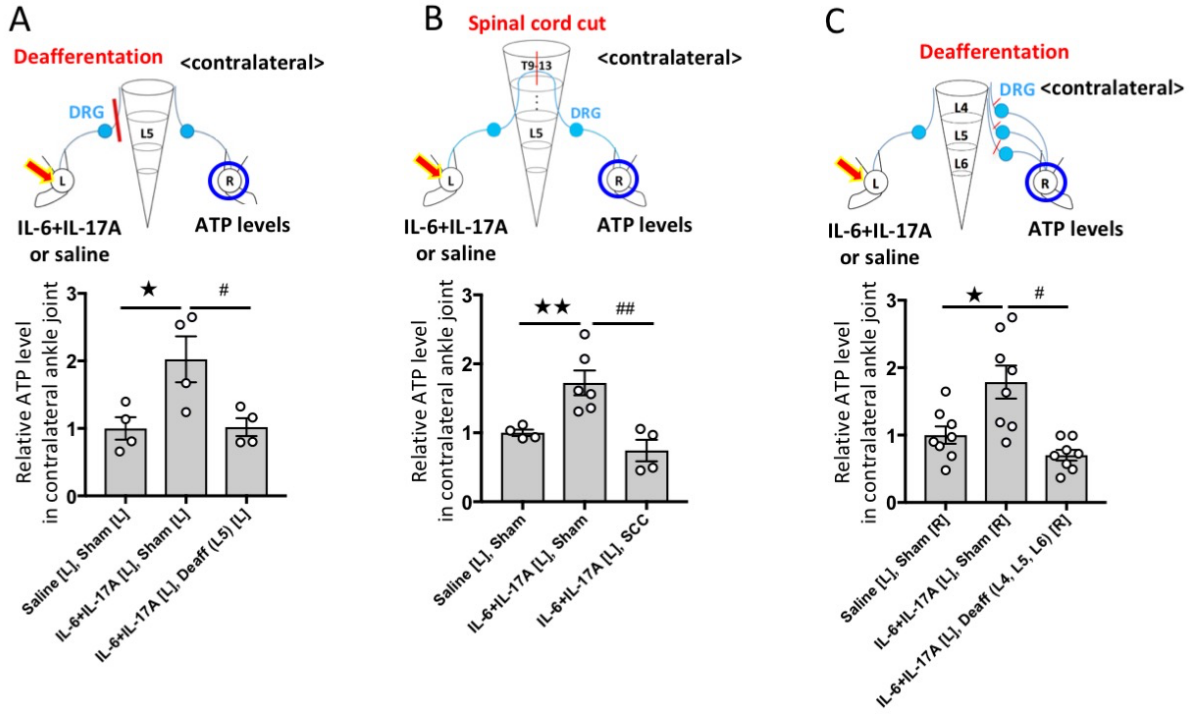

Fig. 22 (A) IL-17A and IL-6 (1 μg each) or saline were injected into the left ankle joint of F759 mice deafferented (Deaff) or sham-operated (Sham) at the L5 DRG of the left side on days 0, 1, and 2, followed by the analysis of ATP levels in the contralateral (right) ankle joint on day 3 using an ATP assay kit (n = 4 per group).

(B) IL-17A and IL-6 (1 μg each) or saline were injected into the left ankle joint of F759 mice with a lengthwise T9-13 spinal cord cut (SCC) or sham-operated (Sham) on days 0, 1, and 2, followed by the analysis of ATP levels in the contralateral (right) ankle joint on day 3 (n = 4-6 per group).

(C) IL-17A and IL-6 (1 μg each) or saline were injected into the left ankle joint of F759 mice deafferented (Deaff) at the L4-L6 DRGs of the right side or sham-operated (Sham) on days 0, 1, and 2, followed by the analysis of ATP levels in the contralateral (right) ankle joint on day 3 (n = 8 per group).

Experiments were performed at least three times independently; representative data are shown. Mean scores ± SEM are shown. *P* values were calculated using Dunnett's test (★ and # $P < 0.05$; ★★ and ## $P < 0.01$). Diagrams illustrate the experimental settings. L, left ankle; L4-L6, fourth to sixth lumbar vertebral level; T9-13, ninth to thirteenth thoracic cord; DRG, dorsal root ganglion; R, right ankle. Arrows indicate cytokine, or saline injection. Blue circles indicate the ankle joints examined.

3-5. Regional ATP induction after ipsilateral joint inflammation functions as a neurotransmitter to activate bilateral sensory neurons followed by contralateral ankle joint inflammation

Next, we examined how ipsilateral joint inflammation activates sensory neurons. Because we previously found that extracellular ATP induced from regional blood vessels by cytokine stimulation enhances the activation of a neural pathway in the brain (**Atsumi *et al.*, 2017)**, we focused our attention on ATP. ATP concentration increased after IL-17A and IL-6 stimulation in synovial cells in a manner dependent on NF-κB activation in vitro **(Fig. 23)**. Moreover, ATP concentration significantly increased in the ankle joint after cytokine injections in a manner dependent on cytokine stimulation in Col1a+ non-immune cells in vivo **(Fig. 24)**. The injection of IL-6 and IL-17A plus A438079 (a selective P2RX7 antagonist) **(Donnelly-Roberts *et al.*, 2009; McGaraughty *et al.*, 2007)** in one ankle joint significantly suppressed the neural activation of L5 DRG neurons **(Fig. 25)** and the increase of ATP concentration in the other ankle joint **(Fig. 26)**. Furthermore, the injection of ATP in one ankle joint increased ATP concentration in the contralateral ankle joint **(Fig. 27)**.

We then examined whether blockade of the ATP signal suppresses spreading inflammation development in a cytokine-injected joint. Arthritis development was suppressed by the injection of A438079 into the same ankle joint **(Fig. 28)**. Importantly, the unilateral injection of A438079 suppressed the development of bilateral arthritis **(Fig. 29, A and B)**. Thus, cytokine stimulation in Col1a+ non-immune cells increases ATP expression to activate sensory pathways in the ankle joint, causing spreading inflammation.

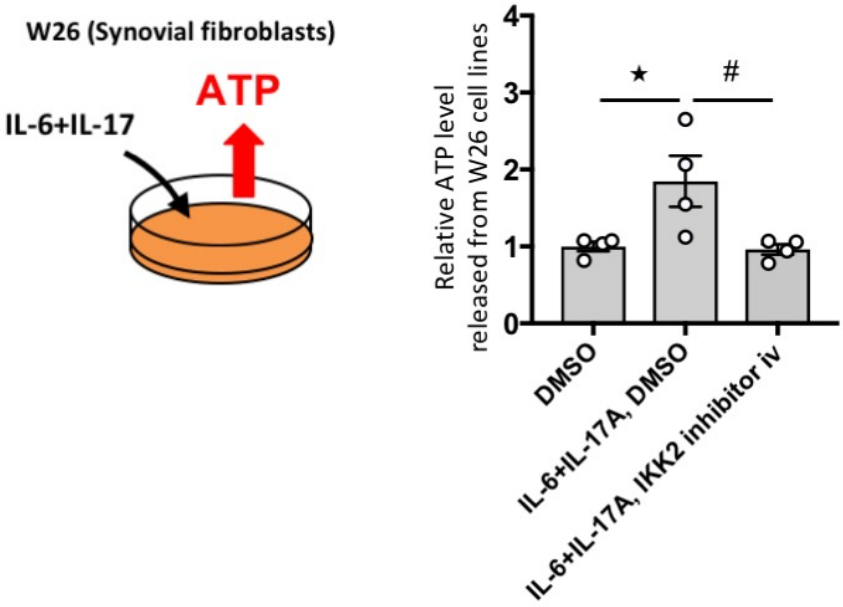

Fig. 23 W26 synovial fibroblasts were stimulated with human IL-6 (50 ng/mL) plus soluble IL-6Rα (50 ng/mL) and/or mouse IL-17A (50 ng/mL) with or without IKK2 inhibitor IV (5 μM). Culture supernatants were collected and assessed using an ATP assay kit (n = 4 per group). Mean scores ± SEM are shown. *P* values were calculated using Dunnett's test (★ and # $P < 0.05$). Diagrams illustrate the experimental settings.

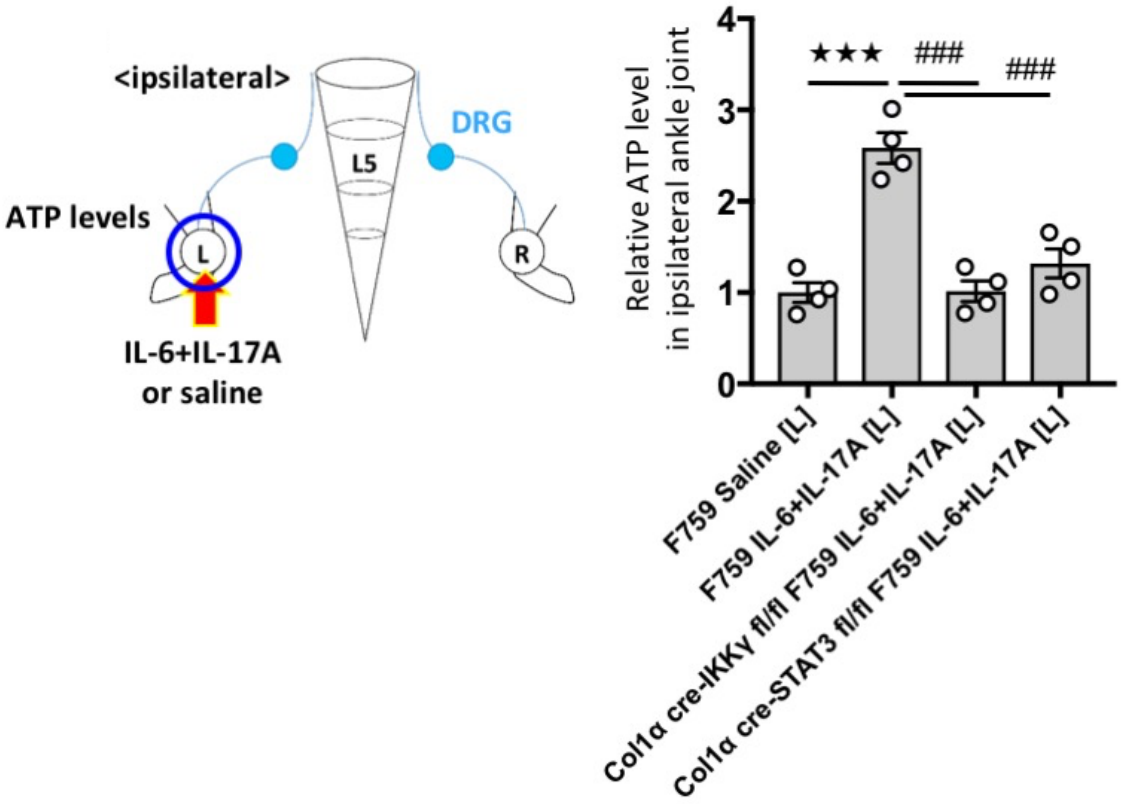

Fig. 24 IL-17A and IL-6 (1 μg each) or saline were injected into the left ankle joint of F759 mice, F759/Col1α-cre IKKγ$^{flox/flox}$ mice, and F759/Col1α-cre STAT3$^{flox/flox}$ mice on days 0, 1, and 2, followed by the analysis of ATP concentration in the ipsilateral (left) ankle joint on day 3 (n = 4 per group). Mean scores ± SEM are shown. *P* values were calculated using Dunnett's test (★★★ and ### $P < 0.001$). Diagram illustrates the experimental setting. L, left ankle; L5, fifth lumbar vertebral level; DRG, dorsal root ganglion; R, right ankle. Arrow indicates cytokine or saline injection. Blue circle indicates the ankle joint examined.

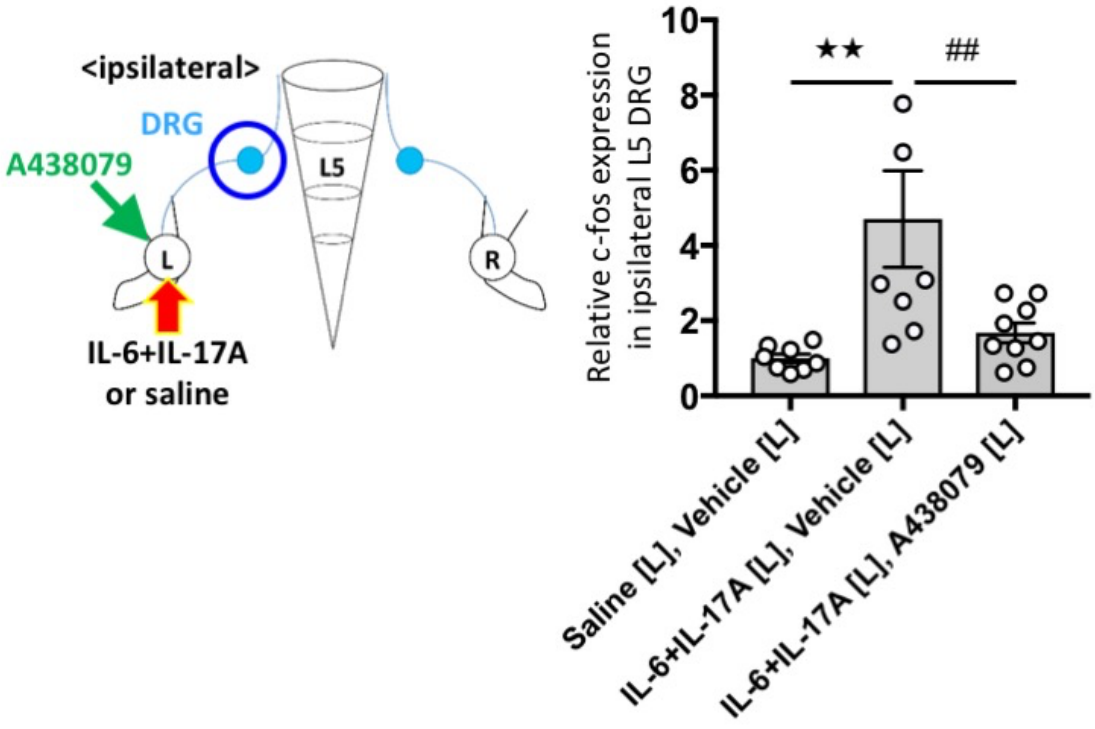

Fig. 25 IL-17A and IL-6 (1 μg each) or saline were injected with or without the P2RX7 inhibitor A438079 into the left ankle joint of F759 mice on days 0, 1, and 2, followed by the analysis of c-fos expression in the ipsilateral (left) L5 DRG on day 3 (n = 8-9 per group). Mean scores ± SEM are shown. *P* values were calculated using Dunnett's test (★★ and ## $P < 0.01$). Diagram illustrates the experimental setting. L, left ankle; L5, fifth lumbar vertebral level; DRG, dorsal root ganglion; R, right ankle. Arrows indicate cytokine, saline, or A438079 injection. Blue circle indicates the DRG examined.

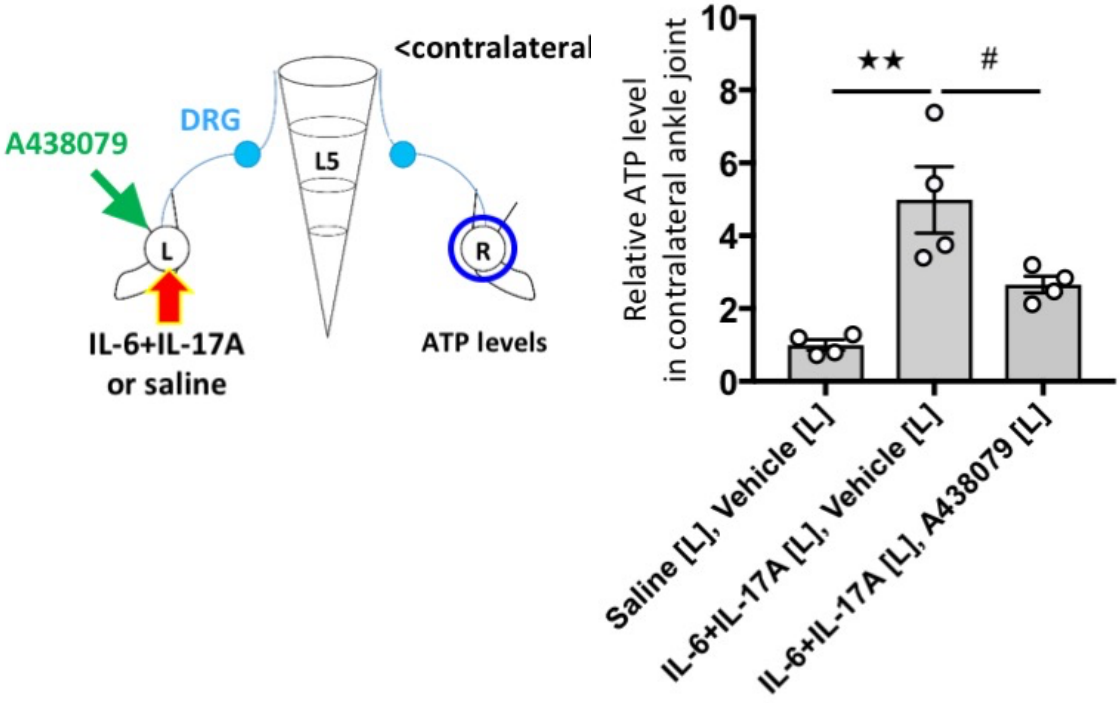

Fig.26 IL-17A and IL-6 (1 μg each) or saline were injected with or without A438079 into the left ankle joint of F759 mice on days 0, 1, and 2, followed by the analysis of ATP concentration in the contralateral (right) ankle joint on day 3 (n = 4 per group). Mean scores ± SEM are shown. *P* values were calculated using Dunnett's test (# $P < 0.05$; ★★ $P < 0.01$). Diagram illustrates the experimental setting. L, left ankle; L5, fifth lumbar vertebral level; DRG, dorsal root ganglion; R, right ankle. Arrows indicate cytokine, saline, or A438079 injection. Blue circle indicates the ankle joint examined.

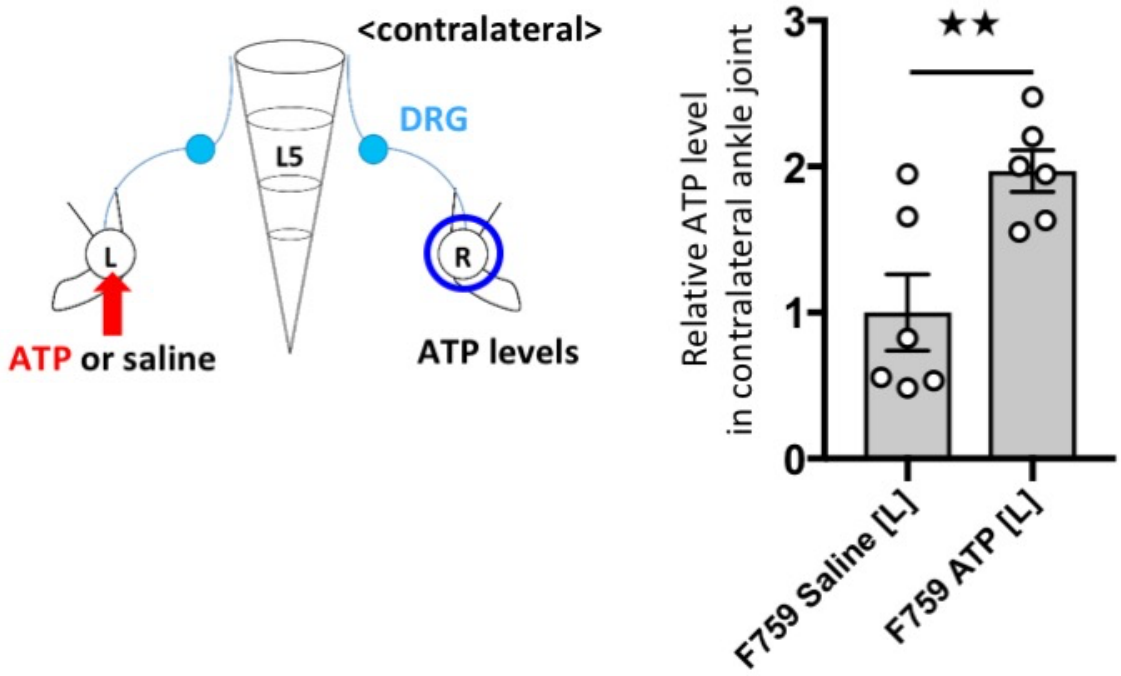

Fig. 27 ATP (2 μg) or saline was injected into the left ankle joint of F759 mice on days 0, 1, and 2, followed by the analysis of ATP concentration in the contralateral (right) ankle joint on day 3 (n = 6 per group). Mean scores ± SEM are shown. *P* values were calculated using Student's t-test (★★ $P < 0.01$). Diagram illustrates the experimental setting. L, left ankle; L5, fifth lumbar vertebral level; DRG, dorsal root ganglion; R, right ankle. Arrow indicates ATP or saline injection. Blue circle indicate the ankle joint examined.

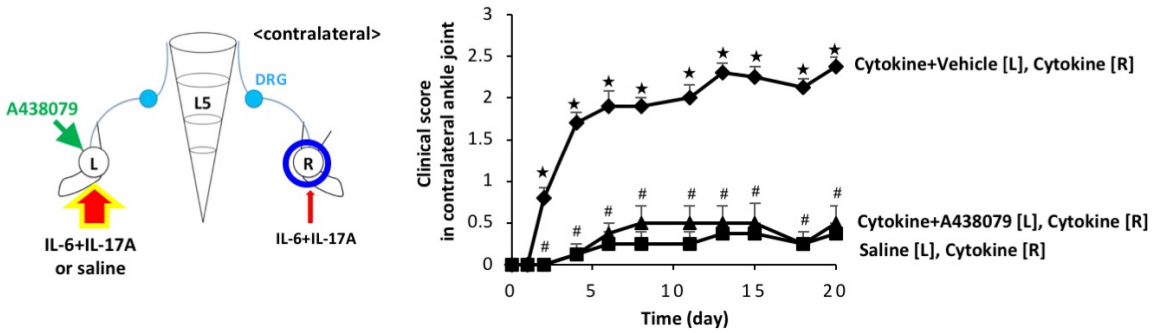

Fig. 28 IL-17A and IL-6 (1 μg each) or saline were injected into the left ankle joint, and a low dose of IL-17A and IL-6 (0.01 μg each) were injected into the right ankle joint with or without A438079 (10 μg) into the left ankle joint of F759 mice on days 0, 1 and 2. Clinical arthritis scores of the right ankle joint of F759 mice were evaluated (n = 14 per group). Mean scores ± SEM are shown. *P* values were calculated using the Wilcoxon rank-sum test (★ and # $P < 0.05$). Diagram illustrates the experimental setting. L, left ankle; L5, fifth lumbar vertebral level; DRG, dorsal root ganglion; R, right ankle. Arrows indicate cytokine, saline, or A438079 injection. Blue circle indicate the ankle joint examined.

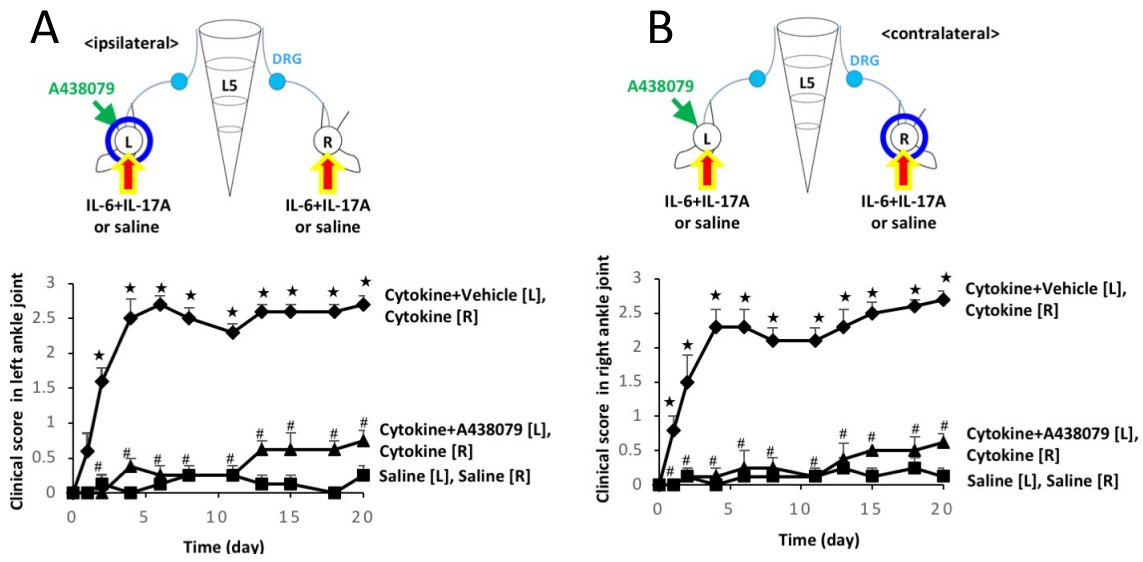

Fig. 29 Clinical arthritis scores from the left (A) or right (B) ankle joint of F759 mice after injections of IL-17A and IL-6 (0.1 μg each) in both ankle joints on days 0, 1, and 2 with or without A438079 (10 μg) (n = 4-5 per group). Mean scores ± SEM are shown. *P* values were calculated using the Wilcoxon rank-sum test (★ and # $P < 0.05$). Diagrams illustrate the experimental settings. L, left ankle; L5, fifth lumbar vertebral level; DRG, dorsal root ganglion; R, right ankle. Arrows indicate cytokine, saline, or A438079 injection. Blue circles indicate the ankle joints examined.

3-6. ATP is secreted in a manner dependent on NF-κB activation and a critical NF-κB stimulator in the contralateral joint

The importance of the ATP-P2RX7 axis on leukocyte function has been reported (Labasi et al., 2002). However, we here investigated the effects of the ATP-P2RX7 axis on nonimmune cells, including sensory neurons, endothelial cells, and fibroblasts, in the contralateral joint where remote inflammation is induced.

ATP injection in the unilateral joint did not increase ATP in the contralateral side in F759 mice deficient of NF-κB or STAT3 signaling in Col1a+ non-immune cells **(Fig. 30**, suggesting that the IL-6 amplifier is critical for the increase of ATP in the contralateral ankle joint. Consistent with these results, we found that vimentin+ cells, including synovial fibroblastic cells and endothelial cells, had phosphorylated NF-κB and STAT3 molecules in the ankle joint after cytokine injections on the opposite side **(Fig. 31)**. Importantly, blockade of P2RX7 signaling by A438079 injection abrogated the contralateral ATP increase in situ **(Fig. 32)**. P2RX7 was expressed by vimentin+ and/or CD31+ cells as well as by Nav1.8+ neurons regardless of cytokine stimulation **(Fig. 33)**. Phosphorylated CREB molecules, which are downstream of ATP signaling, were increased in vimentin+ cells and in CD31+ cells in the contralateral joint after the cytokine stimulation **(Fig. 34)**. These results strongly suggest that synovial fibroblasts and endothelial cells in contralateral joints are responder cells to ATP. Thus, it is possible that these non-immune cells secrete IL-6 and CCL2 as well as more ATP in a manner dependent on NF-κB and STAT3 in the contralateral joint, a phenomenon critical for spreading inflammation.

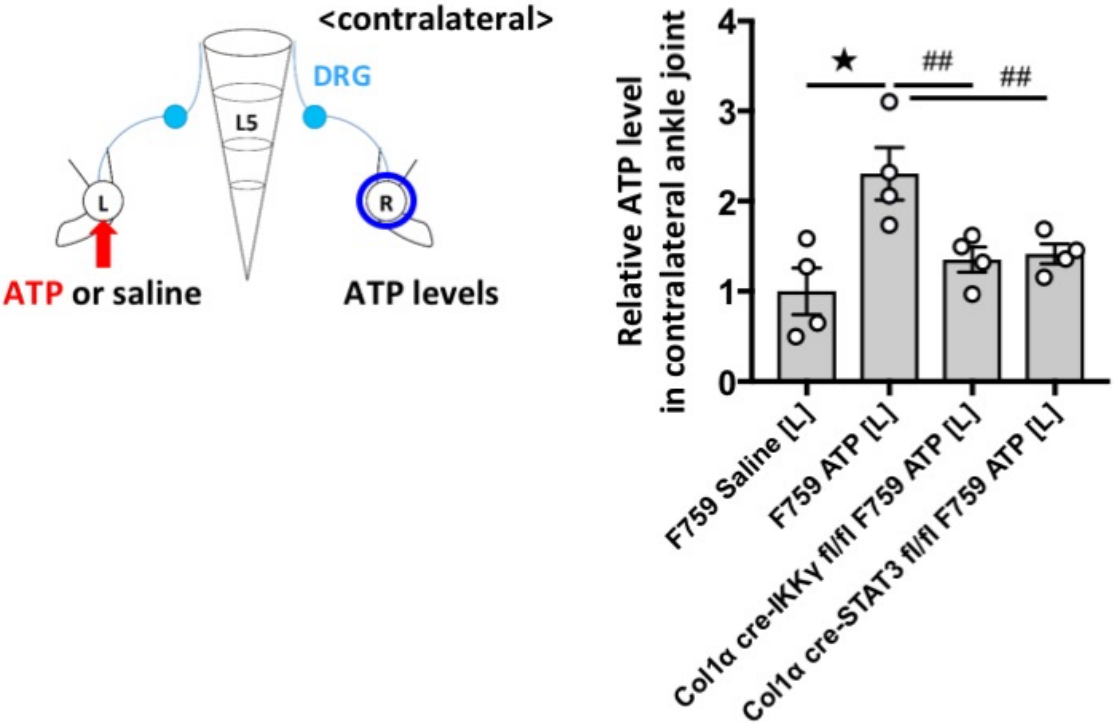

Fig. 30 ATP (2 μg) or saline was injected into the left ankle joint of F759 mice, F759/Col1α-cre IKKγ$^{flox/flox}$ mice, and F759/Col1α-cre STAT3$^{flox/flox}$ mice on days 0, 1, and 2, followed by the analysis of ATP concentration in the contralateral (right) ankle joint on day 3 (n = 4 per group). Experiments were performed at least three times independently; representative data are shown. Mean scores ± SEM are shown. *P* values were calculated using Dunnett's test (★ $P < 0.05$; ## $P < 0.01$). Diagram illustrates the experimental setting. L, left ankle; L5, fifth lumbar vertebral level; DRG, dorsal root ganglion; R, right ankle. Arrow indicates ATP or saline injection. Blue circle indicates the ankle joint examined.

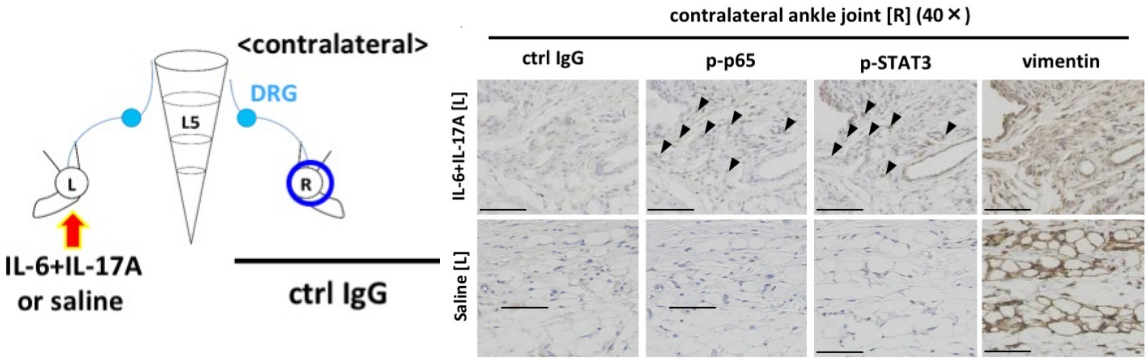

Fig. 31 IL-17A and IL-6 (1 μg each) or saline were injected into the left ankle joint of F759 mice on days 0, 1, and 2, followed by the detection of phosphorylated NF-κB p65 (p-p65) and STAT3 (p-STAT3), and vimentin (non-immune cell marker) in the contralateral (right) ankle joint by immunohistochemistry. Experiments were performed at least three times independently; representative data are shown. Diagram illustrates the experimental setting. L, left ankle; L5, fifth lumbar vertebral level; DRG, dorsal root ganglion; R, right ankle. Arrow indicates cytokine or saline injection. Blue circle indicates the ankle joint examined.

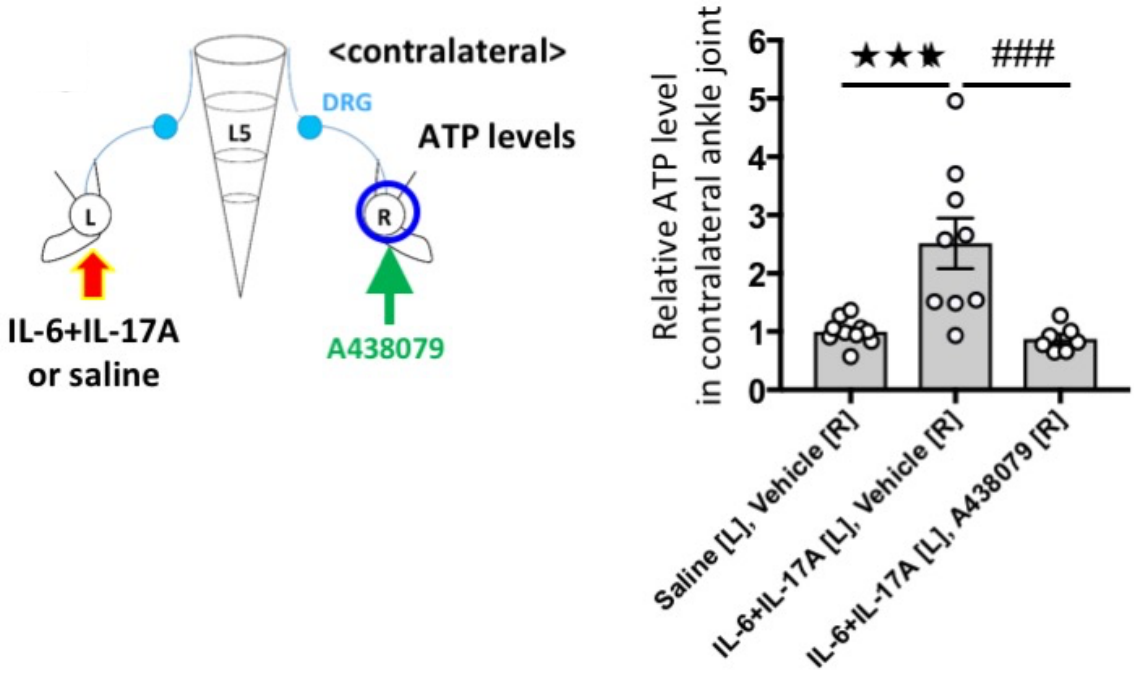

Fig. 32 IL-17A and IL-6 (1 μg each) or saline were injected into the left ankle joint with or without A438079 injection into the right ankle joint of F759 mice on days 0, 1, and 2, followed by the analysis of ATP levels in the contralateral (right) ankle joint on day 3 (n = 7-10 per group). Experiments were performed at least three times independently; representative data are shown. Mean scores ± SEM are shown. *P* values were calculated using Dunnett's test (★★★ and ###, $P < 0.001$). Diagram illustrates the experimental setting. L, left ankle; L5, fifth lumbar vertebral level; DRG, dorsal root ganglion; R, right ankle. Arrows indicate cytokine, saline, or A438079 injection. Blue circle indicates the ankle joint examined.

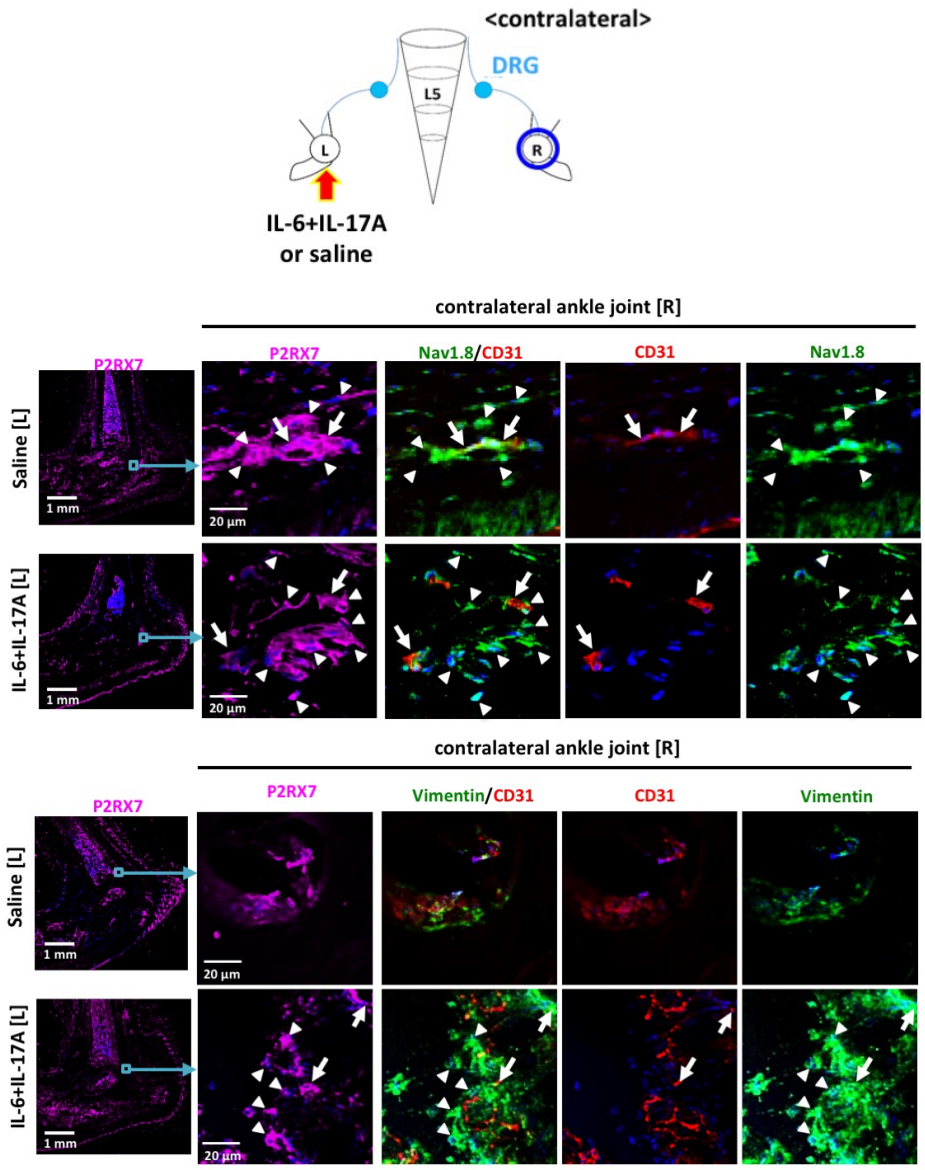

Fig. 33 IL-17A and IL-6 (1 μg each) or saline were injected into the left ankle joint of F759 mice on days 0, 1, and 2, followed by immunostaining for P2RX7, Nav1.8, vimentin, and CD31 in the contralateral (right) ankle joint on day 3. Magenta, P2RX7. Green, Nav1.8 or vimentin. Red, CD31. Blue, Nuclei. Arrows show P2RX7 signals merged with Nav1.8+CD31+ or vimentin+CD31+ signals. Arrowheads show P2RX7 signals merged with Nav1.8 or vimentin signals. Bar, 1 mm or 20 μm. Experiments were performed at least three times independently; representative data are shown. Diagram illustrates the experimental setting. L, left ankle; L5, fifth lumbar vertebral level; DRG, dorsal root ganglion; R, right

ankle. Arrow indicates cytokine or saline injection. Blue circle indicates the ankle joint examined.

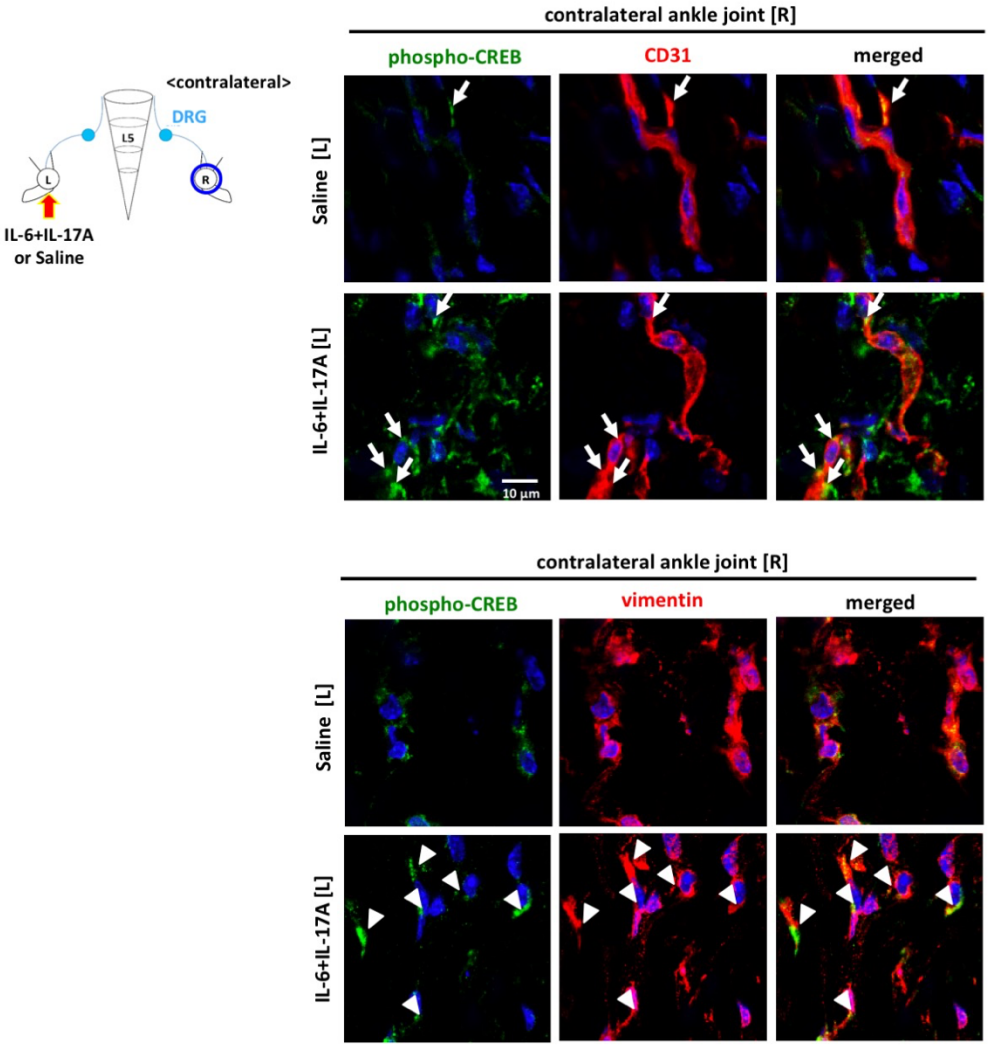

Fig. 34 IL-17A and IL-6 (1 μg each) or saline were injected into the left ankle joint of F759 mice on days 0, 1, and 2, followed by immunostaining for pCREB and CD31 or vimentin in the contralateral (right) ankle joint on day 3. Green, phosphorylated-CREB. Red, CD31 or vimentin. Blue, Nuclei. Arrows (CD31) and arrowheads (vimentin) show merged signals.
The diagram illustrates the experimental settings. L, left ankle; L5, fifth lumbar spinal cord, dorsal root ganglion; R, right ankle. The arrow indicates cytokine or saline injection, and the blue circle shows the ankle joint examined.

3-7. A similar mechanism occurs in collagen-induced arthritis (CIA)

Finally, we investigated whether our observations in the cytokine-induced arthritis model could be applied to more conventional RA models. Accordingly, we employed the CIA model, a common model in which arthritis is induced by active immunization in both joints. We found that intra-articular injections of A438079 significantly suppressed the development of joint inflammation **(Fig. 35)**, as did the intra-articular injections of an anti-IL-6R antibody or anti-IL-17A antibody **(Fig. 36)**, suggesting that this model is locally ATP/NF-κB/STAT3-dependent. In contrast to the levels of other neurotransmitters, ATP levels in the joint increased during the development of CIA **(Fig. 37)**. A lengthwise T9-13 spinal cord cut, which induced the ablation of the proposed sensory neuron-interneuron interaction between the bilateral joints, suppressed ATP induction in the ankle joint and the development of bilateral ankle arthritis **(Fig. 38 and Fig. 39)**. Moreover, unilateral intra-articular injections of A438079 significantly suppressed the development of the bilateral joint inflammation **(Fig. 40)**. Finally, the direct injection of ATP in one ankle joint increased ATP concentration in the other ankle joint in naive wild-type mice **(Fig. 41)**. Thus, we concluded that the sensory neuron-interneuron pathway identified in the cytokine-induced arthritis model is also present in wild-type mice and contributes to the pathogenesis of bilateral ankle inflammation in the CIA model.

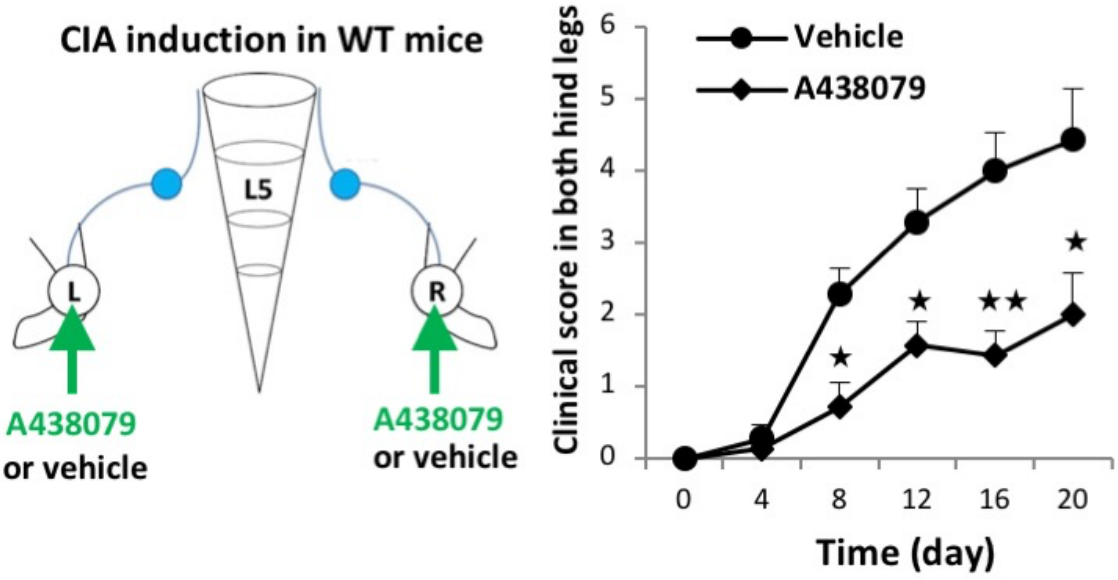

Fig. 35 CIA was induced in C57BL/6 mice. Clinical arthritis scores from both hind legs of CIA mice that received bilateral injections of A438079 every day from days 4-28 after primary immunization (n = 7 per group). Mean scores ± SEM are shown. *P* values were calculated using the Wilcoxon rank-sum test (★ $P < 0.05$; ★★ $P < 0.01$). Diagram illustrates the experimental setting. L, left ankle; L5, fifth lumbar vertebral level; DRG, dorsal root ganglion; R, right ankle. Arrows indicate A438079 or vehicle injection.

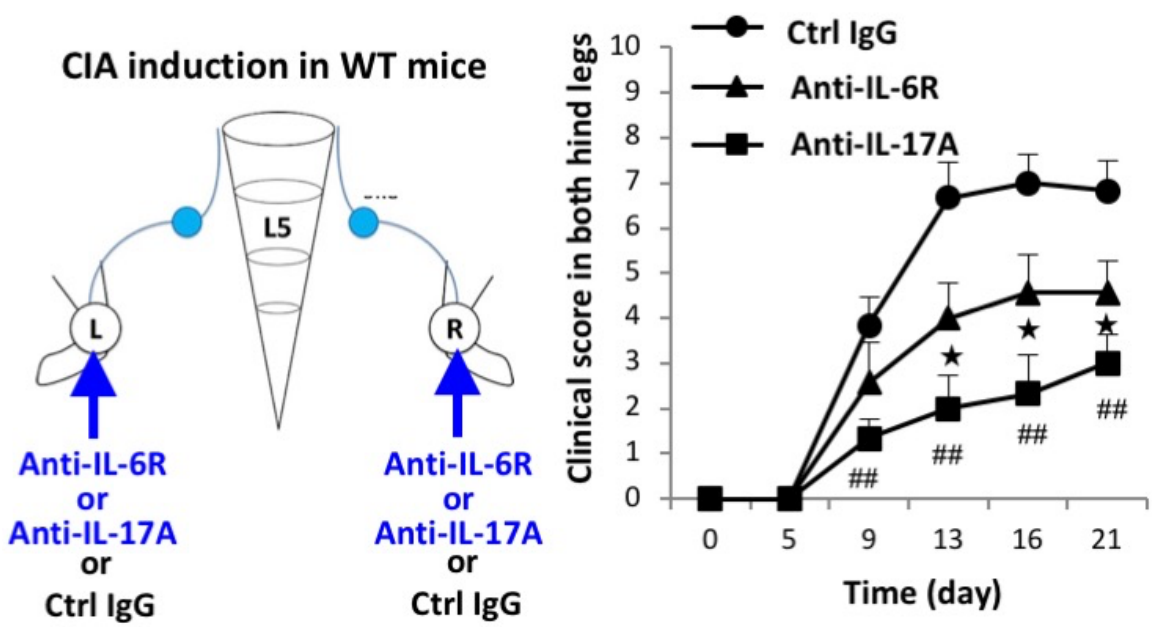

Fig. 36 Clinical arthritis scores from both hind legs of CIA mice that received bilateral injections of anti-IL-6R antibody (2 μg), anti-IL-17A antibody (2 μg), or control antibody every day from days 14-28 after primary immunization (n = 7 per group). Mean scores ± SEM are shown. *P* values were calculated using the Wilcoxon rank-sum test (★ $P < 0.05$; ## $P < 0.01$). Diagram illustrates the experimental setting. L, left ankle; L5, fifth lumbar vertebral level; DRG, dorsal root ganglion; R, right ankle. Arrows indicate antibody injections.

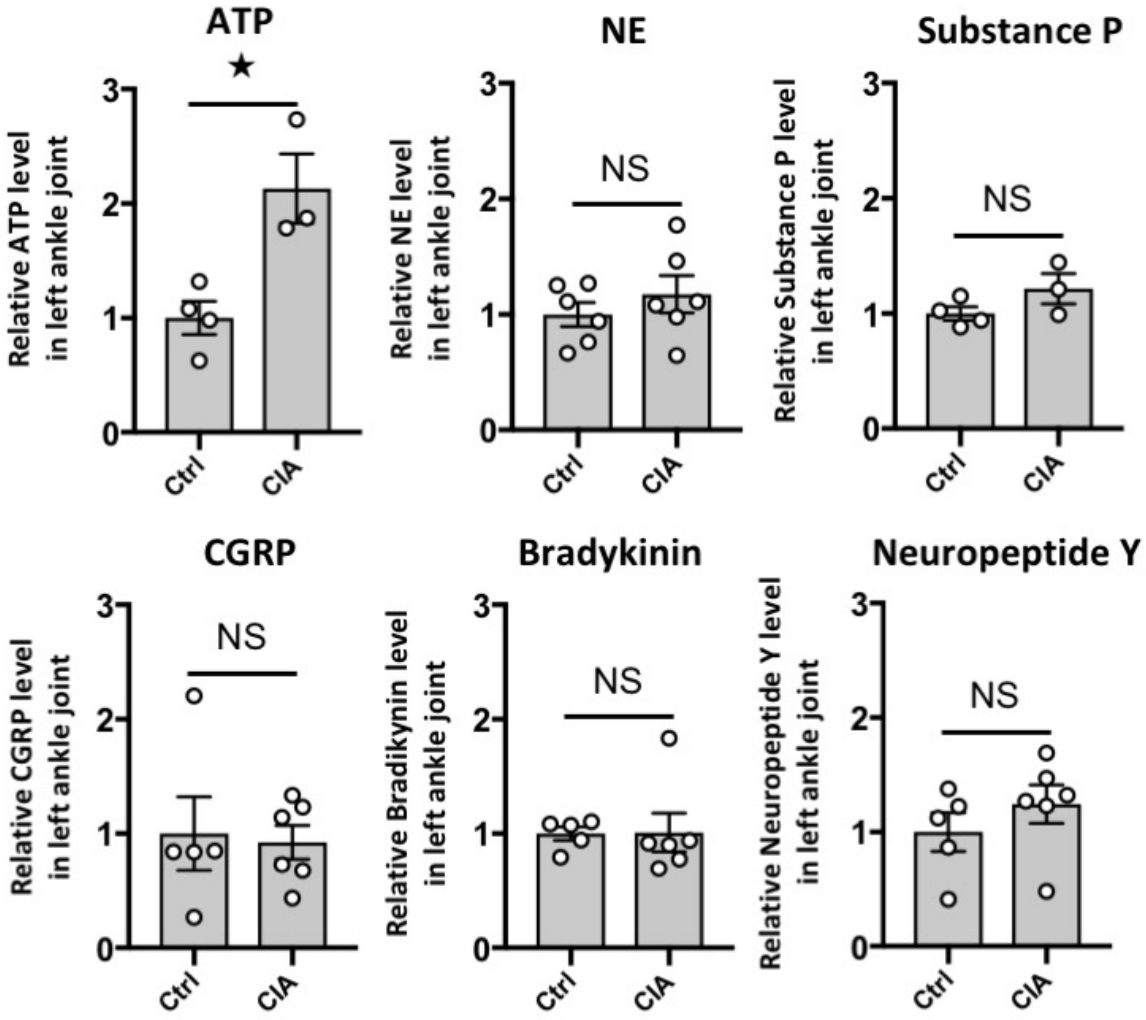

Fig. 37 CIA was induced in C57BL/6 mice, followed by the analysis of ATP, norepinephrine (NE), substance P, CGRP, bradykinin, and neuropeptide Y levels in the right ankle joint on day 23 after primary immunization (n = 4-6 per group). Mean scores ± SEM are shown. *P* values were calculated using the Student's t-test (★ $P < 0.05$; NS, not significant).

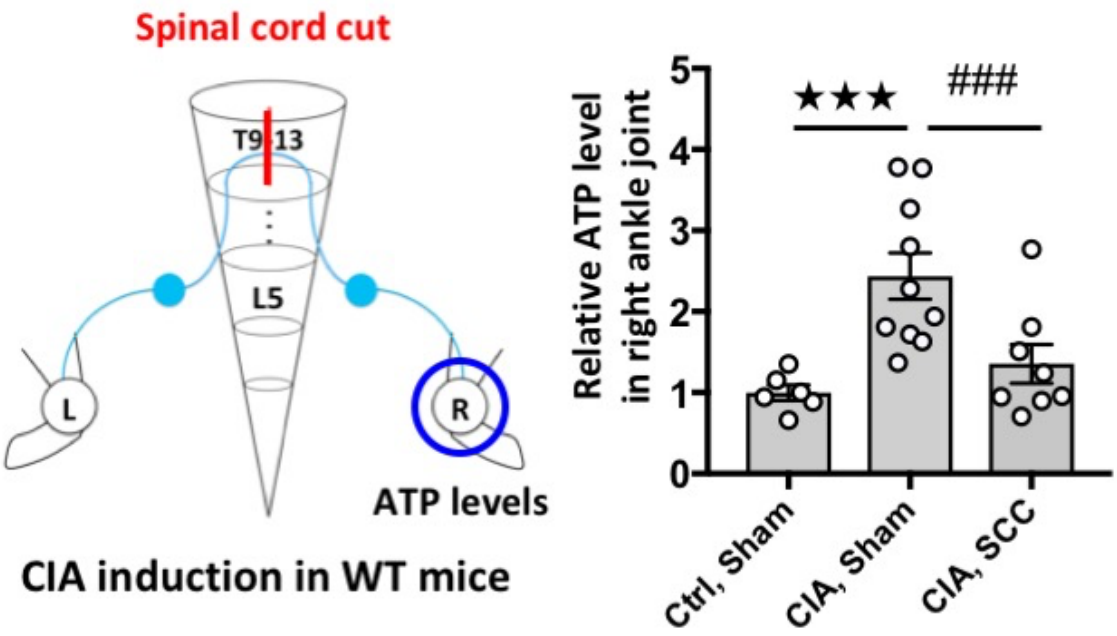

Fig. 38 CIA was induced in C57BL/6 mice after a lengthwise T9-13 spinal cord cut (SCC) or sham-operation (Sham), followed by the analysis of ATP levels in the right ankle joint on day 23 after primary immunization (n = 5-10 per group). Mean scores ± SEM are shown. *P* values were calculated using the Dunnett's test (★★★ and ###, $P < 0.001$). Diagram illustrates the experimental setting. L, left ankle; L5, fifth lumbar vertebral level; T9-13, 9-13th thoracic cords; DRG, dorsal root ganglion; R, right ankle. Blue circle indicates the ankle joint examined.

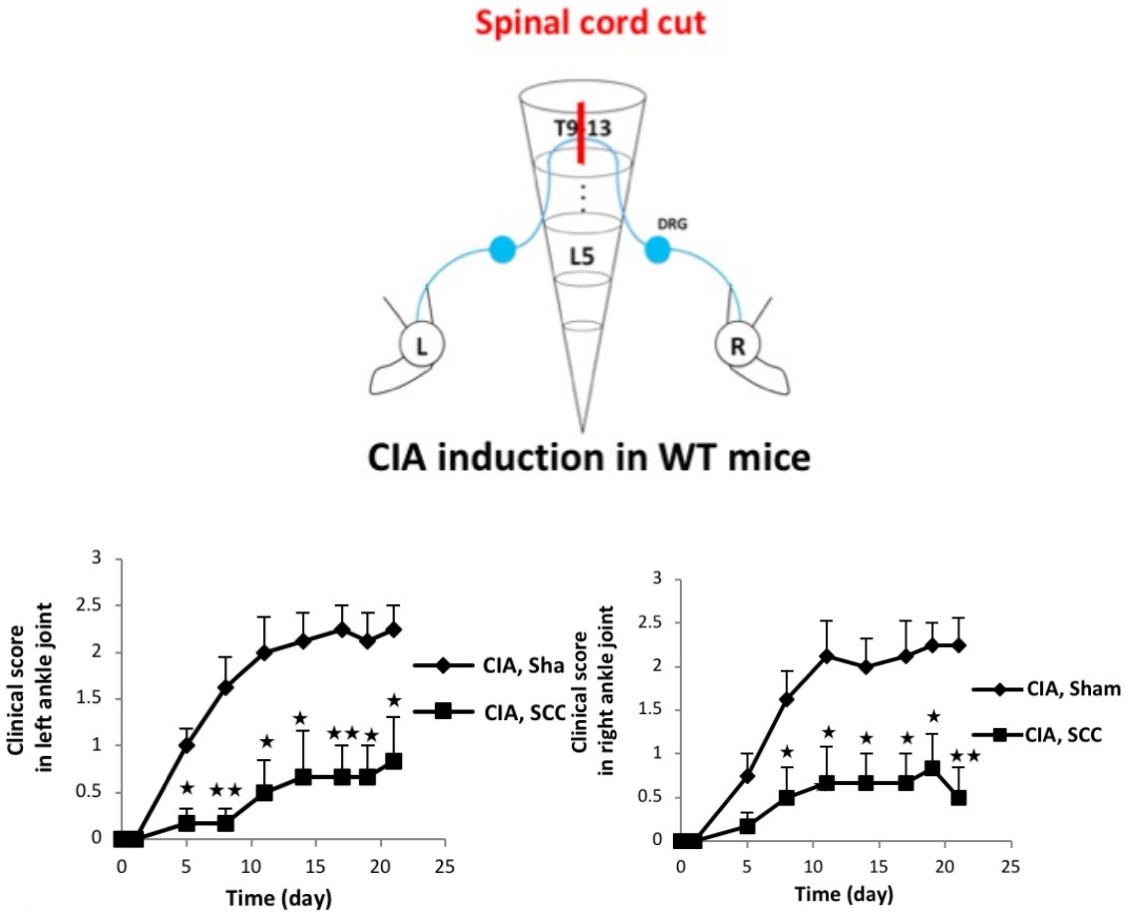

Fig. 39 Clinical arthritis scores from the left or right ankle joint after a lengthwise T9-13 spinal cord cut (SCC) or sham-operation (Sham) (n = 9-10 per group). Mean scores ± SEM are shown. *P* values were calculated using the Wilcoxon rank-sum test (★ $P < 0.05$; ★★ $P < 0.01$). Diagram illustrates the experimental setting. L, left ankle; L5, fifth lumbar vertebral level; T9-13, 9-13th thoracic cords; DRG, dorsal root ganglion; R, right ankle.

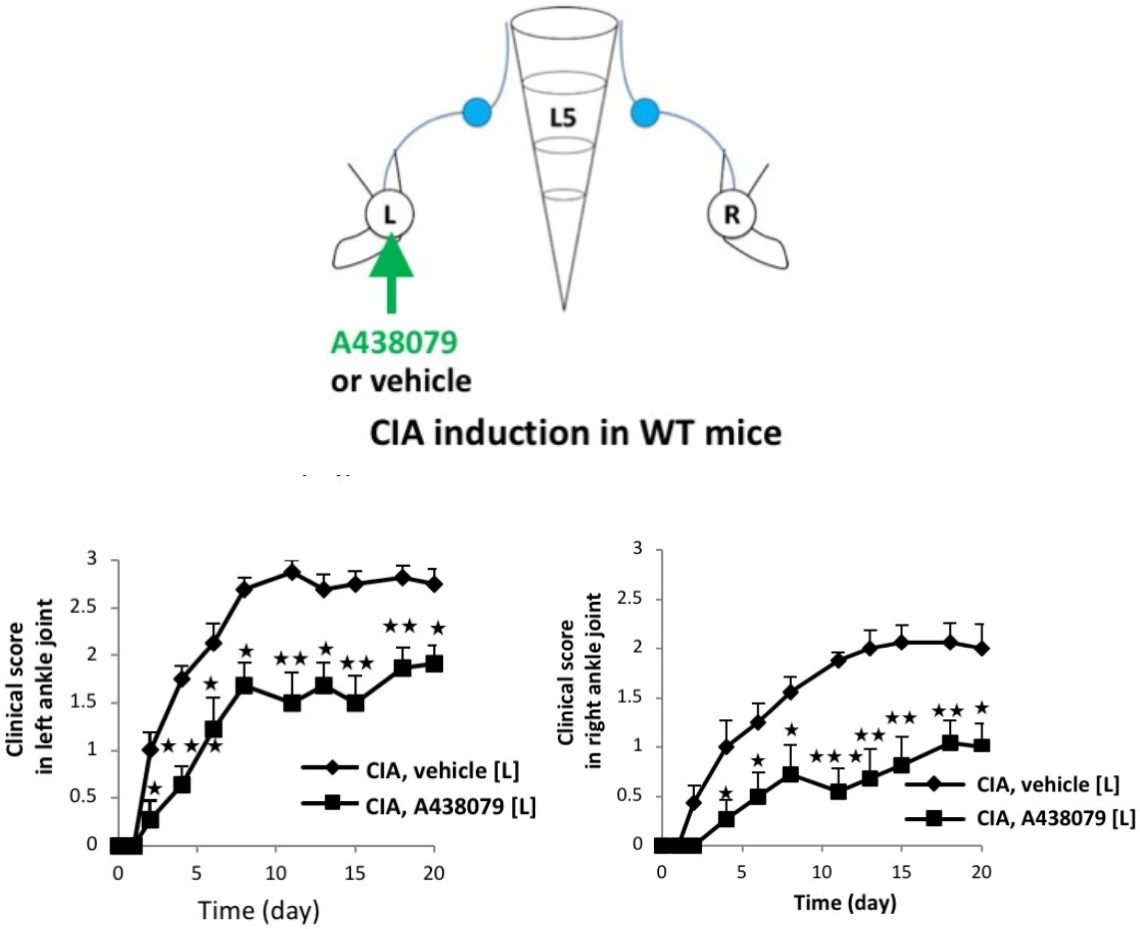

Fig. 40 Clinical arthritis scores from the left or right ankle joint of CIA mice that received unilateral injections of A438079 or vehicle every day from days 14-28 in the left ankle joint (n = 9-10 per group). Mean scores ± SEM are shown. *P* values were calculated using the Wilcoxon rank-sum test (★ $P < 0.05$; ★★ $P < 0.01$). Diagram illustrates the experimental setting. L, left ankle; L5, fifth lumbar vertebral level; DRG, dorsal root ganglion; R, right ankle. Arrows indicate A438079 or vehicle injection.

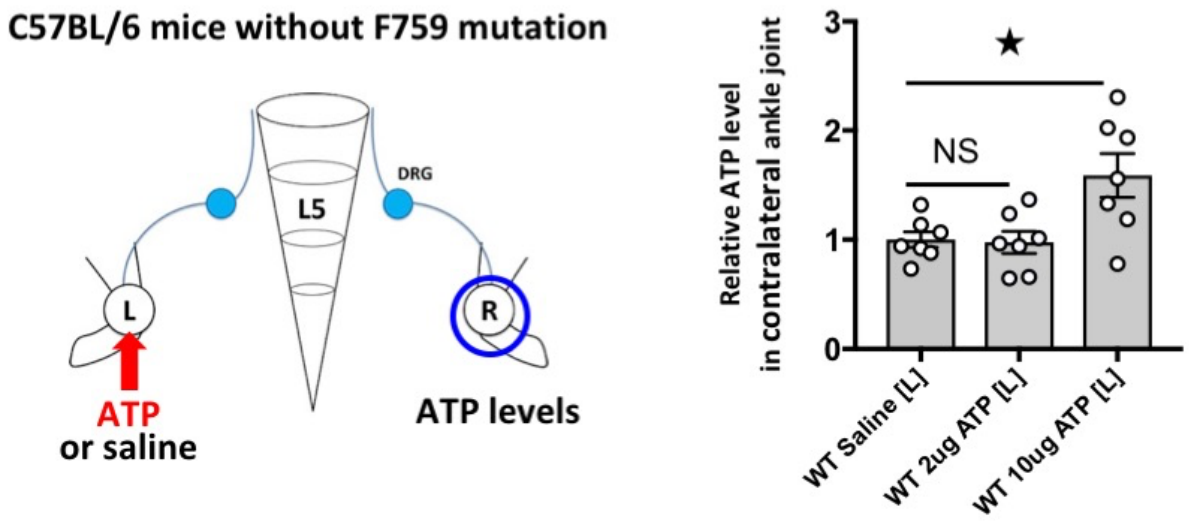

Fig. 41 ATP (2 or 10 μg) or saline was injected into the left ankle joint of naive wild-type mice on days 0, 1, and 2, followed by the analysis of ATP concentration in the contralateral (right) ankle joint on day 3 (n = 7 per group). Mean scores ± SEM are shown. *P* values were calculated using Dunnett's test (★$P < 0.05$; NS, not significant). Diagram illustrates the experimental setting. L, left ankle; L5, fifth lumbar spinal cord; DRG, dorsal root ganglion; R, right ankle. Arrow indicates ATP or saline injection. Blue circle indicates the ankle joint examined.

4. Discussion

Rheumatoid arthritis (RA) is a chronic, auto-immune, inflammatory disease which affects the joints such as the wrist, ankle or hand. Progressive articular damage leads to deformation, local deficiencies, and multiple system inflammation **(Feldmann et al., 1996)** Its prevalence in adults around the world is about 1%, affecting mostly females and increasing with age, The persistent inflammatory process of RA results in progressive damage of joints and may lead to pain and fatigue and systemic complications these symptoms deeply affect the quality of life of RA patients, and trigger the development of depression further affecting the well-being **(da Silva et al., 2019).**

In this study we show a molecular mechanism for spreading inflammation between bilateral ankle joints in cytokine-induced and CIA models **(Fig. 42)**. It was reported that sensory neurons that distribute around the ankle joints mainly connect to L5 DRG, but also to L4 and L6 DRGs, albeit at a lower rate **(Kawano et al., 2004; Russell et al., 2012)**. Consistent with this observation, cytokine injections into one ankle joint of F759 mice induced c-fos expression on both sides of L5 DRG, suggesting that the inflammation signal from one side activates sensory neurons in both the ipsilateral and contralateral sides.

Our results indicate that ATP from non-immune cells, particularly in the ipsilateral ankle joint, is a key neurotransmitter for activating afferent sensory pathways toward the contralateral ankle joint. We also found that ATP is at least in part released from sensory neurons with ATP synthase in the contralateral joint. Interestingly, endothelial cells **(Arima et al., 2017)** and synovial cells **(Fig. 23)** also produced ATP in response to inflammatory cytokines, and ATP stimulated IL-6 amplifier activation in these cells. Therefore, we hypothesized that ATP is both a key neurotransmitter and inflammation mediator in both joints.

It is known that spreading inflammation is common in RA. **Lefèvre et al**. showed that RA synovial fibroblasts (RASFs) are able to migrate and contribute to the spread of the disease between bilateral synovial tissues in SCID mice **(Lefevre et al., 2009)**. Although they identified RASFs as one key factor for spreading inflammation from a single joint to multiple ones, how RASFs reach the other joints remains to be elucidated.

We hypothesized that the local neural regulation for bilateral inflammation shown in this study triggers the initial inflammation and promotes the subsequent recruitment of RASFs by

releasing attracting factors like chemokines via the IL-6 amplifier. **Donaldson et al**. reported that capsaicin-sensitive TRPV1+ fibers are involved in the spread of inflammation to the contralateral side using the complete Freund's adjuvant-induced arthritis model **(Donaldson et al., 1995)**.

Our data also suggest the involvement of Nav1.8+TRPV1+/- sensory neurons in the cytokine-induced arthritis model. In the case of the adjuvant-induced arthritis model, the anterior cingulate cortex (ACC) could be the site from which inflammation spreads to the contralateral side **(Arima et al., 2017a; Bliss et al., 2016)**, which is a different mechanism from that in the F759 model, in which we showed that a regional neural pathway through the lower thoracic cords is the primary mediator. Further study is required to determine the detailed relationship between each neural circuit during spreading inflammation, particularly in clinical cases.

To examine whether circulating cytokine levels injected into the joints of F759 mice contributed to the disease development in addition to local neural concentrations, we measured circulating cytokine levels of mouse and human IL-6 and IL-17A by ELISA after joint injections. Mouse IL-6 levels in serum were equivalent between cytokine-injected and non-injected mice, indicating no major systemic inflammatory responses were induced by the joint cytokine injection, which regionally induced activation of the IL-6 amplifier **(Fig. 43)**. On the other hand, increased circulating levels of human IL-6 and mouse IL-17A were detected after the cytokine injections **(Fig. 43)**, suggesting that a small but certain level of cytokines was systemically absorbed via the blood flow. However, it should be pointed out that these concentrations were too low to activate the IL-6 amplifier in vitro and hardly contributed to the cytokine-induced arthritis in vivo **(Fig. 44, A and B).** These findings argue that the level of circulating cytokines did not affect contralateral ankle joint inflammation after cytokine injection at the ipsilateral side. Thus, we propose that the neural connection between both joints played a main role in spreading inflammation.

It is known that ATP is released both from non-immune cells and sensory neurons **(Arima *et al.*, 2017a; Holton, 1959)** and has neurotransmitter activity **(Burnstock, 2006; Evans et al., 1992; Finger et al., 2005; Gourine et al., 2005)**. Accordingly, we hypothesized that ATP in the ipsilateral joint is not only an inflammation mediator that triggers the development of inflammation but also a neurotransmitter for Nav1.8+TRPV1+/- sensory neuron activation. On the other hand, in the contralateral joint, sensory neurons produced ATP most likely via

ATP synthase expression to activate the IL-6 amplifier in non-immune cells, which in turn produced more ATP as well as IL-6. Namely, in the ipsilateral joint, cytokines activating NF-κB and STAT3 triggered ATP secretion from non-immune cells to stimulate the sensory pathway that connects to the contralateral ankle joint to secrete ATP. The resulting ATP activated the IL-6 amplifier in non-immune cells to secrete more IL-6 and ATP in the contralateral ankle joint. Consistently, the blockade of ATP signaling in the contralateral joints suppressed the contralateral ATP increase in situ. Thus, we propose that positive feedback between the ATP and IL-6 secreted by non-immune cells contributes to the inflammation development in the contralateral joint. consistent with our findings **Da Silva, et al**. reported that binding of ATP to P2X7 promotes the release of IL-6 by Ca2+ influx; IL-6 itself may generate B cell proliferation with antibody production, cytotoxic T cell proliferation, differentiation, hematopoiesis, and thrombopoiesis **(da Silva *et al.*, 2019)**
During cell recruitment, P2X7 is directly involved in the adaptive immune response occurring in RA, by mediating the production of interleukin 2 (IL-2) associated with T cell activation **(Arulkumaran et al., 2011).**
Th17 cells are involved in multiple pathological processes of RA, being recognized as a major player in the pathogenesis of RA, They also upregulate the receptor activator of NF-κB (RANK) expression, which results in joint destruction and bone erosion **(Jørgensen, 2018)**.
The role of activation of P2X7 in the production of Th17 cells has been demonstrated in a study with an animal model of arthritis, which found an increase of mRNA for IL-1β, TGF-β1, IL-23, and IL-6, cytokines, necessary for the development of this cellular subtype**(Fan et al., 2016).** Besides, ATP- P2X7 signaling reduces the viability of Tregs and restricts their sup- pressive activity as well as favoring the differentiation of IL-17-secreting Th17 cells (**Lopez-Castejon et al., 2010)**.
Since Th17 cells are essential for the development of autoimmunity by the production of aforementioned pro-inflammatory cytokines, and Tregs play a key role in the maintenance immunological tolerance, a Th17/Treg balance shift by ATP/P2X7 activation may increase inflammation or initiate autoimmunity ,Conversely, the blockade of P2X7 aids the conversion of naïve CD4+ T cells into Treg and could be a strategy to control autoimmunity **(Niu et al., 2012).**

Our findings suggest that a proenkephalin+ but not calretinin+ interneuron network in the thoracic cords makes up the neural circuit between bilateral joints that regulates spreading inflammation. At the same time, we do not dismiss the possibility that neural crosstalk in the

spinal cord by other interneurons is involved in the development of spreading inflammation. Sensory neurons in DRGs have an antidromic function called the axon reflex and contribute to regional inflammation **(Chavan et al., 2017; Talbot et al., 2016).** We hypothesized that Nav1.8+ sensory neurons in the ipsilateral L5 DRG might be responsible for the orthodromic propagation of action potentials to the spinal cord and that sensory neurons in contralateral L4-L6 DRGs are involved in the antidromic axon reflex, exacerbating the contralateral ankle joint inflammation **(Chavan *et al.*, 2017; Gogan et al., 1983; Talbot *et al.*, 2016)**. Because electrophysiology assays showed that anterograde neural activation is stronger than antidromic neural activation **(Sorkin et al., 2018),** we performed such assays on mice with an electrical stimulation on sciatic nerves. We detected an electrophysiological signal in the ipsilateral side, as expected (data not shown), and around the contralateral DRG but hardly around the contralateral ankle joint **(Fig. 45)**. This finding is consistent with the antidromic sensory neural pathway being involved in the contralateral ankle joint inflammation in our system.

To conclude, we report a molecular mechanism of spreading inflammation in two arthritis models. We show that a regional sensory neuron-interneuron connection between the ankle joints through the thoracic spinal cord is critical for spreading inflammation via the bilateral expression of ATP, which activates a neural pathway and enhances the IL-6 amplifier. Therefore, blockade of this sensory neuron-interneuron axis may be a therapeutic target for various diseases with spreading inflammation including RA.

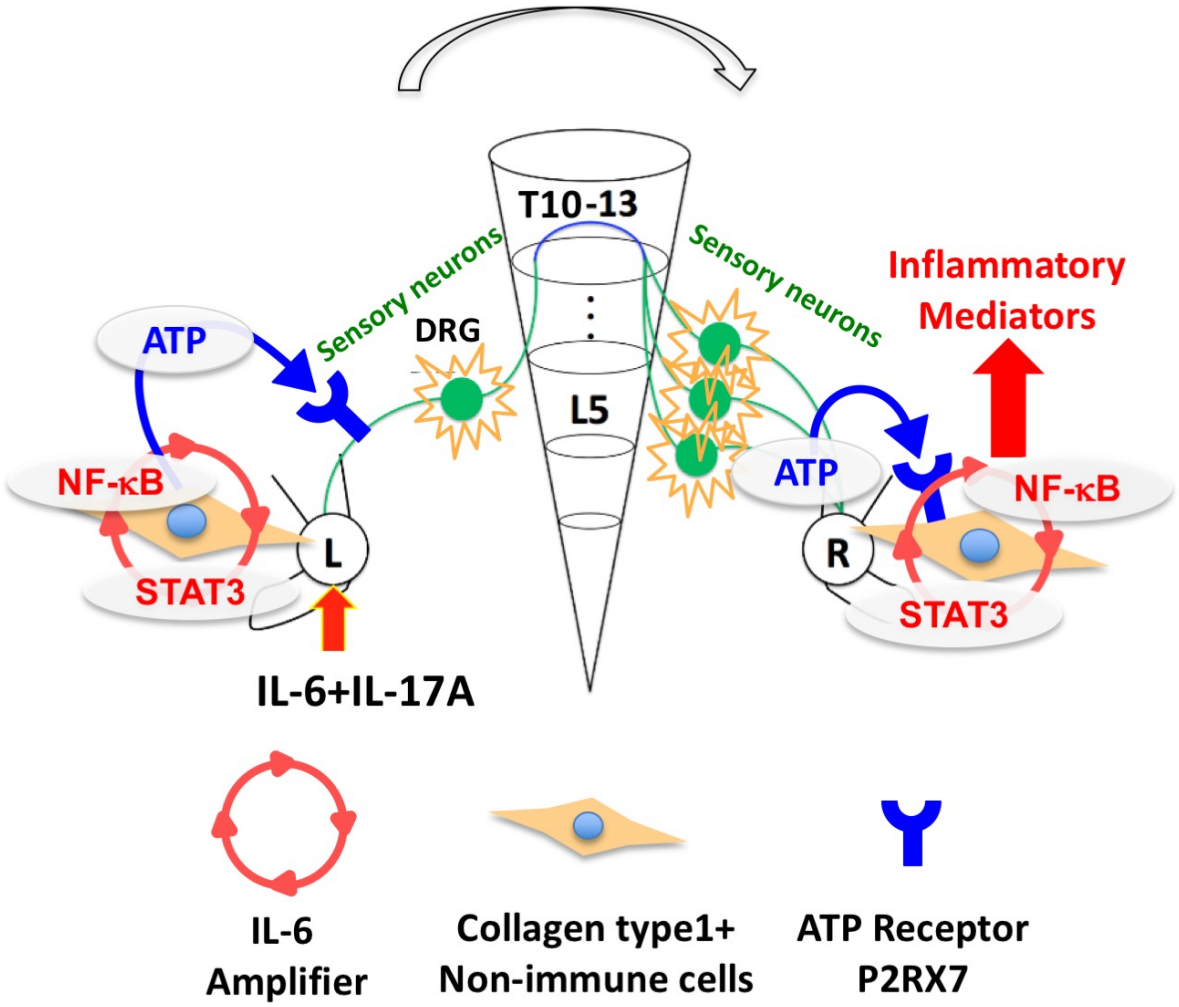

Fig. 42 A schematic model for spreading inflammation

ATP induced by activation of the IL-6 amplifier in collagen type1+ non-immune cells in one side of the ankle joint (left side) activates Nav1.8+ TRPV1+/- sensory neurons, which stimulate the regional sensory neural pathway involving the lower thoracic spinal cord that contains proenkephalin+ interneurons. On the contralateral side (right side), the response of sensory neurons in L4-L6 DRGs releases ATP, which induces inflammatory mediators, including cytokines and chemokines, by activating the IL-6 amplifier in collagen type1+ non-immune cells, including fibroblasts and endothelial cells, through P2RX7.

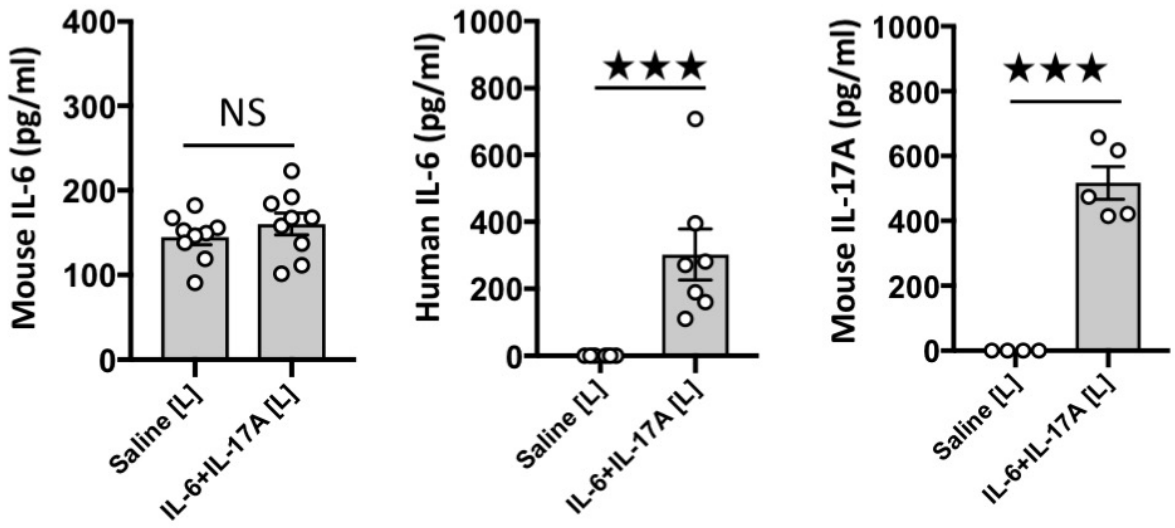

Fig. 43 IL-17A and IL-6 (1 μg each) or saline were injected into the left ankle joint of F759 mice on days 0, 1, and 2, followed by the measurement of mouse IL-6 (n = 9 per group), human IL-6 (n = 6-7 per group), and mouse IL-17A (n = 4-5 per group) levels in serum on day 3. Mean scores ± SEM are shown. *P* values were calculated using Student's t-test (★★★ $P < 0.001$; NS, not significant).

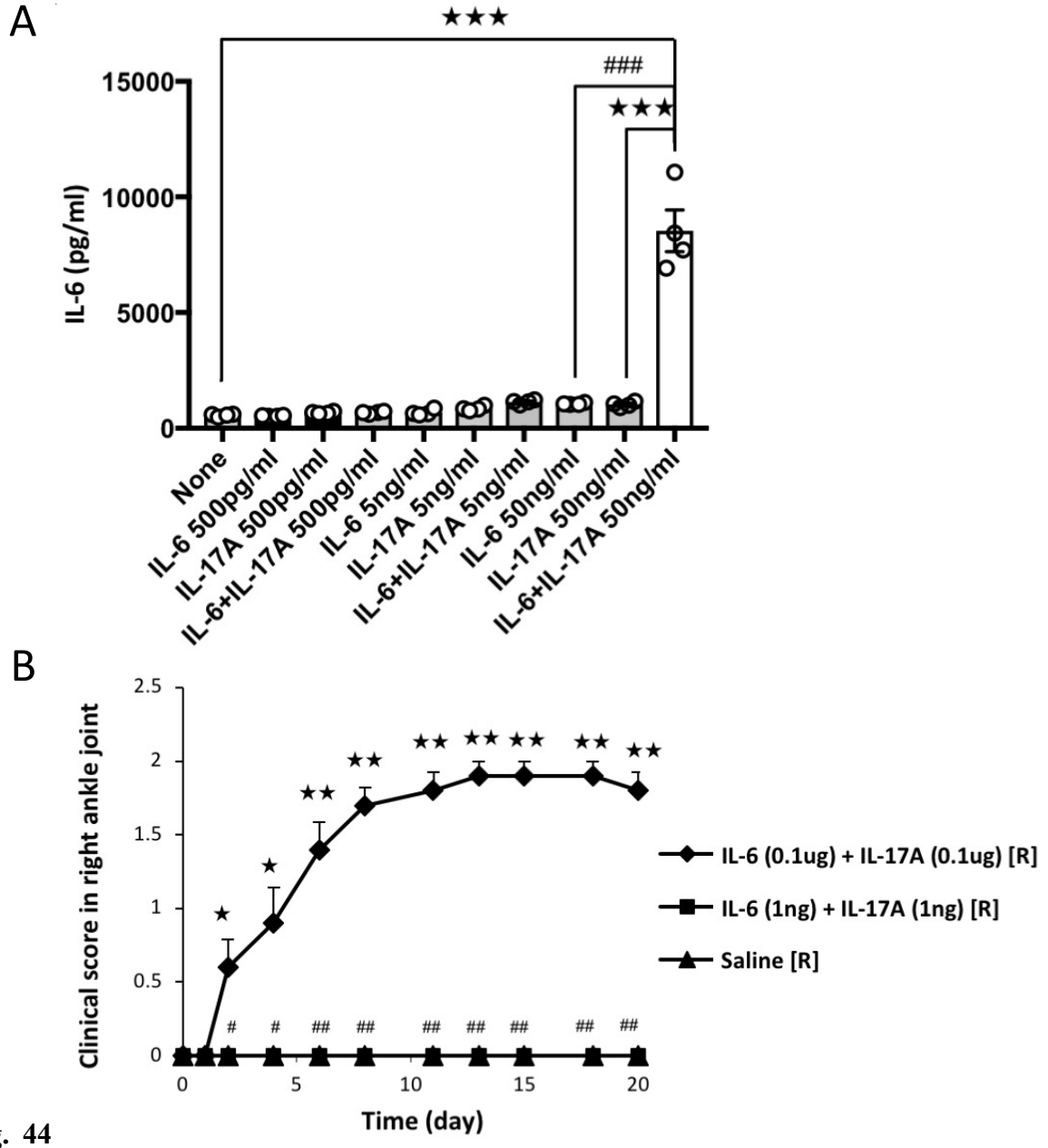

Fig. 44

(A) BC1 endothelial cells were stimulated with a high (50 ng/mL), medium (5 ng/mL each), or low (500 pg/mL each) dose of IL-6 + IL-17A (human IL-6 plus soluble IL-6Rα and/or mouse IL-17A). Culture supernatants were collected and assessed using an ELISA specific for mouse IL-6 (n = 4 per group).

(B) IL-17A and IL-6 (0.1 μg or 1 ng each) or saline were injected into the right ankle joint on days 0, 1, and 2. Clinical arthritis scores of the right ankle joint of F759 mice were evaluated (n = 5 per group). Mean scores ± SEM are shown. *P* values were calculated using Dunnett's

test (A), and the Wilcoxon rank-sum test (B). (★ and # $P < 0.05$; ★★ and ## $P < 0.01$; ★★★ and ###, $P < 0.001$).

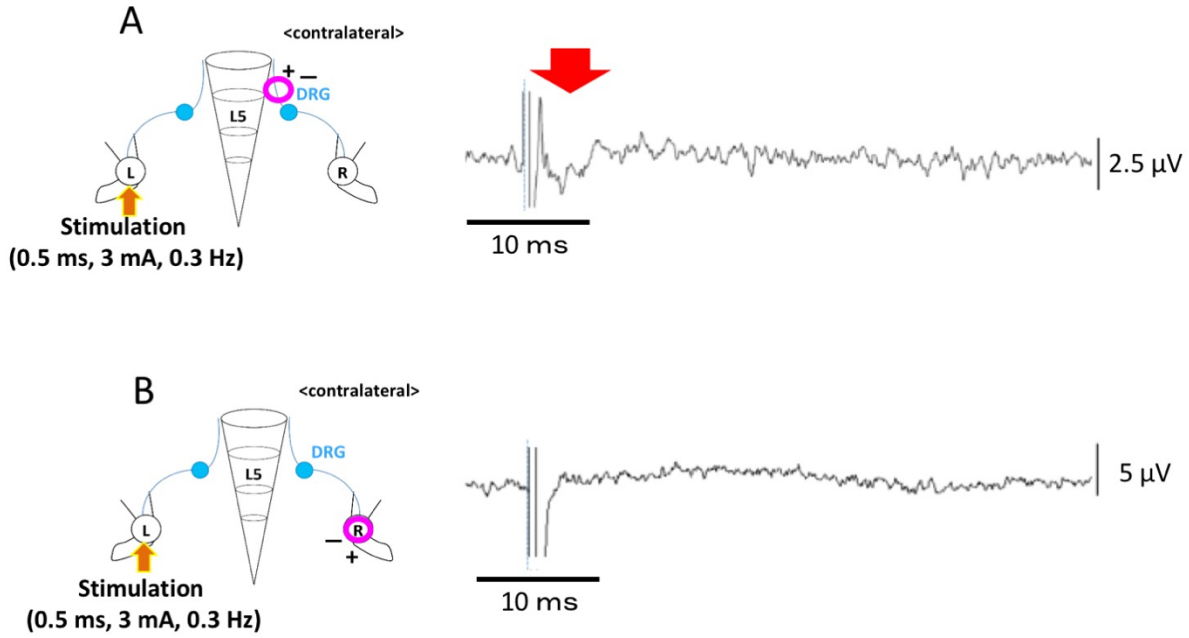

Fig. 45 The tibial nerves around the left ankle were stimulated with 3 mA of electrical pulses (duration: 0.5 ms), and an electrophysiological signal was detected at the contralateral side of the dorsal root (A) or at its sciatic nerves around the right ankle (B) in an anesthetized mouse. A red arrow showed an electrophysiological signal detected.

5. Conclusion

- Surgical ablation or pharmacological inhibition of neural pathway at one side of ankle prevented inflammation development on the other side.
- IL-6 amplifier-mediated ATP induction in collagen type 1+ non-immune cells in one side of ankle joint activates Nav1.8+ TRPV1+/- sensory neurons.
- Nav1.8+ TRPV1+/- sensory neurons stimulates regional sensory neural pathway involving lower thoracic spinal cord that contains proenkephalin+ interneurons.
- Response of sensory neurons in L4-L6 DRGs releases ATP on the contralateral side, and ipsilateral side stimulates collagen type 1+ non-immune cells (fibroblasts and endothelial cells) to induce cytokines and chemokines, resulting in activating the IL-6 amplifier.

Neural circuits between lesions are one mechanism through which local inflammation spreads to remote positions. The present study shows the inflammatory signal on one side of the joint is spread to the other side via sensory neuron-interneuron crosstalk, with ATP at the core. Surgical ablation or pharmacological inhibition of this neural pathway prevented inflammation development on the other side. Mechanistic analysis showed that ATP serves as both a neurotransmitter and an inflammation enhancer, thus acting as an intermediary between the local inflammation and neural pathway that induces inflammation on the other side. These results suggest blockade of this neural pathway may have therapeutic value for inflammatory diseases, particularly those, such as RA, in which inflammation spreads to remote positions.

6. Acknowledgements

At this moment while ending up my Ph.D. , I want to express my deep gratitude for those whom with their support and guidance I reached this point.

As an International student I want to thank the Ministry of Education, Culture, Sports, Science, and technology (MEXT) for the Financial support.

I am deeply grateful to Prof. Dr. Masaaki Murakami for his great guidance, supervision and inspiration. I had learnt a lot from him during or meetings, and very interesting, fruitful scientific discussions.

I also have to thank Dr. Rie Hasebe and Dr. Shintaro Hojyo for supporting, and advising me during the second part of my Ph.D, and for Dr. Daiskue Kamimura for supporting and advising me during the first part of my Ph.D. as well during applying to the MEXT scholarship.

I am also grateful for all Molecular Psychoimmunology lab members for the familial atmosphere we are working in.

7. Conflict of interest

I declare that the research shown in the thesis was conducted in the absence of any commercial or financial relationships that could be construed as a potential conflict of interest.

8. References

Arima, Y., Harada, M., Kamimura, D., Park, J.H., Kawano, F., Yull, F.E., Kawamoto, T., Iwakura, Y., Betz, U.A., Márquez, G., et al. (2012). Regional neural activation defines a gateway for autoreactive T cells to cross the blood-brain barrier. Cell *148*, 447-457. 10.1016/j.cell.2012.01.022.

Arima, Y., Kamimura, D., Atsumi, T., Harada, M., Kawamoto, T., Nishikawa, N., Stofkova, A., Ohki, T., Higuchi, K., Morimoto, Y., et al. (2015a). A pain-mediated neural signal induces relapse in murine autoimmune encephalomyelitis, a multiple sclerosis model. eLife *4*, e08733. 10.7554/eLife.08733.

Arima, Y., Kamimura, D., Atsumi, T., Harada, M., Kawamoto, T., Nishikawa, N., Stofkova, A., Ohki, T., Higuchi, K., Morimoto, Y., et al. (2015b). A pain-mediated neural signal induces relapse in murine autoimmune encephalomyelitis, a multiple sclerosis model. Elife *4*. 10.7554/eLife.08733.

Arima, Y., Ohki, T., Nishikawa, N., Higuchi, K., Ota, M., Tanaka, Y., Nio-Kobayashi, J., Elfeky, M., Sakai, R., Mori, Y., et al. (2017a). Brain micro-inflammation at specific vessels dysregulates organ-homeostasis via the activation of a new neural circuit. eLife *6*, e25517. 10.7554/eLife.25517.

Arima, Y., Ohki, T., Nishikawa, N., Higuchi, K., Ota, M., Tanaka, Y., Nio-Kobayashi, J., Elfeky, M., Sakai, R., Mori, Y., et al. (2017b). Brain micro-inflammation at specific vessels dysregulates organ-homeostasis via the activation of a new neural circuit. Elife *6*. 10.7554/eLife.25517.

Arnett, F.C., Edworthy, S.M., Bloch, D.A., McShane, D.J., Fries, J.F., Cooper, N.S., Healey, L.A., Kaplan, S.R., Liang, M.H., and Luthra, H.S. (1988). The American Rheumatism Association 1987 revised criteria for the classification of rheumatoid arthritis. Arthritis Rheum. *31*, 315-324.

Arulkumaran, N., Unwin, R.J., and Tam, F.W. (2011). A potential therapeutic role for P2X7 receptor (P2X7R) antagonists in the treatment of inflammatory diseases. Expert Opin Investig Drugs *20*, 897-915. 10.1517/13543784.2011.578068.

Atsumi, T., Ishihara, K., Kamimura, D., Ikushima, H., Ohtani, T., Hirota, S., Kobayashi, H., Park, S.J., Saeki, Y., Kitamura, Y., and Hirano, T. (2002). A point mutation of Tyr-759 in interleukin 6 family cytokine receptor subunit gp130 causes autoimmune arthritis. J Exp Med *196*, 979-990. 10.1084/jem.20020619.

Atsumi, T., Singh, R., Sabharwal, L., Bando, H., Meng, J., Arima, Y., Yamada, M., Harada, M., Jiang, J.J., Kamimura, D., et al. (2014). Inflammation amplifier, a new paradigm in cancer biology. Cancer Res *74*, 8-14. 10.1158/0008-5472.Can-13-2322.

Atsumi, T., Suzuki, H., Jiang, J.J., Okuyama, Y., Nakagawa, I., Ota, M., Tanaka, Y., Ohki, T., Katsunuma, K., Nakajima, K., et al. (2017). Rbm10 regulates inflammation development via alternative splicing of Dnmt3b. Int Immunol *29*, 581-591. 10.1093/intimm/dxx067.

Biggioggero, M., Crotti, C., Becciolini, A., and Favalli, E.G. (2019). Tocilizumab in the treatment of rheumatoid arthritis: an evidence-based review and patient selection. Drug Des Devel Ther *13*, 57-70. 10.2147/dddt.S150580.

Bliss, T.V., Collingridge, G.L., Kaang, B.K., and Zhuo, M. (2016). Synaptic plasticity in the anterior cingulate cortex in acute and chronic pain. Nat Rev Neurosci *17*, 485-496. 10.1038/nrn.2016.68.

Burnstock, G. (2006). Historical review: ATP as a neurotransmitter. Trends Pharmacol Sci *27*, 166-176. 10.1016/j.tips.2006.01.005.

Chavan, S.S., Pavlov, V.A., and Tracey, K.J. (2017). Mechanisms and Therapeutic Relevance of Neuro-immune Communication. Immunity *46*, 927-942. 10.1016/j.immuni.2017.06.008.

Clarke, G.S., Buckland-Wright, J.C., and Grahame, R. (1994). Symmetry of radiological features in the wrist and hands of patients with early to moderate rheumatoid arthritis: a quantitative microfocal radiographic study. Br J Rheumatol. *33*, 249-254.

da Silva, J.L.G., Passos, D.F., Bernardes, V.M., and Leal, D.B.R. (2019). ATP and adenosine: Role in the immunopathogenesis of rheumatoid arthritis. Immunol Lett *214*, 55-64. 10.1016/j.imlet.2019.08.009.

Donaldson, L.F., McQueen, D.S., and Seckl, J.R. (1995). Neuropeptide gene expression and capsaicin-sensitive primary afferents: maintenance and spread of adjuvant arthritis in the rat. J Physiol *486 (Pt 2)*, 473-482.

Donnelly-Roberts, D.L., Namovic, M.T., Han, P., and Jarvis, M.F. (2009). Mammalian P2X7 receptor pharmacology: comparison of recombinant mouse, rat and human P2X7 receptors. Br J Pharmacol. *157*, 1203-1214.

Evans, R.J., Derkach, V., and Surprenant, A. (1992). ATP mediates fast synaptic transmission in mammalian neurons. Nature *357*, 503-505.

Fan, Z.D., Zhang, Y.Y., Guo, Y.H., Huang, N., Ma, H.H., Huang, H., and Yu, H.G. (2016). Involvement of P2X7 receptor signaling on regulating the differentiation of Th17 cells and type II collagen-induced arthritis in mice. Sci Rep *6*, 35804. 10.1038/srep35804.

Feldmann, M., Brennan, F.M., and Maini, R.N. (1996). Rheumatoid arthritis. Cell *85*, 307-310. 10.1016/s0092-8674(00)81109-5.

Finger, T.E., Danilova, V., Barrows, J., Bartel, D.L., Vigers, A.J., Stone, L., Hellekant, G., and Kinnamon, S.C. (2005). ATP signaling is crucial for communication from taste buds to gustatory nerves. Science *10*, 1495-1499.

Fujita, M., Yamamoto, Y., Jiang, J.J., Atsumi, T., Tanaka, Y., Ohki, T., Murao, N., Funayama, E., Hayashi, T., Osawa, M., et al. (2019). NEDD4 Is Involved in Inflammation Development during Keloid Formation. J Invest Dermatol *139*, 333-341. 10.1016/j.jid.2018.07.044.

Fukada, T., Hibi, M., Yamanaka, Y., Takahashi-Tezuka, M., Fujitani, Y., Yamaguchi, T., Nakajima, K., and Hirano, T. (1996). Two signals are necessary for cell proliferation induced by a cytokine receptor gp130: involvement of STAT3 in anti-apoptosis. Immunity *5*, 449-460. 10.1016/s1074-7613(00)80501-4.

Gogan, P., Gueritaud, J.P., and Tyc-Dumont, S. (1983). Comparison of antidromic and orthodromic action potentials of identified motor axons in the cat's brain stem. J Physiol *335*, 205-220.

Gourine, A.V., Llaudet, E., Dale, N., and Spyer, K.M. (2005). ATP is a mediator of chemosensory transduction in the central nervous system. Nature. *436*, 108-111.

Grassel, S.G. (2014). The role of peripheral nerve fibers and their neurotransmitters in cartilage and bone physiology and pathophysiology. Arthritis Res Ther *16*, 485.

Harada, M., Kamimura, D., Arima, Y., Kohsaka, H., Nakatsuji, Y., Nishida, M., Atsumi, T., Meng, J., Bando, H., Singh, R., et al. (2015). Temporal expression of growth factors triggered by epiregulin regulates inflammation development. Journal of immunology *194*, 1039-1046. 10.4049/jimmunol.1400562.

Hashizume, M., and Mihara, M. (2011). The roles of interleukin-6 in the pathogenesis of rheumatoid arthritis. Arthritis *2011*, 765624. 10.1155/2011/765624.

Higuchi, H., Kamimura, D., Jiang, J.J., Atsumi, T., Iwami, D., Hotta, K., Harada, H., Takada, Y., Kanno-Okada, H., Hatanaka, K.C., et al. (2020). Orosomucoid 1 is involved in the development of chronic allograft rejection after kidney transplantation. Int Immunol *32*, 335-346. 10.1093/intimm/dxaa003.

Hirano, T. (1992). Interleukin-6 and its relation to inflammation and disease. Clin Immunol Immunopathol *62*, S60-65. 10.1016/0090-1229(92)90042-m.

Hirano, T. (1998). Interleukin 6 and its receptor: ten years later. Int Rev Immunol *16*, 249-284. 10.3109/08830189809042997.

Hirano, T., Matsuda, T., Turner, M., Miyasaka, N., Buchan, G., Tang, B., Sato, K., Shimizu, M., Maini, R., Feldmann, M., and et al. (1988). Excessive production of interleukin 6/B cell stimulatory factor-2 in rheumatoid arthritis. Eur J Immunol *18*, 1797-1801. 10.1002/eji.1830181122.

Hirano, T., and Murakami, M. (2020). COVID-19: A New Virus, but a Familiar Receptor and Cytokine Release Syndrome. Immunity *52*, 731-733. 10.1016/j.immuni.2020.04.003.

Hirano, T., Taga, T., Yasukawa, K., Nakajima, K., Nakano, N., Takatsuki, F., Shimizu, M., Murashima, A., Tsunasawa, S., Sakiyama, F., and et al. (1987). Human B-cell differentiation factor defined by an anti-peptide antibody and its possible role in autoantibody production. Proceedings of the National Academy of Sciences of the United States of America *84*, 228-231. 10.1073/pnas.84.1.228.

Holton, P. (1959). The liberation of adenosine triphosphate on antidromic stimulation of sensory nerves. J Physiol *145*, 494-504.

Houssiau, F.A., Devogelaer, J.P., Van Damme, J., de Deuxchaisnes, C.N., and Van Snick, J. (1988). Interleukin-6 in synovial fluid and serum of patients with rheumatoid arthritis and other inflammatory arthritides. Arthritis Rheum *31*, 784-788. 10.1002/art.1780310614.

Igarashi, H., Hashimoto, J., Tomita, T., Yoshikawa, H., and Ishihara, K. (2010). TP53 mutations coincide with the ectopic expression of activation-induced cytidine deaminase in the fibroblast-like synoviocytes derived from a fraction of patients with rheumatoid arthritis. Clin Exp Immunol *161*, 71-80. 10.1111/j.1365-2249.2010.04163.x.

Ishihara, K., and Hirano, T. (2002). IL-6 in autoimmune disease and chronic inflammatory proliferative disease. Cytokine Growth Factor Rev *13*, 357-368. 10.1016/s1359-6101(02)00027-8.

Jørgensen, N.R. (2018). The purinergic P2X7 ion channel receptor-a 'repair' receptor in bone. Curr Opin Immunol *52*, 32-38. 10.1016/j.coi.2018.03.016.

June, R.R., and Olsen, N.J. (2016). Room for more IL-6 blockade? Sarilumab for the treatment of rheumatoid arthritis. Expert Opin Biol Ther *16*, 1303-1309. 10.1080/14712598.2016.1217988.

Kamimura, D., Ishihara, K., and Hirano, T. (2003). IL-6 signal transduction and its physiological roles: the signal orchestration model. Rev Physiol Biochem Pharmacol *149*, 1-38. 10.1007/s10254-003-0012-2.

Kawamoto, T., and Kawamoto, K. (2014). Preparation of thin frozen sections from nonfixed and undecalcified hard tissues using Kawamot's film method (2012). Methods Mol Biol *1130*, 149-164. 10.1007/978-1-62703-989-5_11.

Kawano, F., Ishihara, A., Stevens, J.L., Wang, X.D., Ohshima, S., Horisaka, M., Maeda, Y., Nonaka, I., and Ohira, Y. (2004). Tension- and afferent input-associated responses of neuromuscular system of rats to hindlimb unloading and/or tenotomy. Am J Physiol Regul Integr Comp Physiol *287*, R76-86. 10.1152/ajpregu.00694.2003.

Kawano, F., Matsuoka, Y., Oke, Y., Higo, Y., Terada, M., Wang, X.D., Nakai, N., Fukuda, H., Imajoh-Ohmi, S., and Ohira, Y. (2007). Role(s) of nucleoli and phosphorylation of ribosomal protein S6 and/or HSP27 in the regulation of muscle mass. American journal of physiology. Cell physiology *293*, C35-44. 10.1152/ajpcell.00297.2006.

Kelly, S., Dunham, J.P., and Donaldson, L.F. (2007). Sensory nerves have altered function contralateral to a monoarthritis and may contribute to the symmetrical spread of inflammation. Eur J Neurosci *26*, 935-942. 10.1111/j.1460-9568.2007.05737.x.

Kidd, B.L., Mapp, P.I., Gibson, S.J., Polak, J.M., O'Higgins, F., Buckland-Wright, J.C., and Blake, D.R. (1989). A neurogenic mechanism for symmetrical arthritis. Lancet *2*, 1128-1130.

Kim, S.S., Wang, H., Li, X.Y., Chen, T., Mercaldo, V., Descalzi, G., Wu, L.J., and Zhuo, M. (2011). Neurabin in the anterior cingulate cortex regulates anxiety-like behavior in adult mice. Mol Brain. *19*, 4-6.

Kitabayashi, C., Fukada, T., Kanamoto, M., Ohashi, W., Hojyo, S., Atsumi, T., Ueda, N., Azuma, I., Hirota, H., Murakami, M., and Hirano, T. (2010). Zinc suppresses Th17 development via inhibition of STAT3 activation. . Int. Immunol. *22*, 375-386.

Labasi, J.M., Petrushova, N., Donovan, C., McCurdy, S., Lira, P., Payette, M.M., Brissette, W., Wicks, J.R., Audoly, L., and Gabel, C.A. (2002). Absence of the P2X7 receptor alters leukocyte function and attenuates an inflammatory response. Journal of immunology *168*, 6436-6445. 10.4049/jimmunol.168.12.6436.

Larsson, J., Ekblom, A., Henriksson, K., Lundeberg, T., and Theodorsson, E. (1991). Concentration of substance P, neurokinin A, calcitonin gene-related peptide, neuropeptide Y and vasoactive intestinal polypeptide in synovial fluid from knee joints in patients suffering from rheumatoid arthritis. Scand J Rheumatol *20*, 326-335.

Lee, J., Nakagiri, T., Kamimura, D., Harada, M., Oto, T., Susaki, Y., Shintani, Y., Inoue, M., Miyoshi, S., Morii, E., et al. (2013). IL-6 amplifier activation in epithelial regions of bronchi after allogeneic lung transplantation. Int Immunol *25*, 319-332. 10.1093/intimm/dxs158.

Lefevre, S., Knedla, A., Tennie, C., Kampmann, A., Wunrau, C., Dinser, R., Korb, A., Schnaker, E.M., Tarner, I.H., Robbins, P.D., et al. (2009). Synovial fibroblasts spread rheumatoid arthritis to unaffected joints. Nat Med *15*, 1414-1420. 10.1038/nm.2050.

Lopez-Castejon, G., Theaker, J., Pelegrin, P., Clifton, A.D., Braddock, M., and Surprenant, A. (2010). P2X(7) receptor-mediated release of cathepsins from macrophages is a cytokine-independent mechanism potentially involved in joint diseases. J Immunol *185*, 2611-2619. 10.4049/jimmunol.1000436.

Malmberg, A.B., and Basbaum, A.I. (1998). Partial sciatic nerve injury in the mouse as a model of neuropathic pain:
behavioral and neuroanatomical correlates. Pain *76*, 215-222.

Mausset-Bonnefont, A.L., Cren, M., Vicente, R., Quentin, J., Jorgensen, C., Apparailly, F., and Louis-Plence, P. (2019). Arthritis sensory and motor scale: predicting functional deficits from the clinical score in collagen-induced arthritis. Arthritis Res Ther *21*, 264. 10.1186/s13075-019-2047-z.

McGaraughty, S., Chu, K.L., Namovic, M.T., Donnelly-Roberts, D.L., Harris, R.R., Zhang, X.F., Shieh, C.C., Wismer, C.T., Zhu, C.Z., Gauvin, D.M., et al. (2007). P2X7-related modulation of pathological nociception in rats. Neuroscience. *148*, 1817-1828.

Meng, J., Jiang, J.J., Atsumi, T., Bando, H., Okuyama, Y., Sabharwal, L., Nakagawa, I., Higuchi, H., Ota, M., Okawara, M., et al. (2016). Breakpoint Cluster Region-Mediated Inflammation Is Dependent on Casein Kinase II. Journal of immunology *197*, 3111-3119. 10.4049/jimmunol.1601082.

Miller, L.E., Grifka, J., Scholmerich, J., and Straub, R.H. (2002). Norepinephrine from synovial tyrosine hydroxylase positive cells is a strong indicator of synovial inflammation in rheumatoid arthritis. J Rheumatol *29*, 427-435.

Moretto, J.N., Duffy Á, M., and Scharfman, H.E. (2017). Acute restraint stress decreases c-fos immunoreactivity in hilar mossy cells of the adult dentate gyrus. Brain Struct Funct *222*, 2405-2419. 10.1007/s00429-016-1349-z.

Murakami, K., Tanaka, Y., and Murakami, M. (2021). The gateway reflex: breaking through the blood barriers. Int Immunol. 10.1093/intimm/dxab064.

Murakami, M., Harada, M., Kamimura, D., Ogura, H., Okuyama, Y., Kumai, N., Okuyama, A., Singh, R., Jiang, J.J., Atsumi, T., et al. (2013). Disease-association analysis of an inflammation-related feedback loop. Cell Rep *3*, 946-959. 10.1016/j.celrep.2013.01.028.

Murakami, M., Kamimura, D., and Hirano, T. (2019). Pleiotropy and Specificity: Insights from the Interleukin 6 Family of Cytokines. Immunity *50*, 812-831. 10.1016/j.immuni.2019.03.027.

Murakami, M., Okuyama, Y., Ogura, H., Asano, S., Arima, Y., Tsuruoka, M., Harada, M., Kanamoto, M., Sawa, Y., Iwakura, Y., et al. (2011). Local microbleeding facilitates IL-6- and IL-17-dependent arthritis in the absence of tissue antigen recognition by activated T cells. J Exp Med *208*, 103-114. jem.20100900 [pii]10.1084/jem.20100900.

Nakagawa, T., Tsuruoka, M., Ogura, H., Okuyama, Y., Arima, Y., Hirano, T., and Murakami, M. (2010). IL-6 positively regulates Foxp3+CD8+ T cells in vivo. Int Immunol *22*, 129-139. 10.1093/intimm/dxp119.

Narváez, J., Oton, T., J, L.L., Mora-Limiñana, M., Nolla, J.M., and Loza, E. (2021). Response to interleukin-6 receptor antagonists in patients with rheumatoid arthritis is independent of the number of prior used TNF inhibitors: A systematic review and metaanalysis. Joint Bone Spine *88*, 105112. 10.1016/j.jbspin.2020.105112.

Niu, Q., Cai, B., Huang, Z.C., Shi, Y.Y., and Wang, L.L. (2012). Disturbed Th17/Treg balance in patients with rheumatoid arthritis. Rheumatol Int *32*, 2731-2736. 10.1007/s00296-011-1984-x.

Norgren, R.B.J., and Lehman, M.N. (1998). Herpes simplex virus as a transneuronal tracer. Neurosci Biobehav Rev. *22*, 695-708.

O'Connor, T.M., O'Connell, J., O'Brien, D.I., Goode, T., Bredin, C.P., and Shanahan, F. (2004). The role of substance P in inflammatory disease. J Cell Physiol *201*, 167-180. 10.1002/jcp.20061.

Ogata, A., Kato, Y., Higa, S., and Yoshizaki, K. (2019). IL-6 inhibitor for the treatment of rheumatoid arthritis: A comprehensive review. Mod Rheumatol *29*, 258-267. 10.1080/14397595.2018.1546357.

Ogura, H., Murakami, M., Okuyama, Y., Tsuruoka, M., Kitabayashi, C., Kanamoto, M., Nishihara, M., Iwakura, Y., and Hirano, T. (2008). Interleukin-17 promotes autoimmunity by triggering a positive-feedback loop via interleukin-6 induction. Immunity *29*, 628-636. 10.1016/j.immuni.2008.07.018.

Ohtani, T., Ishihara, K., Atsumi, T., Nishida, K., Kaneko, Y., Miyata, T., Itoh, S., Narimatsu, M., Maeda, H., Fukada, T., et al. (2000). Dissection of signaling cascades through gp130 in vivo: reciprocal roles for STAT3- and SHP2-mediated signals in immune responses. Immunity *12*, 95-105. 10.1016/s1074-7613(00)80162-4.

Okuyama, Y., Tanaka, Y., Jiang, J.J., Kamimura, D., Nakamura, A., Ota, M., Ohki, T., Higo, D., Ogura, H., Ishii, N., et al. (2018a). Bmi1 Regulates IkappaBalpha Degradation via Association with the SCF Complex. Journal of immunology *201*, 2264-2272. 10.4049/jimmunol.1701223.

Okuyama, Y., Tanaka, Y., Jiang, J.J., Kamimura, D., Nakamura, A., Ota, M., Ohki, T., Higo, D., Ogura, H., Ishii, N., et al. (2018b). Bmi1 Regulates IκBα Degradation via Association with the SCF Complex. J Immunol *201*, 2264-2272. 10.4049/jimmunol.1701223.

Ota, M., Tanaka, Y., Nakagawa, I., Jiang, J.J., Arima, Y., Kamimura, D., Onodera, T., Iwasaki, N., and Murakami, M. (2020). Role of Chondrocytes in the Development of Rheumatoid Arthritis Via Transmembrane Protein 147-Mediated NF-kappaB Activation. Arthritis Rheumatol *72*, 931-942. 10.1002/art.41182.

Peirs, C., Williams, S.P., Zhao, X., Walsh, C.E., Gedeon, J.Y., Cagle, N.E., Goldring, A.C., Hioki, H., Liu, Z., Marell, P.S., and Seal, R.P. (2015). Dorsal Horn Circuits for Persistent Mechanical Pain. Neuron *87*, 797-812. 10.1016/j.neuron.2015.07.029.

Raimondo, M.G., Biggioggero, M., Crotti, C., Becciolini, A., and Favalli, E.G. (2017). Profile of sarilumab and its potential in the treatment of rheumatoid arthritis. Drug Des Devel Ther *11*, 1593-1603. 10.2147/dddt.S100302.

Russell, F.A., Schuelert, N., Veldhoen, V.E., Hollenberg, M.D., and McDougall, J.J. (2012). Activation of PAR(2) receptors sensitizes primary afferents and causes leukocyte rolling and adherence in the rat knee joint. Br J Pharmacol *167*, 1665-1678. 10.1111/j.1476-5381.2012.02120.x.

Sadikot, R.T., and Blackwell, T.S. (2008). Bioluminescence: imaging modality for in vitro and in vivo gene expression. Methods Mol Biol *477*, 383-394. 10.1007/978-1-60327-517-0_29.

Sasai, M., Saeki, Y., Ohshima, S., Nishioka, K., Mima, T., Tanaka, T., Katada, Y., Yoshizaki, K., Suemura, M., and Kishimoto, T. (1999). Delayed onset and reduced severity of collagen-induced arthritis in interleukin-6-deficient mice. Arthritis Rheum. *42*, 1635-1643.
Sawa, S., Kamimura, D., Jin, G.H., Morikawa, H., Kamon, H., Nishihara, M., Ishihara, K., Murakami, M., and Hirano, T. (2006). Autoimmune arthritis associated with mutated interleukin (IL)-6 receptor gp130 is driven by STAT3/IL-7-dependent homeostatic proliferation of CD4+ T cells. J Exp Med *203*, 1459-1470. 10.1084/jem.20052187.

Schmidt-Supprian, M., Bloch, W., Courtois, G., Addicks, K., Israël, A., Rajewsky, K., and Pasparakis, M. (2000). NEMO/IKK gamma-deficient mice model incontinentia pigmenti. Mol . Cell *5*, 981-992.

Seltzer, Z., Dubner, R., and Shir, Y. (1990). A novel behavioral model of neuropathic pain disorders produced in rats by partial sciatic nerve injury. Pain *43*, 205-218.

Shenker, N., Haigh, R., Roberts, E., Mapp, P., Harris, N., and Blake, D. (2003). A review of contralateral responses to a unilateral inflammatory lesion. Rheumatology (Oxford). *42*, 1279-1286.

Sorkin, L.S., Eddinger, K.A., Woller, S.A., and Yaksh, T.L. (2018). Origins of antidromic activity in sensory afferent fibers and neurogenic inflammation. Semin Immunopathol *40*, 237-247. 10.1007/s00281-017-0669-2.

Stofkova, A., Kamimura, D., Ohki, T., Ota, M., Arima, Y., and Murakami, M. (2019). Photopic light-mediated down-regulation of local α(1A)-adrenergic signaling protects blood-retina barrier in experimental autoimmune uveoretinitis. Sci Rep *9*, 2353. 10.1038/s41598-019-38895-y.

Stotz-Potter, E.H., Morin, S.M., and DiMicco, J.A. (1996). Effect of microinjection of muscimol into the dorsomedial or paraventricular hypothalamic nucleus on air stress-induced neuroendocrine and cardiovascular changes in rats. Brain Res *742*, 219-224. 10.1016/s0006-8993(96)01011-6.

Takeda, K., Kaisho, T., Yoshida, N., Takeda, J., Kishimoto, T., and Akira, S. (1998). Stat3 activation is responsible for IL-6-dependent T cell proliferation through preventing apoptosis: generation and characterization of T cell-specific Stat3-deficient mice. J Immunol *161*, 4652-4660.

Talbot, S., Foster, S.L., and Woolf, C.J. (2016). Neuroimmunity: Physiology and Pathology. Annu Rev Immunol *34*, 421-447. 10.1146/annurev-immunol-041015-055340.

Tanaka, Y., Arima, Y., Higuchi, K., Ohki, T., Elfeky, M., Ota, M., Kamimura, D., and Murakami, M. (2017). EAE Induction by Passive Transfer of MOG-specific CD4(+) T Cells. Bio Protoc *7*, e2370. 10.21769/BioProtoc.2370.

Tanaka, Y., Sabharwal, L., Ota, M., Nakagawa, I., Jiang, J.J., Arima, Y., Ogura, H., Okochi, M., Ishii, M., Kamimura, D., and Murakami, M. (2018). Presenilin 1 Regulates NF-kappaB Activation via Association with Breakpoint Cluster Region and Casein Kinase II. Journal of immunology *201*, 2256-2263. 10.4049/jimmunol.1701446.

Turner, S.L., and Jenkins, F.J. (1997). The roles of herpes simplex virus in neuroscience. J Neurovirol. *3*, 110-125.

Uchida, M., Yamamoto, R., Matsuyama, S., Murakami, K., Hasebe, R., Hojyo, S., Tanaka, Y., and Murakami, M. (2021). Gateway reflexes, neuronal circuits that regulate the gateways for autoreactive T cells in organs that have blood barriers. Int Immunol. 10.1093/intimm/dxab022.

Vetrugno, G.C., Lachuer, J., Perego, C., Miranda, E., De Simoni, M.G., and Tappaz, M. (1993). Lack of glucocorticoids sustains the stress-induced release of noradrenaline in the anterior hypothalamus. Neuroendocrinology *57*, 835-842. 10.1159/000126442.

Xie, Z., Dai, J., Yang, A., and Wu, Y. (2014). A role for bradykinin in the development of anti-collagen antibody-induced arthritis. Rheumatology (Oxford) *53*, 1301-1306. 10.1093/rheumatology/keu015.

Yoshizaki, K., Matsuda, T., Nishimoto, N., Kuritani, T., Taeho, L., Aozasa, K., Nakahata, T., Kawai, H., Tagoh, H., Komori, T., and et al. (1989). Pathogenic significance of interleukin-6 (IL-6/BSF-2) in Castleman's disease. Blood *74*, 1360-1367.

Yun, S., Reynolds, R.P., Petrof, I., White, A., Rivera, P.D., Segev, A., Gibson, A.D., Suarez, M., DeSalle, M.J., Ito, N., et al. (2018). Stimulation of entorhinal cortex-dentate gyrus circuitry is antidepressive. Nat Med *24*, 658-666. 10.1038/s41591-018-0002-1.